Multistatic Radar Optimization for Radar Sensor Network Applications

by

Moez BEN KILANI

THESIS PRESENTED TO ÉCOLE DE TECHNOLOGIE SUPÉRIEURE
IN PARTIAL FULFILLMENT FOR THE DEGREE OF
DOCTOR OF PHILOSOPHY
Ph.D.

MONTREAL, APRIL 30, 2018

ÉCOLE DE TECHNOLOGIE SUPÉRIEURE
UNIVERSITÉ DU QUÉBEC

BOARD OF EXAMINERS

THIS THESIS HAS BEEN EVALUATED

BY THE FOLLOWING BOARD OF EXAMINERS

Mr. Ghyslain Gagnon, Thesis Supervisor
Department of electrical engineering at École de technologie supérieure

Mr. François Gagnon, Thesis Co-supervisor
Department of electrical engineering at École de technologie supérieure

Mr. Roger Champagne, President of the Board of Examiners
Department of software and IT engineering at École de technologie supérieure

Mr. Charles Despins, Member of the jury
Department of electrical engineering at École de technologie supérieure

Mr. Chahé Nerguizian, External Independent Examiner
Department of electrical engineering at Polytechnique Montreal.

THIS THESIS WAS PRENSENTED AND DEFENDED

IN THE PRESENCE OF A BOARD OF EXAMINERS AND PUBLIC

MARCH, 14TH, 2018

AT ÉCOLE DE TECHNOLOGIE SUPÉRIEURE

ACKNOWLEDGMENT

OPTIMISATION DES RADARS MULTISTATIQUES POUR DES APPLICATIONS DE RÉSEAUX DE CAPTEURS RADAR

Moez BEN KILANI

RÉSUMÉ

La conception de réseaux de capteurs radar a subi une croissance considérable durant les dernières années. En effet, ce genre de systèmes est caractérisé par un degré de flexibilité élevé du point de vue de la conception. Ceci est grâce à la multiplicité de nœuds radar ainsi que les méthodes de fusion de données. Cette thèse se concentre particulièrement sur le développement et l'analyse des architectures de réseaux de capteurs radar dans le but d'optimiser la détection et le positionnement de la cible. Un intérêt spécial est porté aux systèmes de réseaux de capteurs radar distribués, où la diversité spatiale peut être exploitée afin d'améliorer les capacités du radar en termes de détection de cible.

Dans une première partie de cette thèse, la diversité spatiale est utilisée en conjonction avec des techniques cognitives de conception et de sélection de formes d'ondes afin de s'adapter rapidement et en temps réel aux variations de l'environnement où se situe la cible. Dans une seconde partie, on étudie l'impact de la géométrie de réseaux de capteurs radar, en particulier, l'emplacement des récepteurs du radar multistatique sur la précision de positionnement de la cible. On développe un système basé sur une sélection cognitive de formes d'ondes radar ainsi qu'une stratégie adaptative de placement de récepteurs pour gérer les caractéristiques de dispersion propre à la cible. Ces caractéristiques sont variables dans le temps ainsi que les paramètres de distribution d'objets radars non désirés dans la milieu radar dynamique.

La troisième partie de la thèse est consacrée au thème de la coexistence entre les systèmes radar et de communication et leur opération conjointe à travers deux architectures possibles. Dans la première architecture, plusieurs nœuds de communication opèrent séparément en fréquences. Chaque nœud tire profit de la diversité à plusieurs vues du système distribué afin d'activer le traitement radar sur les multiples signaux radar bistatiques et monostatique reçus au niveau de chaque nœud. L'architecture est basée sur le fait que le signal de communication, comme la forme d'onde Orthogonal Frequency Division Multiplexing (OFDM), peut être utilisé pour du traitement radar par l'intermédiaire d'un choix judicieux de paramètres. Ceci permettra de réaliser simultanément des tâches radar et de communication de données. L'avantage d'utiliser la même forme d'onde pour les deux applications est d'assurer les fonctions en permanence des systèmes radar et de communication à la suite d'une meilleure utilisation du spectre utilisé et à l'intérieur de la même plateforme matérielle. La deuxième principale architecture est plus complexe et permet de traiter le cas où les entités radar et de communication sont séparés dans l'environnement mais avec une contrainte de partage complet ou partiel du spectre de fréquences. On étudie dans le cadre de cette thèse l'emplacement optimal des récepteurs

radar dans le but d'améliorer la précision de positionnement de la cible d'intérêt tout en réduisant les erreurs de mesures radars. Ceci est réalisé en minimisant les interférences causées par l'opération en simultanée du système de communication. Des meilleures performances en termes de réduction d'interférence au niveau radar ont été obtenues en appliquant la technique proposée d'emplacement des récepteurs, comparée à la technique basée uniquement sur la minimisation du geometric dilution of precision (GDOP).

Mots-clés: réseaux de capteurs radar, détection et positionnement de la cible, opération conjointe des systèmes radar et de communication.

MULTISTATIC RADAR OPTIMIZATION FOR RADAR SENSOR NETWORK APPLICATIONS

Moez BEN KILANI

ABSTRACT

The design of radar sensor networks (RSN) has undergone great advancements in recent years. In fact, this kind of system is characterized by a high degree of design flexibility due to the multiplicity of radar nodes and data fusion approaches. This thesis focuses on the development and analysis of RSN architectures to optimize target detection and positioning performances. A special focus is placed upon distributed (statistical) multiple-input multiple-output (MIMO) RSN systems, where spatial diversity could be leveraged to enhance radar target detection capabilities.

In the first part of this thesis, the spatial diversity is leveraged in conjunction with cognitive waveform selection and design techniques to quickly adapt to target scene variations in real time. In the second part, we investigate the impact of RSN geometry, particularly the placement of multistatic radar receivers, on target positioning accuracy. We develop a framework based on cognitive waveform selection in conjunction with adaptive receiver placement strategy to cope with time-varying target scattering characteristics and clutter distribution parameters in the dynamic radar scene. The proposed approach yields better target detection performance and positioning accuracy as compared with conventional methods based on static transmission or stationary multistatic radar topology.

The third part of this thesis examines joint radar and communication systems coexistence and operation via two possible architectures. In the first one, several communication nodes in a network operate separately in frequency. Each node leverages the multi-look diversity of the distributed system by activating radar processing on multiple received bistatic streams at each node level in addition to the pre-existing monostatic processing. This architecture is based on the fact that the communication signal, such as the Orthogonal Frequency Division Multiplexing (OFDM) waveform, could be well-suited for radar tasks if the proper waveform parameters are chosen so as to simultaneously perform communication and radar tasks. The advantage of using a joint waveform for both applications is a permanent availability of radar and communication functions via a better use of the occupied spectrum inside the same joint hardware platform. We then examine the second main architecture, which is more complex and deals with separate radar and communication entities with a partial or total spectrum sharing constraint. We investigate the optimum placement of radar receivers for better target positioning accuracy while reducing the radar measurement errors by minimizing the interference caused by simultaneous operation of the communication system. Better performance in terms of communication interference handling and suppression at the radar level, were obtained with the proposed placement approach of radar receivers compared to the geometric dilution of precision (GDOP)-only minimization metric.

Keywords: RSN, target detection and positioning, joint radar and communication.

TABLE OF CONTENTS

LIST OF TABLES

LIST OF FIGURES

Page

LIST OF ABREVIATIONS

RSN	Radar Sensor Networks
MSRSs	multisite radar systems
RF	Radio Frequency
MIMO	Multiple Input Multiple Output
RCS	Radar Cross Section
CR	Cognitive Radar
ULA	Uniform Linear Array
UWB	Ultra Wide Band
NP	Neyman Pearson
CRLB	Cramer-Rao Lower Bound
PCRB	Posterior Cramer-Rao Bound
TOA	Time of Arrival
UAV	Unmanned Aerial Vehicle
GDOP	Geometric Dilution of Precision
OFDM	Orthogonal Frequency Division Multiplexing
SAR	Synthetic Aperture Radar
RSSI	Received Signal Strength Indication
LFM	Linear Frequency Modulation
SNR	Signal to Noise Ratio
STAP	Space Time Adaptive Processing
BER	Bit Error Rate

SIMO	Single Input Multiple Output
GLRT	Generalized Likelihood Ratio Test
AMF	Adaptive Matched Filter
TDOA	Time difference of Arrival
AOA	Angle of Arrival
MLE	Maximum Likelihood Estimator
LS	Least Squares
BLUE	Best Linear Unbiased Estimator
KF	Kalman Filter
EKF	Extended Kalman Filter
CP	Circular Polarization
GPS	Global Positioning System
RFID	Radio-Frequency Identification
LP	Linear Polarization
ISM	Industrial Scientific and medical
LEE	Location Estimation Error
WSS	Wide Sense Stationary
PDF	Probability Density Function
AWGN	Additive White Gaussian Noise
SCNR	Signal-to-Clutter-plus-Noise Ratio
SINR	Signal-to-Interference-plus-Noise Ratio
AF	Ambiguity Function
PAPR	Peak to Average Power Ratio

LOS   Line of Sight

PPS   Pulse per Second

FFT   Fast Fourier Transform

BPSK   Binary Phase-Shift Keying

SSPARC   Shared Spectrum Access for Radar and Communications

CN   Complex Normal

CDF   Cumulative Distribution Function

INTRODUCTION

The word "radar" is an abbreviation of "radio detection and ranging". In general, radar systems use modulated waveforms and directive antennas to transmit and radiate electromagnetic energy into a specific volume in space to search for targets (Mahafza & Elsherbeni, 2005). Objects (targets) within the search volume will reflect portions of incident energy (radar returns or echoes) in the direction of the radar. These echoes are then processed to extract target information such as range, velocity, angular position and other target identifying characteristics (Mahafza & Elsherbeni, 2005).

Radar systems were initially developed for military applications, and can be classified as ground-based, airborne, spaceborne, or ship-based. Another type of radar systems classification could be applied based on the frequency band, the antenna type and the waveform. Today, radars are used to accomplish several missions ranging from weather, acquisition and search, tracking, fire control, early warning, terrain following and collision avoidance (Mahafza & Elsherbeni, 2005).

In recent years, the design and operation of radar systems have become increasingly complex. New radar systems should be able to offer more accuracy in terms of target detection in harsh indoor and outdoor environments, intelligently adjust their parameters to cope with dynamic and time-varying radar scenes and cooperate with existent wireless systems to ensure the operability of all systems at acceptable performance levels and under spectrum-sharing constraints.

0.1   Background on radar sensor networks

A radar sensor network (RSN) belongs to the category of multisite radar systems (MSRSs), named also: multi radar or netted radar systems. A RSN is defined as a radar system including several spatially separated transmitting, receiving and/or transmitting-receiving

facilities, where all the sensors' information on each target is fused and jointly processed (Chernyak, 1998).

From the above definition, any radar system that is principally composed of a multiplicity of transmitter and receiver elements, and which applies a fusion or joint processing of received target information, could be categorized as an RSN.

As shown in Figure 0.1, RSNs are classified based on several metrics:

- Type of target of interest: an active RSN is composed of at least one transmitting station that is, used to detect non-radiating targets, which are simply reflecting targets. By contrast, passive RSNs are principally based on only receiving stations and are used to detect radiating targets. A mixed passive-active RSN could also be used for both types of target detection;

- Degree of spatial coherence: RSN's spatial coherence is defined as its ability to maintain strong dependence between signal RF phases in separated stations, and consequently to make use of relevant information contained in those phase relations (Chernyak, 1998). It represents the phase stability of RSN equipment. It should be distinguished from the spatial coherence of signals at the inputs of the RSN receiving stations, which depends on baselengths between stations, signal wavelength, target size and fluctuations of the propagation medium characteristics (Chernyak, 1998).
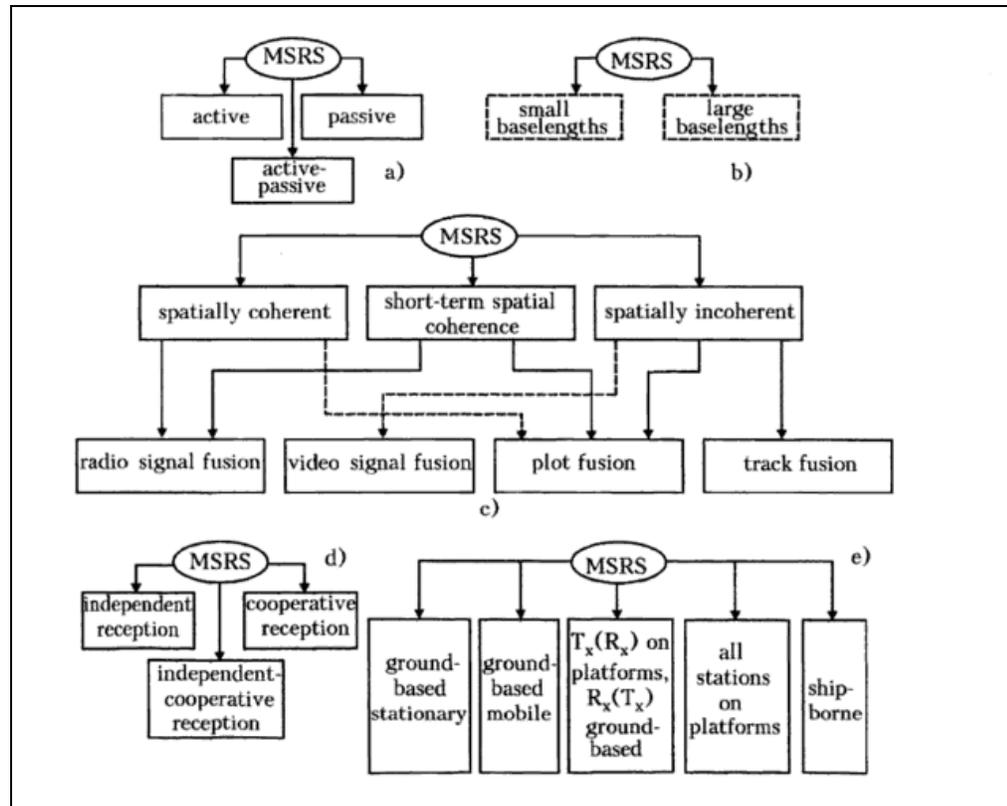
Figure 0.1 Classification of MSRS
Taken from Chernyak (1998)

Considering the spatial configuration of radar elements, four major classes of RSN could be defined:

- Distributed RSN: this type of RSN is composed of several monostatic radar stations that operate independently. Each radar station performs target radar processing individually and sends its decision to a cluster head (i.e., fusion center), which receives detection signals from different radar stations and make a final decision on target detection based on specific combination algorithms (Liang & Liang, 2011).

- Collocated (coherent) MIMO RSN: inspired by the development of the MIMO concept in communication system, the concept of MIMO radar has been initially introduced in

(Fishler et al., 2004). A MIMO radar simultaneously transmits multiple orthogonal waveforms by multiple antennas. A bank of matched filters is used at each receiver level in order to match the received signal to different orthogonal transmitted waveforms. The outputs of the matched filters are then processed for target detection. Collocated MIMO RSN are a type of MIMO radar sensors, wherein transmit and receive antennas are collocated. The signals received by different receivers are highly correlated due to proximity between the receivers. Thus, coherent processing could be enabled on collocated MIMO RSNs, leading to maximization of the processing gain. It was shown that collocated configuration can be used for beamforming application around targets of interest by proper choice of transmit waveforms and processing (Stoica, Li & Xie, 2007); (Li & Stoica, 1998). In addition, the collocated MIMO configuration offers accurate parameters estimation (Xu, Li, Stoica &, 2008); (Li, Stoica & Xu, 2007), high resolution, high degrees of freedom (Bliss & Forsythe, 2003), and better sensitivity (Forsythe, Bliss & Fawcett, 2004) to ground-moving targets.

- Distributed (also called statistical) MIMO RSN: unlike coherent MIMO RSN, which counts on coherent processing gain due to correlated responses received at the closely-spaced receivers, a statistical MIMO radar, initially introduced in (Fishler et al., 2006), leverages the diversity of uncorrelated target scattering responses received at different receivers. In real scenarios, a radar target is composed of several point scatterers. Small fluctuations at the response of the point scatterers and their number result in variation of the target Radar Cross Section (RCS). This variation can cause target fades, which is a synonym of radar performance degradation (since closely-spaced antenna systems are more sensitive to target fades). In the case of distributed (statistical) MIMO radar, spatial separation between antenna elements at the transmitter and at the receiver ensure independent target scattering responses at different receiver element. This improves the radar performance in a different manner by leveraging the spatial diversity offered by the system (since target angular spread is manifested).
- Netted radar sensor systems (Baker & Hume, 2003); (Hume & Baker, 2001): these are a general form of RSN, wherein each node can operate monostatically and bistatically with

other nodes of the network. It can be seen from the definition of "netted radar" concept that these systems are somewhat like combination of the distributed RSN and the MIMO RSN types.

Regarding the fusion approach used in radar sensor networks, the detection could either be centralized or distributed. In centralized detection, the signals received at different stations are directly fed to the fusion center for joint processing (although a few basic operations could be carried out at each station level, such as linear filtering). In distributed detection, the radar processing, including thresholding and parameter estimation, is carried out at each station level. Then only useful information such as the presence or absence of target, is fed to the fusion center, where a final decision is made as a result of combining the preliminary decisions sent by different stations.

RSN presents a variety to advantages compared to monostatic radar or a collection of non-integrated radars, due to its information fusion and spatial diversity capabilities. The main advantages of RSN are improved capabilities of target detection and parameters estimation, classification and location capabilities, and extended coverage and availability of spatial diversity for distributed systems. It can offer a counter to stealth technology and can improve the system countermeasure and jamming resistance capabilities. In addition, RSN systems may offer power gain benefits, especially in the case of cooperative signal reception and fusion.

Despite the great number of advantages that RSN systems offer, many shortcomings are also present due to the nature of these systems. One of the main drawbacks is the increased cost and complexity compared to single monostatic or bistatic radars, and the increased demand on data processors and computer systems. In addition, a high level of synchronization is required for basic RSN operation, because there is a minimum requirement of frequency and time synchronization for non-coherent networks in addition to the phase synchronization required in the case of coherent networks.

RSN systems are mainly used in military applications (Chernyak, 1998), although there have been increasingly important civil applications, chiefly for marine, air navigation and remote sensing purposes (Chernyak, 1998). Depending on the type of application, ground-based, air, space, or shipborne RSNs could be used with or without stations mobility.

0.2 Recent advances and research scope

The purpose of this section is to highlight recent advances in the design of radar sensor networks and to describe the research scope of this thesis. In particular, this thesis focuses on three main domains:

- Radar waveform selection and design approaches for target detection in RSN;

- Receiver placement optimization strategies for target positioning in RSN;

- Joint radar and communication system design.

0.2.1 Radar waveform selection and design approaches for target detection in RSNs

Adaptive waveform selection and design in radar has always been a major part of cognitive radar (CR) (Haykin, 2006), which aims to optimize traditional radar performances within a dynamic environment. The concept is essentially based on continuous learning through radar interactions with its surrounding world, and also from iterative feedback from the receiver to the transmitter, which facilitates the adaptation of radar transmission parameters in real time. The transmitter's reaction agility to the updated information coming from the feedback loop has a crucial impact on the ability of the CR to intelligently adapt to the environment.

Figure 0.2 shows the block diagram of CR architecture (Haykin, 2006). The transmitter begins by illuminating the environment using an initial waveform. The radar returns generated by the environment are fed into two functional blocks: the radar-scene analyzer

and a Bayesian target-tracker. The tracker makes decisions on the possible presence of targets on a continuous time basis (detection through tracking), considering information provided by the radar-scene analyzer. The transmitter, in turn, illuminates the environment considering the decisions made on possible targets, which are fed back to it by the receiver. The entire cycle is then repeated iteratively.

It should be noted that the continuous learning about the environment and the feedback loop between radar receiver and transmitter units allow the transmitter to intelligently adjust its illumination parameters to cope with dynamic changes in the environment. Such intelligent illumination is what distinguishes a cognitive radar from a simple adaptive radar (Haykin, 2006); in the latter, intelligence is limited to reception strategies without being integrated into the transmitter side.
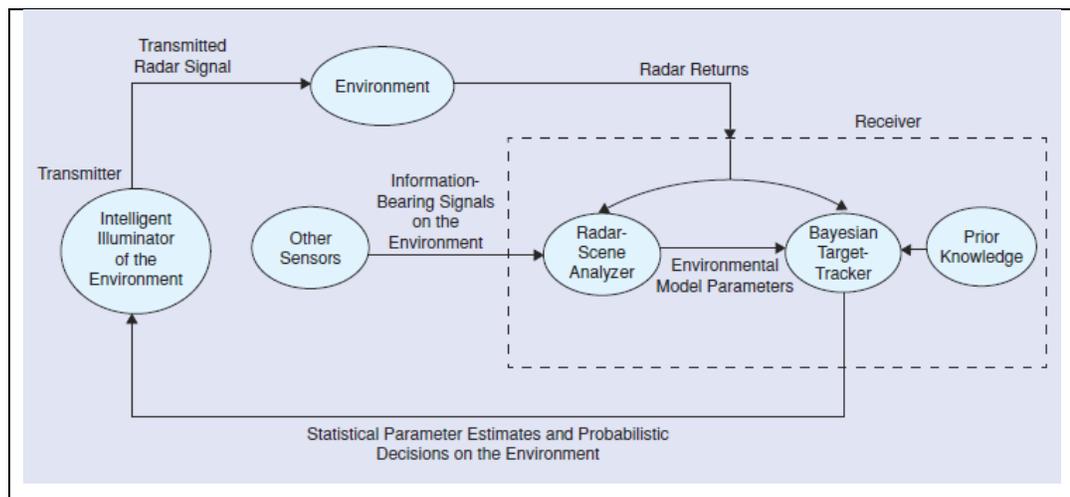
Figure 0.2 Block Diagram of CR Architecture
Taken from Haykin (2006)

The topic of radar waveform optimization has been treated following several optimization criteria. In (Pillai et al., 2000), a joint design of the transmit radar pulse and the receiver impulse response was proposed with the goal of maximizing the signal to interference plus noise (SINR) in presence of clutter and noise. A similar joint design was investigated in (Garren et al., 2001) to maximize either the probability of target detection or the probability

of correct identification between two target classes. The optimal waveform design based on maximization of SINR has also been applied in the context of sensing through the wall application (Estephan et al., 2010).

An information-theoretic approach was initially proposed in (Bell., 1993). The idea is to maximize the mutual information between the extended target impulse response and the received radar returns. Waveform design approaches based on either information theory or SINR maximization have been integrated with a sequential testing framework that controls when hard decisions on target classes may be made with adequate confidence and sufficient understanding of propagation channel (Goodman et al., 2007). An extension of the information theoretic approach presented in (Goodman et al., 2007) to the signal-dependent clutter problem was investigated in (Romero et al., 2007).

The topic of waveform design in a RSN context has recently drawn greater attention from radar researchers. In (Kay et al., 2009), the optimal Neyman-Pearson (NP) detector was derived in the context of multistatic radar. Based on this work, a divergence criterion was then proposed as a metric to find the optimal waveform for extended target detection in the presence of extended clutter, interference, and noise. In (Zhang et al., 2010), the author proposes an algorithm for adaptively designing orthogonal frequency hopping waveforms based on range and velocity ambiguity function in the context of separated transmit/receive ULA_MIMO radar. Several MIMO radar transmit beampattern design problems such as beampattern matching design and minimum side lobe beampattern design, have been considered in (Stoica et al., 2007). The idea is to design the covariance matrix of the probing signal vector to achieve specific goals, especially to minimize the cross-correlation of the signals reflected back to the radar by the targets of interest, or, in addition, to maximize the power around the locations of targets of interest. Other papers (Yang et al., 2006); (Jajamovich et al., 2010); (Yang et al., 2009); (Song et al., 2010) extended the approach presented in (Bell., 1993) by using the mutual information between the random target response and the reflected signal as a waveform optimization criterion in MIMO radar. An MI-based chaotic UWB-MIMO waveform selection mechanism for multitarget detection and

classification purposes was proposed in (Nijsure et al., 2015) in the context of distributed MIMO radar. The optimal waveform was selected within a set of chaos-based UWB waveforms with the objective of maximizing the statistical similarity between successive target echoes for better target signature estimation. A similar idea was proposed in (Chen et al., 2013), wherein a two-stage information-theoretic design was investigated with emphasis on phase-coded UWB Gaussian pulses as applied radar waveform.

Research Scope

In a multistatic radar scenario composed of a distributed transmitter and several receivers, the spatial diversity offered by the radar architecture should be leveraged for better extended target detection, especially in the presence of signal-dependent interference (clutter) and noise. If this multisatic radar scenario is empowered with a cognitive capability, it could enhance radar detection performance in a constantly changing environment. The cognitive approach is applied by enabling permanent interactions of the radar with its surrounding world, as well as iterative feedback from the receivers to the transmitter. The feedback contains updated information regarding the target impulse response, clutter and the noise covariance matrix.

Data acquired by the transmitter could be leveraged for better waveform design to fit the real-time radar scene. In this thesis, chapter 2 extends the relevant works on cognitive waveform design in a multistatic radar context. The aim is a better detection of an extended target in the context of a highly dynamic harsh environment. In this chapter, the maximization objective of the mutistatic probability of detection is used to design and select the radar waveform for better extended target detection. The maximization algorithm takes into consideration the constantly changing environment parameters for adaptive choice of radar waveform.

0.2.2   Receiver placement optimization strategies for target positioning in RSN

The topic of receiver placement optimization in the context of passive RSNs has recently been treated with special attention in the literature. The pioneering works in (Kaplan, 2006); (Kaplan, 2006) have proposed global and local node selection mechanisms for localization in the general case of distributed sensor networks. In (Anastasio et al., 2010), the CRLB for target positioning estimation was derived and then used to select the broadcast transmitters and receiver locations that offer the best accuracy in a multistatic passive radar context. The derived CRLB expression includes the effect of a sensor probability of detection that is lower than unity. A similar scenario of passive multistatic radar-based two transmitters of opportunity and one receiver was treated in (Gumiero et al., 2011) in a real air traffic context. The selection of radar node locations is controlled by a maximization of the 2D target positioning accuracy. In (Nguyen et al., 2014), a joint adaptive selection of transmitted waveform and receiver placement in a multistatic radar with moving receiver's context was proposed. The joint approach aims at minimizing the trace of the target tracking error covariance matrix. The proposed approach does not account for extended target considerations. In addition, the environment is assumed to be clutter-free. An interesting approach was recently presented in (Nguyen et al., 2016), where the optimum multistatic radar geometry of one transmitter and several receivers was analyzed from a 2D TOA target localization perspective. The proposed search algorithm for better radar geometry is based on minimization of the area of the estimation confidence region equivalent to maximization of the determinant of a Fisher information matrix. The output of the proposed algorithm is the optimal angular separation between sensors instead of their absolute positions. A UAV case study was used to validate the proposed algorithm, where each UAV was deployed as a moving receiver platform. A similar work was presented in (Nguyen et al., 2015), which considers the Doppler shift information in the objective function optimization instead of TOA information.

Recent work in (Yang et al., 2015) in particular focuses upon the choice of multistatic radar antenna placement that optimizes both detection capability and localization accuracy. The

aforementioned optimization goal is achieved by maximizing a radar coverage ratio and an average GDOP of the surveillance region. A multi-objective particle swarm optimization algorithm was devised in order to resolve the high dimensionality constraint of the original multi-objectives problem. A global optimization based on genetic algorithms was used to search for the best multistatic radar sensor placement that minimizes the error on target range and velocity estimation (Lei et al., 2012). The multistatic CRLBs for range and velocity estimation were derived for this problem.

A similar approach based on genetic algorithm but minimizing the target localization error instead of radar parameters (range, velocity) estimation was proposed in (Lackpour et al., 2016). In (Bradaric et al., 2006); (Bradaric et al., 2009), the multistatic radar ambiguity function was defined and used to relate the radar performance measures to systems parameters such as radar geometry and waveforms. More general expressions of the multistatic ambiguity functions were derived in (Derham et al., 2010) to account for spatial coherence of target fluctuations observed at each receiver of the multistatic radar. Similarly, these expressions were used to link the ambiguity in target position and velocity to the choice of transmitted waveform and employed multistatic radar topology. In fact, the derived expression of the multistatic ambiguity function in (Derham et al., 2010) depends on the optimal multistatic detector expressions, which in turn depend on spatial coherence of the multistatic radar geometry.

Two deployment strategies: hexagonal deployment strategy (HDS) and diamond deployment strategy (DDS) were investigated in order to deploy a distributed radar sensor network for multi-target detection (Yang et al., 2014). A fusion center was used to make a final detection decision after receiving local decisions from different radar nodes. It has been shown that compared with random deployment strategy (RDS), the proposed HDS and DDS strategies can improve the detection probability while being energy efficient (Yang et al., 2014). The concept of operating RSN in subsets or clustering was introduced in (Godrich et al., 2012). The goal was to identify the optimal sets of nodes that deliver the required localization estimation performance while minimizing the number of required radar nodes, which results

in better radar resources management in terms of central processing loads and communication link needs (Godrich et al., 2012).

In (Tharmarasa, 2007), an iterative local search was applied to minimize the PCRB and find the subset of antennas to be employed for tracking multiple targets in the presence of clutter. In (He et al., 2010), a search for the best antenna placement in a distributed MIMO radar context was analyzed in order to minimize the CRB of the velocity estimation error. The work in (Godrich et al., 2010) focuses on the analysis of relations between sensor locations, target location and localization accuracy by deriving the CRLB for target localization accuracy for both coherent and noncoherent processing in a widely distributed MIMO radar context.

A notion of random sensor network was proposed in (Daher & Adve, 2007). The proposed system is a trade-off between two types of detection: distributed detection using several distributed monostatic radar sensors and centralized detection using collocated antennas, specifically where each radar sensor is equipped with an array of collocated antennas. A geometry design trade-off between spatial diversity and interference cancellation has also been analyzed (Daher & Adve, 2007).

Research Scope

In addition to the transmitted waveform, the geometry of RSN and mutistatic radars has a direct impact on radar detection performance and target accuracy. The degree of spatial coherence of target returns observed at different radar receivers has a major effect on the choice of the signal processing to be used for target parameters estimation, and therefore on the overall system performance.

Geometric dilution of precision (GDOP) is a metric initially used in satellite navigation to characterize the impact of system geometry on positioning accuracy (Yarlagadda et al., 2000). Recently, the GDOP metric has been applied in the general context of indoor and

outdoor wireless sensor networks (Sharp et al., 2009); (Torrieri, 1984); (Sharp et al., 2012). In chapter 2, we extend the multistatic radar receiver optimization placement literature to derive the expression of a GDOP metric based on the multiplicity of bistatic range and Doppler expressions in the multistatic radar context in addition to the current target position estimate generated by a LS geolocation process. The derived expression is then used to search for the suitable radar receivers' placement that minimizes the target positioning estimation error. The target positioning error could be high if the multistatic radar receivers are placed randomly. Our proposed approach in chapter 2 attempts to find the best multistatic radar geometry in order to enhance target positioning accuracy.

Chapter 4 deals with the case of coexistence between radar and communication systems with a challenge of spectrum sharing. It presents and analyzes a new adaptive radar receivers placement mechanism that jointly maximizes the signal to clutter plus noise ratio (SCNR) of each communication transmitter-radar receiver channel, while minimizing the GDOP. The goal of our proposed approach is to minimize the impact of communication interference on the performance of the radar system resulting in less radar measurement errors, while enhancing the target positioning accuracy.

0.2.3   Joint radar and communication system design

In the past, radar and communication systems were treated as two separate fields. The goal of a communication system in general is to achieve the best data transfer in a noisy channel with power and bandwidth constraints. From a radar system of view, the main goal is the detection of targets of interest and estimation of their parameters with minimum errors in the presence of clutter and noise. Recently, the joint operation of radar and communication has started to become a real requirement due to a variety of constraints, especially: the increasing demand on spectrum resources from both sides in addition to the increasing similarities in carrier frequencies, hardware and software architectures and resources.

In the research literature, the topic of radar and communication coexistence has been treated in different ways depending on the deployment scenario and application. We can highlight three main categories of joint radar and communication operation. The first one is related to the presence of wireless nodes, where both communication and radar functionalities are enabled at each node level (Sturm & Wiesbeck, 2010); (Garmatyuk et al., 2007); (Garmatyuk et al., 2011); (Nijsure et al., 2012). The proof of concept of OFDM capabilities for use as radar waveform has enabled simultaneous use of the same OFDM communication waveform for monostatic radar detection in several areas: an intelligent transportation context (Sturm & Wiesbeck, 2010), SAR imaging applications (Garmatyuk et al., 2007); (Garmatyuk et al., 2011) and cognitive radar radio networks for the purpose of safety (Nijsure et al., 2012).

The second category of joint radar and communication operation focuses on the incorporation of communication as secondary to the primary radar function as reported in several papers (Surrender & Narayanan, 2011); (Euziere et al., 2014); (Hassanien et al., 2015); (Blunt & Yantham, 2007). An OFDM communication signal is inserted within a notched band-limited radar noise signal in (Surrender & Narayanan, 2011) for a secure communication network between multi-site radars. Side lobe control is used to enable a communication link without interference with the radar function in the main lobe (Euziere et al., 2014). The side lobe control technique in tandem with waveform diversity was proposed in (Hassanien et al., 2015).

The third main category of joint radar and communication operation consists of separate communication and radar systems operation, wherein each system has its own nodes and architecture but coexistence is mandatory because both systems are deployed in the same environment with a partial or total spectrum sharing constraint (Jacyna et al., 2016); (Turlapaty & Jin, 2014). From this perspective, works like (Jacyna et al., 2016); (Richmond et al., 2016); (Bliss, 2014) focused on investigating the joint radar and communications performance bounds for spectrum sharing while ensuring each system achieves its mission objectives. These theoretical bounds studies resulted in several waveform design approaches that mitigate interference between systems while keeping the performance of each one at

acceptable level (Chiriyath et al., 2015); (Paul et al., 2016); (Guerci et al., 2015). Another interesting approach to the spectral design of separate radar and communication waveforms was investigated in (Turlapaty & Jin, 2014) and is based on maximization of the mutual information of the joint system.

Research Scope

There are many challenges involved in the design of joint communication and radar systems. The traditional approach has been to separate both systems operation in time, space or frequency band. However, the increasing demand on spectrum resources and simultaneous operation demands cooperation between the two systems for the purpose of better resource sharing and utilization. In the case of full control over both systems' architecture, a joint operation can be enabled at each node scale, where the same transmitted waveform could be used for communication with other nodes and simultaneously leveraged for monostatic radar operation. Such an approach requires the waveform to be suitable for both radar and communication operation as mentioned above in the description of the first category of joint radar and communication operation. Additionally, simultaneous transmission by multiple nodes should be handled via standard collision avoidance techniques in communication networks, in order to avoid any interference between them.

The third category, in which separate and uncontrolled radar and communication architectures are deployed in the environment, is even more challenging. In this case, cooperative spectrum sharing between both systems is required to ensure proper operation of each system with acceptable performance in the presence of each other.

Chapter 3 of this thesis investigates the first category of joint radar and communication operation, where several communication nodes in a network operate separately in frequency and are able to simultaneously perform radar tasks. A novel architecture at node scale has been proposed to leverage the multi-look diversity of the distributed system in order to

activate radar processing on multiple received bistatic streams at each node level in addition to the pre-existing monostatic processing.

Chapter 4 focuses on the third category of joint radar and communication operation, where separate point-to-point communication and multistatic radar systems are present with a partial or total spectrum sharing constraint. This chapter investigates the optimum placement of radar receivers in order to optimize target positioning accuracy while minimizing the interference caused by the simultaneous operation of the communication system.

0.3   Motivation for RSN operation

The performance of radar systems is dictated by target scintillation characteristics (Fishler et al., 2006). Targets are complex bodies composed of many scatterers. The target's distance to the radar and its orientation determines the amount of energy reflected by the scatterers composing the target. Any movement of the target causes changes in range and orientation, which result in variation of the energy reflected by the target and captured by the radar receiver platform. The scintillations are responsible for signal fading, which can cause a large degradation in radar detection capabilities (Skolnik, 2001); (Trees, 1968).

The only way to mitigate the effect of target fading is to maximize the energy received from the target. One well-known approach is to maximize the system coherent processing gain by deploying an array of radar antenna elements for both radar transmission and reception functionalities. The array is composed of closely-spaced antenna elements in order to guarantee spatial coherence between signals received at radar receiver inputs, which enables adaptive array and beamforming techniques. This type of system is called collocated (coherent) MIMO RSN and has been described in section 0.1 of this chapter.

Another way to mitigate the target fading caused by target RCS scintillations is to deploy widely separated transmitter and receiver elements. This allow the transceiver units to view the target from distinct aspect angles and thus exploit the spatial diversity of the RSN channels. Orthogonal waveforms are to be used in the case of multiple transmitter elements.

As the transmitting and receiving transmitting antenna elements are far from each other relative to target distance, the target RCSs are independent random variables for different transmit-receive paths. This spatial diversity, in addition to waveform diversity, can be leveraged for better detection performance (Fishler et al., 2006). This type of RSN is known as distributed (also called statistical) MIMO RSN, as details in section 1.1. The main advantage of this system is that the average received energy is approximately constant across all the independent radar transmit-received paths, i.e., it does not fade as in conventional systems (Fishler et al., 2006). It has been shown that the spatial diversity gain outweighs the coherent processing gain in several scenarios (Fishler et al., 2006) where target fading can significantly degrade the coherent processing-based systems.

0.4 Major contributions and thesis outline

In this thesis, we develop and analyze RSN architectures to optimize target detection and parameters estimation in the context of dynamic radar scene with mobile extended target and non-target scatterers. The aim of this work is to leverage the advantages offered by RSN architectures to improve target detection and positioning. There is a special focus on distributed (statistical) MIMO RSN systems, wherein spatial diversity could be utilized in conjunction with cognitive waveform selection and design techniques for optimization of target detection.

We also analyze the impact of a distributed MIMO RSN geometry, specifically a multistatic radar with multiple receiver stations on target positioning accuracy. We develop a cognitive framework based on cognitive waveform selection in conjunction with adaptive receiver placement strategy, in order to cope with time-varying target scattering characteristics and clutter distribution parameters in the dynamic radar scene and optimize the extended target detection and positioning. Finally, we investigate the RSN systems with extended functionality by developing joint communication and radar systems.

The Chapters of this thesis are organized as follows:

- **Chapter 1** presents a detailed literature survey covering the research ideas discussed in section 0.2. Special attention is paid to recent advances in radar sensor networks, joint radar and communication systems and target geolocation and tracking.

- **Chapter 2** develops and analyzes a cognitive waveform and receiver selection mechanism for multistatic radar. In this work, a cognitive selection mechanism of the radar waveform is enabled based on real-time target and clutter scene parameters estimation. In conjunction, an adaptive receiver allocation / selection is proposed that aims to enhance target positioning accuracy. Simulation results demonstrate the ability of the proposed approach to optimize target detection performance and positioning accuracy as compared to conventional methods that are based on static transmission or the topology of stationary multistatic receivers.

- **Chapter 3** investigates the first category of joint radar and communication operation, wherein several communication nodes in a network operate separately in frequency. A novel architecture at each node level is proposed to leverage the multi-look diversity of the distributed system by activating radar processing on multiple received bistatic streams at each node level, in addition to the pre-existing monostatic processing. The demonstration of the OFDM ability to be used as a radar waveform has allowed each network node to simultaneously employ the same OFDM communication waveform for monostatic and bistatic radar functionalities.

- **Chapter 4** focuses on the third type of joint radar and communication operation, wherein separate communication and multistatic radar systems are present with a partial or total spectrum sharing constraint. This chapter investigates the optimum placement of radar receivers in order to optimize target positioning accuracy while minimizing interference caused by simultaneously operating the communication system.

- Finally, we conclude the thesis and we discuss potential future works based on this research.

0.5   Publications

1. Ben-Kilani, M., Raymond, A. J., Gagnon, F., Gagnon, G., & Lavoie, P. (2014, March). *RSSI-based indoor tracking using the extended Kalman filter and circularly polarized antennas*. Paper presented at the Workshop on Positioning, Navigation and Communication, Dresden, Germany.

2. Ben-Kilani, M., Nijsure, Y., Gagnon, G., Kaddoum, G., & Gagnon, F. (2016). Cognitive waveform and receiver selection mechanism for multistatic radar. *IET Radar, Sonar & Navigation, 10(2), 417-425.*

3. Ben-Kilani, M., Gagnon, G., & Gagnon, F. (2018). Multistatic Radar Placement Optimization for Cooperative Radar-Communication Systems (submitted to *IEEE Communications Letters).*

CHAPTER 1

LITERATURE SURVEY

1.1   Introduction

In the general introduction, we introduced the main objective of this thesis, which is to propose novel approaches in the design of Radar Sensor Networks. In section 0.2, the link between the existing research ideas and the contribution of this thesis was presented. We provide in this chapter a detailed survey of the literature on these research ideas. Specifically, we discuss recent advances in radar sensor networks, target geolocation and joint radar and communication systems. This will help underline the main contributions of this thesis, which are as follows: an approach to the cognitive waveform design and selection in the particular context of multistatic radar, a radar receiver placement optimization strategy for target positioning and a proposed method of joint radar and communication operation in the context of variable degrees of both systems architecture control and spectrum sharing resources.

Section 1.3 of this chapter shares the same review of literature as a publication by the same author. Some passages are taken directly from (Ben-Kilani et al., 2014), with the addition of other information that applies to this thesis.

1.2   Radar sensor networks

Radar sensor networks are the general framework of a radar composed of several transmitting and receiving stations, where information of each target from all sensors is fused and jointly processed (Chernyak, 1998). From this general definition, RSN could have several variants such as the system geometry and the target data fusion approach. These variants justify the importance of RSN for modern radar applications, since the system flexibility could be leveraged to fit any radar application requirements. Indeed, the geometry

of a RSN, the number of radar stations, the transmission parameters and the fusion of radar data can be adapted to suit any specific application and radar scene. It has been shown in subsection 1.1 that four main categories of RSN may be identified based on the radar network geometry, data fusion technique, and degree of cooperation between different radar stations. In this subsection, we describe recent advances in different RSN categories presented in the literature.

A conventional distributed RSN is composed of several monostatic radar stations that operate independently. Each monostatic station considers the other stations to be sources of interference, and a cluster head is used to combine different decisions/detected signals sent by the stations in order to make a final decision on target detection (Liang & Liang, 2011). The challenge is to come up with a waveform design in distributed RSNs that will reduce inter-stations interference. Orthogonal LFM waveforms could be used for this purpose (Liang, 2006) in conjunction with a RAKE structure for waveform diversity combining in the context of automatic target recognition (ATR). A similar structure, except with constant frequency (CF) pulse waveform design instead of LFM waveforms, has been proposed in (Liang, 2006). Information theory is used to design the transmitted waveform for extended detection in RSNs (Xu & Liang, 2010). An algorithm for radar-to-radar interference cancellation in distributed RSNs was investigated in (Wang & Shao, 2014). Spatial-temporal frequency diversity techniques were also investigated for better target detection and clutter suppression in a RSN context (Ly & Liang, 2009).

An optimal fusion scheme in distributed RSNs as well as a power control scheme in MIMO-RSNs, were analyzed in flat fading channels and compared in terms of target detection performance (Liu & Liang, 2014). In (Liang & Liang, 2011), orthogonal waveforms and spatial diversity were studied under the condition of the Doppler shift in both coherent and non-coherent distributed RSNs. It has been shown that coherent RSNs provide better performance than non-coherent RSNs in the case of the same SNR and the same Doppler shift. A selection combiner was used, which chooses the radar branch with the maximum SNR. The work in (Daher & Adve, 2010) analyzes the trade-off between distributed

detection using several distributed monostatic radar sensors and centralized detection using collocated antennas, where each radar sensor is equipped with an array of collocated antennas. A notion of diversity order in a general distributed RSN context was defined in contrast with the asymptotically high signal-to-noise ratio (SNR) definition in wireless communications, as the slope of probability of detection (P_D) versus the SNR curve at $P_D = 0.5$. Test statistics were characterized for the distributed system and the diversity order was determined for various fusion rules (Daher & Adve, 2010). In (Shu & Liang, 2007) different fusion techniques used in a distributed RSN were analyzed in the presence of fluctuating multi-targets.

The sensing capability of a distributed MIMO RSN for target detection and localization has been analyzed in terms of detection probability (Sun et al., 2012). Detection performance of the radar network was analyzed under both centralized and decentralized detection strategies. Target localization error performance was analyzed in terms of CRLB.

The concept of MIMO was first discovered in the field of communication. Then it has been recently explored in the field of sensor and radar systems (Fishler et al., 2004). Unlike the standard phased array radar that transmits a single waveform at a time, MIMO radar transmits multiple orthogonal waveforms via multiple antennas simultaneously. These waveforms are extracted by a bank of matched filters at the receiver, and then all the matched filter outputs are combined to obtain the information of interest (Fishler et al., 2004); (Stoica et al., 2007). As detailed in the general introduction, two main categories of MIMO radars are distinguished in the literature, distributed (statistical) MIMO RSNs and collocated (coherent) MIMO RSNs.

In collocated MIMO RSN, the distances between transmitting antennas (and likewise between receiving antennas) are small enough relative to the distance between the target and the radar stations such that the target RCS is identical for all transmitting paths. Thus, the signals received by different receivers are highly correlated due to proximity and coherent processing could be enabled so as to maximize the processing gain. It has been shown that

collocated configuration can be used for beamforming application around targets of interest by proper choice of transmit waveforms and processing (Stoica et al., 2007); (Li & Stoica, 2007); (Robey et al., 2004); (Xu et al., 2007). In addition, the collocated MIMO configuration offers accurate parameters estimation (Xu et al., 2008), (Li et al., 2007), high resolution (Li et al., 2008), high degrees of freedom (Bliss & Forsythe, 2003) and better sensitivity (Forsythe et al., 2004) to ground-moving targets. Recent advances in collocated MIMO radars focus on the waveform design and optimization techniques for better waveform orthogonality (Fuhrmann & Antonio, 2008); (Ahmed & Alouini, 2014), target detection optimization (Maio et al., 2008); (Wang et al., 2011); (Wang et al., 2013), the specific case of constant-modulus waveforms (Maio et al., 2008) and a frequency-hopping scheme (Chen & Vaidyanathan, 2008). One approach to waveform design in the presence of clutter is presented in (Liu et al., 2016) and using prior information of the extended target and clutter is investigated in (Chen & Vaidyanathan, 2009). An imperfect clutter knowledge condition has been considered in waveform design in the context of MIMO-STAP (Wang et al., 2014). The design of a MIMO transmitter with a frequency diverse array for improved target and angle estimation was investigated in (Gao et al., 2016).

Distributed (statistical) MIMO RSN systems have been widely investigated in the literature. The key point in this radar network architecture is that sensors at both the transmitter and the receiver of the radar are separated such that they experience a target angular spread, which is defined as the target RCS variability as a function of the aspect ratio (Fishler et al., 2006). Consequently, the spatial diversity offered by independent target scattering responses at different receiver elements can be leveraged to combat target fades caused by variation in target range and orientation and therefore to improve radar detection capabilities. The pioneering work in (Fishler et al., 2006) investigated the detection performance of statistical MIMO RSNs through the analysis of optimal detector statistics. The performances of both statistical MIMO RSNs and conventional phased-array radars were compared. It has been demonstrated that statistical MIMO RSNs outperform the conventional phased-array radars whenever the probability of detection is at a reasonable level above 80% (Fishler et al., 2006). The superiority of MIMO radars over the conventional phased-array radars in terms of

other aspects such as lower range, location and angle of arrival as well as lower Doppler estimation errors has been demonstrated in related works (Fishler et al., 2006); (Scharrenbroich & Zatman, 2014).

The particular case of SIMO radar also called multistatic radar has been investigated in (Kay et al., 2009). The optimal Neyman-Pearson (NP) detector was derived for a general case of multiple distance separated radar receivers. Based on that, a divergence criterion was then proposed as a metric for finding the optimal waveform for extended target detection in the presence of extended clutter, interference and noise. A generalized canonical correlation detector for multistatic passive detection was proposed in (Liu & Himed, 2014). It has been shown that the proposed detector performs better than the generalized likelihood ratio test (GLRT) detector only in the case of known noise statistics (Liu & Himed, 2014). In (Bruyere & Goodman, 2008), the likelihood ratio test (LRT) for multistatic detection is derived for the case where each sensor platform is a coherent space-time radar. It has been shown that when clutter is considered, the diversity benefit of a MIMO radar is strongly dependent on system geometry. The relationship between geometry and diversity gain for multistatic airborne space-time radar was analyzed in the context of centralized and decentralized detection (Bruyere & Goodman, 2008).

The work in (Bruyere & Goodman, 2008) was extended to include a comparative study between the adaptive matched filter (AMF) detector and the GLRT detector in (Goodman & Bruyere, 2007) for multistatic space-time radar, where each sensor platform has a coherent multi-channel array. It is shown that the GLRT outperforms AMF in the case of unknown noise and target scattering statistics. Both detectors exhibit better performances with an increasing number of receiver platforms (Goodman & Bruyere, 2007).

In (Nelms & Collins, 2011), a multistatic UWB random noise radar network architecture was investigated. The system was based on four monostatic noise radar stations, where bistatic processing was also enabled between stations. The sixteen available signal channels were processed in a fusion center to extract highly resolved imagery of the target scene (Nelms &

Collins, 2011). As detailed in the general introduction, this type of RSN where each node can operate monostatically and/or bistatically with other nodes of the network is also known as netted radar system (Baker & Hume, 2003), (Hume & Baker, 2001). If orthogonal waveforms are used at different transmitters and coherent sensing is enabled in the network (i.e., the radar sensors comprising the network have a common and highly precise shared knowledge of time and space), each node of the netted radar system will be able to simultaneously operate in both monostatic and multistatic modes (Deng, 2004); (Deng, 2012). In the case of a non-coherent network, each radar node will operate only in monostatic mode without taking into consideration the bistatic data coming from the other remote nodes, which corresponds to a distributed RSN case.

In chapter 2, we investigate a cognitive waveform and receiver selection mechanism in the context of multistatic radar. We show how the spatial diversity offered by the RSN could be leveraged for improvement of target detection and positioning accuracy via proper cognitive waveform design and receiver placement that enable quick adaptation to the dynamically changing environment.

1.3   Target geolocation

1.3.1   Overview on target geolocation and tracking in RSN

Wireless positioning systems have received a great deal of attention in recent years. Various types of wireless sensor networks have been investigated for different types of sensors (radio-frequency, infrared, optical, inertial, etc.) and estimation algorithms (Fink & Beikirch, 2011). For radio-frequency-based systems, several signal metrics, such as time of flight measurements (TOA, TDOA) and direction of arrival measurements (AoA), were detailed in (Fink & Pahlavan, 2004); (Liu et al., 2007). Systems based on received signal strength indicators (RSSI) have also been studied extensively, as they have a comparatively low cost and can leverage pre-existing infrastructure, such as Wi-Fi and Bluetooth networks (Laitinen et al., 2007).

Wireless positioning systems based on radar technology have recently attracted more and more attention of radar researchers. Target localization based on both coherent and non-coherent (widely separated antennas) MIMO radar was investigated in (Kohler et al., 2009). It was shown that both cases benefit from a MIMO gain that is directly proportional to the product of the number of transmitting and receiving radars (Kohler et al., 2009).

Distributed MIMO radars can directly or indirectly estimate the target location and velocity (Du & Wei, 2014); (Liang et al., 2016). The direct method is achieved by collecting all the observations of receivers and searching in the possible grid (Du & Wei, 2014); (Liang et al., 2016). Although direct methods, such as maximum likelihood estimator (MLE) (Godrich et al., 2010); (Niu et al., 2012); (He et al., 2010) and sparse recovery (Gogineni & Nehorai, 2011), provide asymptotically optimal solutions, their computational complexity is impractically high due to high dimensional search and the large number of grid points. On the other hand, the localization can be performed indirectly, where the system can estimate the radar time delays and Doppler shifts, which are then used to compute the target position and velocity (Du & Wei, 2014). Several approaches, such as the best linear unbiased estimator (BLUE) method (Kohler et al., 2009); (Godrich et al., 2010) and the Least Squares (LS) method (Dianat et al., 2013) could be used for target indirect localization.

Many recent studies like (Liang et al., 2016); (Yan & Chun, 2016); (Wanchun et al., 2017); and (Noroozi & Sebt, 2016) focus on the improving target localization accuracy in distributed coherent and non-coherent MIMO RSN scenarios. The goal is to leverage the diversity information for better target localization accuracy by taking into consideration time synchronization errors and antenna position uncertainties (Liang et al., 2016), a variety of measurement sets such as squared range-sum measurements (Zou et al., 2016) and the range and range rate (Zou & Want, 2016) and algorithmic improvement techniques (Yi et al., 2016); (Gogineni & Nehorai, 2011). An approach for multi-target classification in multistatic radar systems has been analyzed in (Stinco et al., 2014), where information on target class is provided by the sensors of the system and the final classification decision is made using a fusion rule that combines the decisions coming from each channel of the radar network

(Stinco et al., 2014). Unlike the classical fusion rule based on the energy path loss, the proposed approach (Stinco et al., 2014) is made to favour the channels that are more suited to recognize the targets, considering both SNR and geometry. Thus, the spatial diversity of the multistatic radar system has been leveraged for higher probability of targets recognition (Stinco et al., 2014). A new UWB collaborative mobile target imaging algorithm for target classification purpose in RSNs has been presented in (Arik & Akan, 2010).

One research group has completed a detailed treatement of multiple target tracking in UWB radar sensor networks using particle filter (Sobhani et al., 2014); (Sobhani et al., 2016).

Another group has recently studied the impact of UWB RSN topology, waveform processing methods and tracking algorithm parameters on target localization performance (Bartoletti et al., 2015); (Bartoletti et al., 2013); (Bartoletti et al., 2014). It was demonstrated that a proper selection of representative observations (Bartoletti et al., 2015) and the use of subset diversity radars (Bartoletti et al., 2013) could help mitigate the ranging errors caused by harsh environmental conditions such as multipath, clutter and non-line-of-sight.

1.3.2   RSSI-based indoor tracking using the Extended Kalman Filter and circularly polarized antennas

In (Ben-Kilani et al., 2014), we investigate an RSSI-based indoor tracking scenario based on extended Kalman Filter and circularly-polarized antennas. The target of interest was a radiating source (an emitter) present in an environment composed of multiple RF receivers.

The RSSI-based indoor positioning technique is highly dependent on the propagation environment, which can lead to significant localization errors. For instance, permanent changes in the physical environment can yield inaccuracies with respect to the propagation model. Those permanent changes can be caused by multipath fading due to signal reflections, which is problematic in RSSI-based localization systems.

In order to mitigate those issues, many improvements have been proposed (Fink & Beikirch, 2011). The first type of improvement is mainly algorithmic. Different estimators have been investigated for enhancing the positioning accuracy.

In (Laitinen et al., 2007); (Li, 2006) a least square (LS) estimator was proposed for RSSI-based location estimation. This linear estimator attempts to minimize the error term between measurements and a propagation model. An adaptive approach was proposed in (Li, 2006), which takes into account the dynamic changes in the propagation environment. Specifically, a joint estimation technique of unknown location coordinates and path-loss exponent was investigated. We note that applying the non-linear LS algorithm requires a linearization step based on the first-order Taylor series expansion and the Levenberg-Marquardt method, which entails additional complexity.

A maximum likelihood (ML) based estimator was detailed in (Mazuelas et al., 2009). The proposed approach also dynamically estimates the propagation parameters, based on real-time RSSI measurements. The main drawback of such an approach is again the amount of calculations needed to perform the algorithm.

A second type of location estimation improvement was investigated in (Fink et al., 2010); (Kao & Lin, 2010); (Schmid et al., 2011). This type involves the fusion of RSSI measurements with data from other types of sensors (inertial, laser, etc.). This approach was shown to clearly increase the accuracy of the proposed localization techniques.

The Kalman filter (KF) is one of the best-known prediction-correction algorithms. It can easily be adapted to tracking scenarios (Kalman, 1960); (Welch & Bishop, 1995). However, since RSSI measurements relate to physical coordinates in a non-linear fashion, the extended Kalman filter (EKF) is more suitable, because it applies some linearization and approximation around the current estimate using the partial derivatives of the process and measurement functions (Welch & Bishop, 1995); (Yim et al., 2008). In (Caceres et al., 2009),

adaptive approaches using the EKF with direct RSSI measurements were proposed, and better results were obtained compared to more traditional LS estimators.

Recently, circularly polarized (CP) antennas have shown much promise in mitigating the effects of multipath fading in indoor environments (Nepa et al., 2010); (Szumny et al., 2007). Such antennas also allow for more flexible reciprocal orientation of the transmitter and the receiver. As such, they are becoming widely used in several wireless applications, such as the global positioning system (GPS) and synthetic aperture radar (SAR), as well as radio-frequency identification systems (RFID) (Nepa et al., 2010).

Circular polarization was also shown to reduce the root-mean-square delay spread by about one-half compared to linear polarization (LP), and the bit error rate (BER) due to multipath propagation in high-speed transmission channels (Rappaport & Hawbaker, 1992); (Manabe et al., 1995). In (Nepa et al., 2010), circular polarization was applied to an RSSI-based localization system. A direct comparison between measured and estimated position based on a standard Hata-like model was proposed for both LP and CP antennas. It was clearly shown that lower localization errors were obtained using CP antennas. In our proposed work (Ben-Kilani et al., 2014), we extend the study investigated in (Nepa et al., 2010) by offering a method of reducing the estimation errors in tracking scenarios.

In (Ben-Kilani et al., 2014) we aimed to design and evaluate the accuracy of a simple and robust algorithm, which is based on the EKF estimator and suitable for indoor tracking of mobile nodes. The proposed algorithm directly processes raw RSSI measurements, which are taken from wireless receivers equipped with CP antennas. The combination of the CP antennas – which yield more stable RSSI values – and the EKF, which offer excellent tracking performance, is evaluated in a real deployment scenario.

- **Extended Kalman Filter**

The tracking approach in (Ben-Kilani et al., 2014) is based on an extended Kalman filter, operating in the discrete time domain. This filter recursively estimates the state of a dynamic system modeled by the following state equation:

$$X_k = f(X_{k-1}) + w_k \qquad (1.1)$$

Taken from Caceres et al. (2009)

Where X_k is the state vector at time k, $f(.)$ is the state transition function which projects a state vector X_{k-1} forward in time, and $w_k \sim N(0, Q_k)$ is a random vector modeling random process noise, normally distributed with zero mean and covariance matrix Q_k.

We use the position-velocity model to characterize the state vector X which is defined as:

$$X = [x \; y \; v_x \; v_y]^T \qquad (1.2)$$

Taken from Caceres et al. (2009)

Where x and y are the coordinates of the node on a two-dimensional plane, and v_x and v_y are the corresponding velocities along those axes, respectively. The node's height is assumed constant in this model.

We also assume that the mobile node moves with a constant velocity between adjacent time intervals. Any change in target velocity is modeled as acceleration noise included in w_k; it also models non-linearities and system perturbations.

The transition function models a constant-speed, linear motion:

$$f(X_{k-1}) = F_k X_{k-1} = \begin{bmatrix} 1 & 0 & \Delta t & 0 \\ 0 & 1 & 0 & \Delta t \\ 0 & 0 & 1 & 0 \\ 0 & 0 & 0 & 1 \end{bmatrix} X_{k-1} \qquad (1.3)$$

Where Δt is the short time interval during which the mobile node velocity is assumed constant. The value of Δt is chosen to be $0.1\ s$ due to hardware limitations.

Q_k is computed under the assumption that the acceleration is a white noise random vector. This assumption takes into consideration different forces that could temporally cause changes in target directions as described in (Kohler, 1997). Q_k is calculated as follows:

$$Q_k = a^2 \begin{bmatrix} \dfrac{\Delta t^3}{3} & 0 & \dfrac{\Delta t^2}{2} & 0 \\ 0 & \dfrac{\Delta t^3}{3} & 0 & \dfrac{\Delta t^2}{2} \\ \dfrac{\Delta t^2}{2} & 0 & \Delta t & 0 \\ 0 & \dfrac{\Delta t^2}{2} & 0 & \Delta t \end{bmatrix} \tag{1.4}$$

Taken from Kohler (1997)

Where a is the maximum amplitude of the noise process. The measurements are considered during the update phase. They are incorporated into the filter using:

$$Z_k = \mathrm{h}(X_k) + v_k \tag{1.5}$$

Where $v_k \sim N(0, R_k)$, Z_k is the measurement vector at instant k, and $\mathrm{h}(.)$ is the observation function that estimates the expected measurements at the true state X_k. v_k is the measurement noise vector, modeled as a normally distributed random variable with zero mean and covariance matrix R_k, which we set to a diagonal matrix because we assume that the measurements errors are independent.

In order to take advantage of the non-linear capabilities of the EKF, the system makes direct use of the RSSI measurements P_{ref} produced by L separate receivers (RSSI values at different receivers) in the observation vector Z, in addition to the measured velocities:

$$\boldsymbol{Z} = [v_x \; v_y \; P_{ref_1} \dots P_{ref_L}]^T \tag{1.6}$$

The measurements v_x and v_y contained in the measurement vector gives additional information regarding the node's state, which the algorithm uses to improve tracking accuracy. Inaccuracies related to the measured velocities are also taken into account through the measurement noise covariance matrix:

$$\boldsymbol{R}_k = diag(\sigma_{v_x}^2 \; \sigma_{v_y}^2 \; \sigma_{dBm_{ref_{1,k}}}^2 \; \cdots \; \sigma_{dBm_{ref_{L,k}}}^2) \tag{1.7}$$

The matrix $\boldsymbol{R}_k$ characterizes the errors between measured and propagation-model-based RSSI values. More stable RSSI measurements allow us to have smaller error variances. Good tracking performance can therefore be achieved provided that the RSSI measurements are accurate.

The observation function is derived from the log-normal propagation model applied to each receiver:

$$h(\boldsymbol{X}_k) = \begin{bmatrix} v_x \\ v_y \\ P_{0_1} - 10\alpha_1 log_{10}(dist(\boldsymbol{X}_k, \boldsymbol{X}_{ref_1})/d_0) \\ \vdots \\ P_{0_L} - 10\alpha_L log_{10}(dist(\boldsymbol{X}_k, \boldsymbol{X}_{ref_L})/d_0) \end{bmatrix} \tag{1.8}$$

Where α_i is the path loss exponent related to receiver i, L is the number of receivers, P_{0_i} is the mean power received at a distance d_0 (typically 1 m) from the receiver $\boldsymbol{X}_{ref_i}$ is the position of the receiver i and $dist(.)$ is the Euclidean distance function.

- **CP Antennas**

Compared to LP antennas, CP antennas offer better performance by reducing multipath effects, which yields more stable RSSI measurements. These characteristics reduce estimation errors, especially those due to first-order signal reflections. Indeed, when a circularly polarized wave is reflected, its handedness is reversed. Thus, if the transmitting and receiving antennas are circularly polarized with the same handedness (both right-handed or left-handed CP), multipath-delayed waves caused by single reflections will be effectively rejected by the receiving antennas. This characteristic is of great interest because channel fading is generally caused by first-order reflections, and because the field amplitude of such reflections is much higher than those of higher-order reflections (Nepa et al., 2010); (Szumny et al., 2007).

In order to characterize the advantages of using CP antennas compared to LP antennas, we carried out RSSI measurements using both types. The results are presented in Figure 1.1. High RSSI fluctuations are obtained for the LP case, due to the superposition of incident and reflected waves, resulting in constructive and destructive interference. Conversely, reduced oscillations can be observed when CP antennas are used, as expected, due to the reduced amplitude of the first-order reflections. The RSSI error-term variance $\sigma^2_{dBm_{ref_{LP}}}$ was found to be 19.87 dBm^2 for the LP antenna, compared to 7.73 dBm^2 for CP one. In both cases, propagation parameters were determined ensuring minimum error term variances between the measurements and the propagation model. The same transmitted power was used for both experiments. Note that the fact that higher values of RSSI were obtained with the CP antenna is related to its higher gain compared to the LP one.
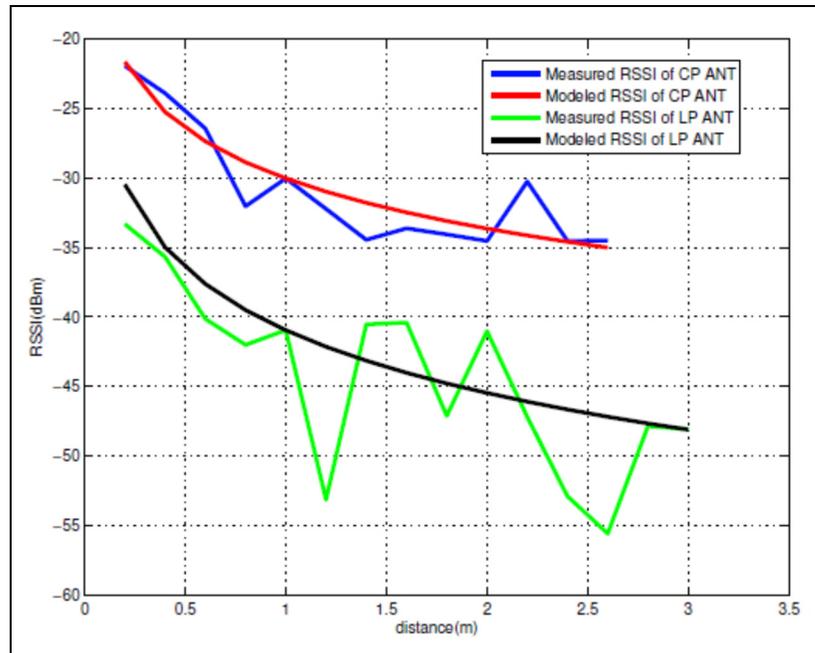
Figure 1.1 Experimental and modeled propagation characteristics of CP and LP antennas

In order to test the performance of the proposed system, a localization experiment was devised.

- **Experimental Setup**

Our experimental setup consists of four sensor nodes, or anchor nodes, positioned inside a capture area of $4\,m \times 4\,m$, as illustrated in Figure 1.2 (a). Both the transmitter and the receivers are equipped with circularly polarized, omnidirectional antennas operating at 2.4 GHz.

Experiments were carried out using custom-built receivers based on Texas Instruments CC2510 2.4 GHz radio transceivers, and equipped with the four-leaf receiver antennas shown in Figure 1.3 (a). Those receivers are connected, via Ethernet links, to a central processing server where data is saved for offline processing.

The emitter also consists of a CC2510 module, programmed to permanently transmit a sinusoidal signal on an unused channel of the 2.4 GHz ISM band. The mobile node makes use of a three-leaf transmitter antenna, as presented in Figure 1.3 (b). We installed the emitter on top of an iRobot Roomba robot, depicted in Figure 1.2 (b), programmed to follow a piecewise-linear trajectory at a constant speed of $0.2\ m/s$ This trajectory is illustrated in Figure 1.2 (a).

(a) Anchor Positions   (b) Robot and Emitter
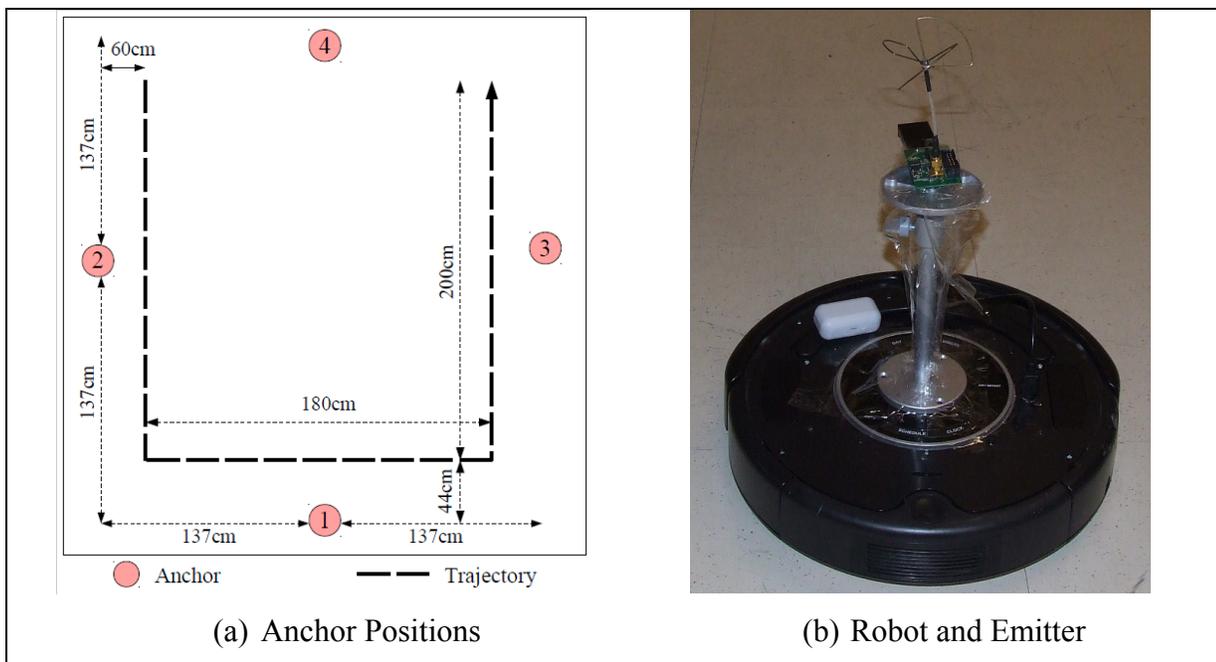
Figure 1.2 Experimental Configuration

Due to the presence of Wi-Fi signals in the same frequency band, we were careful to choose an unused channel to limit the amount of interference.

Figure 1.4 describes the acquisition system from a high-level point of view. As pictured, the four receivers are connected to a computer server via an ethernet link. To reduce the number of wires required, the receivers are powered using a power-over-ethernet-compatible ethernet switch. The computer server gathers RSSI measurements from each receiver at 100 ms

intervals. Those measurements are stored in a plain-text file for offline processing using MATLAB.

(a) Receiver (Anchor node) (b) Emitter
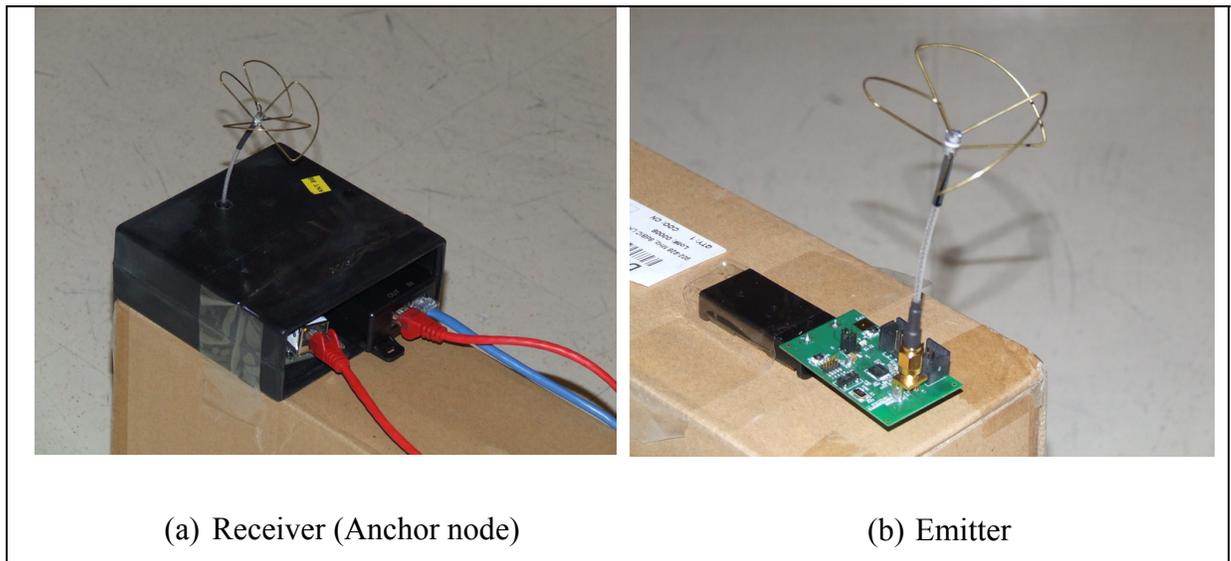
Figure 1.3 Custom-built receivers and emitter, equipped with circularly
polarized 2.4 GHz antennas
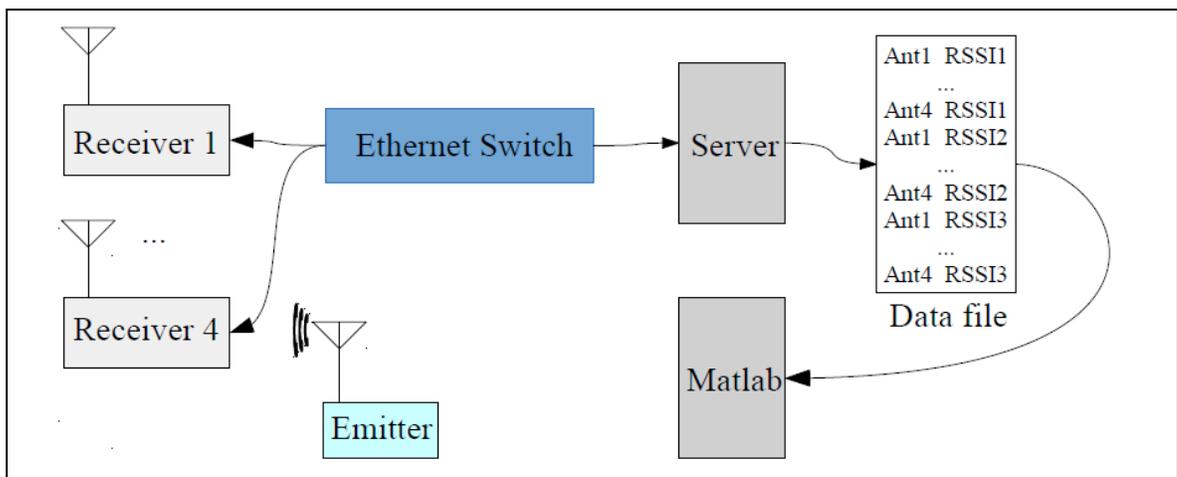
Figure 1.4 High level description of the acquisition system

- **Calibration phase**

In order to model the propagation characteristics of the receiver antennas, an offline calibration phase was first carried out. 100 RSSI measurements were recorded after placing the emitter at various distances from each receiver, in 20 cm increments.

The received values were then imported into MATLAB for analysis, and the parameters of each antenna were computed by minimizing the error term variance $\sigma^2_{dBm_{ref_i}}$, assuming a log-normal propagation model. The resulting model parameters are illustrated in Figure 1.5. Table 1.1 summarizes the mean received power at distance $d_0 = 1$ m, path-loss exponent α_i of the adjusted model, and the error-term variances.

Table 1.1 Propagation parameters

Antenna i	P_{0_i} (dBm)	α_i	$\sigma^2_{dBm_{ref_i}}$
1	-31.79	1.4	7.32
2	-30.84	3.1	7.73
3	-34.55	1.5	4.79
4	-30.035	1.2	3.06
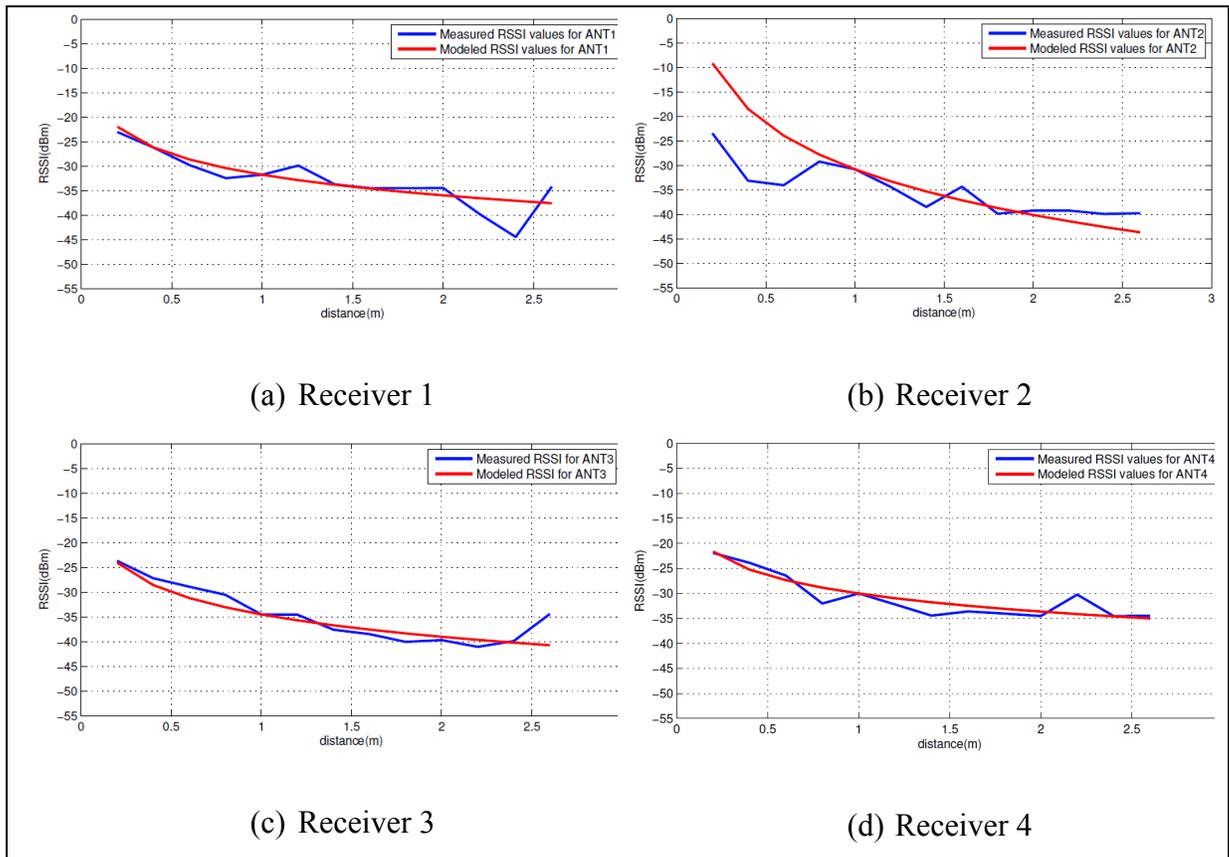
Figure 1.5 Log-normal channel model of different receivers

- **Localization Accuracy**

After this initial calibration step, which characterized the antennas as well as the propagation environment, we carried out a tracking scenario to quantitatively evaluate the precision of the proposed system.

The mobile node was moved along the trajectory presented in Figure 1.2(a). RSSI measurements were gathered from all four receivers and sent to the computer server. A total of 471 measurements were gathered from each receiver. These measurements were then processed using the EKF implemented in MATLAB code.

After processing, the target's estimated trajectory was computed and compared to a known ground truth. Comparative results are shown in Figure 1.6. The maximum location estimation error (LEE) is found to be 0.52 m. The location error is high compared to the environment dimensions since the RSSI-based indoor positioning technique is highly dependent on the propagation environment. We can see from the estimation curve that changes in direction are also well-predicted by the EKF.

The tracking precision is essentially dependent on the stability of measurements obtained from CP antennas, as detailed in previous sections, as well as the additional noisy velocity measurements supplied to the algorithm. This latter point is corroborated by Figure 1.7, which demonstrates, as an example, the effectiveness of the proposed EKF model in estimating the y-axis velocity during the tracking scenario. It also illustrates the fluctuations of v_y caused by changes in target direction along its path. The additional information regarding measured velocities allow us to increase the tracking ability of the proposed system, and to avoid the imprecisions introduced by the simplistic PV model. the x-axis velocity is also effectively estimated during the tracking scenario.
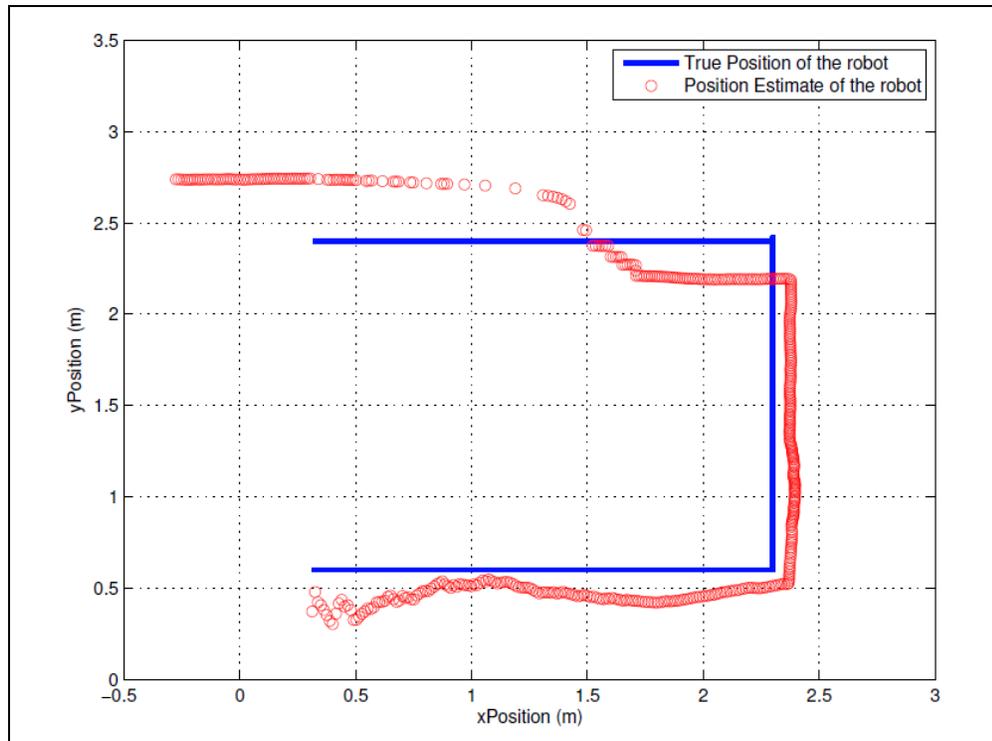
Figure 1.6 Position tracking performance
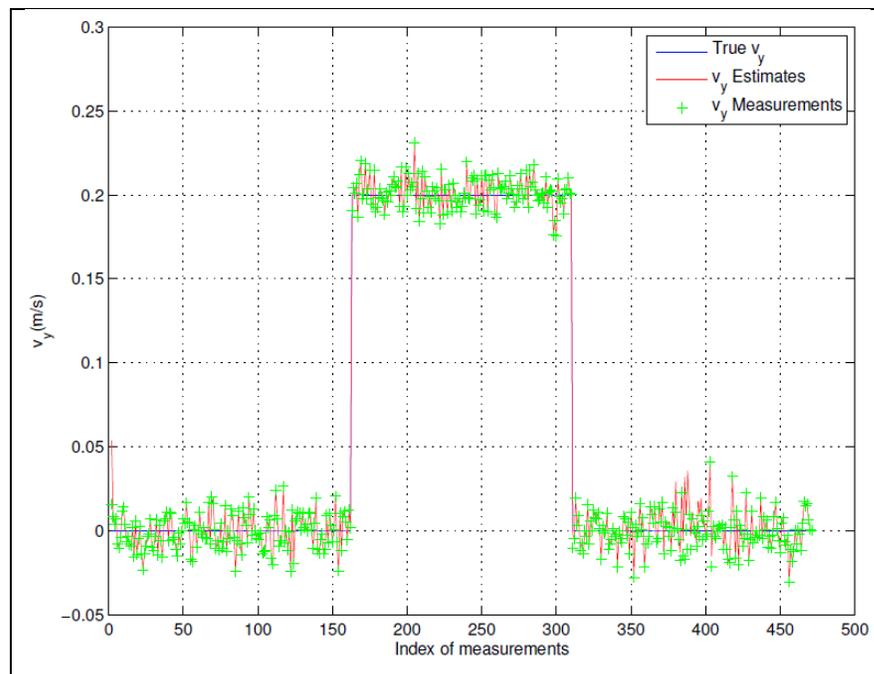
Figure 1.7 Velocity tracking performance in the y direction

1.4 Joint radar and communication systems

RF front-end architectures for both radar and communication are becoming increasingly similar. In particular, most functionalities are now carried out via digital signal processing rather than by hardware components. At the same time, similarities in carrier frequencies between radar and communication systems are also becoming more prominent. The overall similarities between both systems dictate a joint operation between them with a minimum of mutual interference. As detailed in section 0.2.3, the joint radar and communication systems investigated in the literature can be separated into three main categories. The first category is related to the presence of wireless nodes, where both communication and radar functionalities are enabled at each node level (Sturm & Wiesbeck, 2010); (Garmatyuk et al., 2007); (Garmatyuk et al., 2011); (Nijsure et al., 2012). The same communication waveform is used for monostatic radar detection in an intelligent transportation context (Sturm & Wiesbeck, 2010), in SAR imaging applications (Garmatyuk et al., 2007); (Garmatyuk et al., 2011), and in the context of cognitive radar radio networks for safety purposes (Nijsure et al., 2012).

A second category of joint radar and communication operation focuses on incorporation of communication as secondary to the primary radar function, as reported in several papers (Surrender & Narayanan, 2011); (Euziere et al., 2014); (Hassanien et al., 2015); (Blunt & Yantham, 2007).

The third main category of joint radar and communication operation consists of separate communication and radar systems operation, wherein each system has its own nodes and architecture, but coexistence is mandatory because both systems are deployed in the same environment with a partial or total spectrum sharing constraint (Jacyna et al., 2016); (Turlapaty & Jin, 2014).

Chapter 3 investigates the first category of joint radar and communication operation, where several communication nodes in a network operate separately in frequency. A novel

architecture at each node level is proposed in order to leverage the multi-look diversity of the distributed system. This is done by activating radar processing on multiple received bistatic streams at each node level in addition to the pre-existing monostatic processing. The proof of concept of OFDM capabilities for use as a radar waveform has enabled the same OFDM communication waveform to be used for simultaneous monostatic and bistatic radar functionalities.

Chapter 4 focuses on the third category of joint radar and communication operation, where separate communication and multistatic radar systems are present with a partial or total spectrum sharing constraint. This chapter investigates the optimum placement of radar receivers in order to optimize target positioning accuracy while minimizing the interference caused by the simultaneous operation of the communication system.

CHAPTER 2

COGNITIVE WAVEFORM AND RECEIVER SELECTION MECHANISM FOR MULTISTATIC RADAR

In this chapter, a novel Cognitive Radar (CR) approach to improve the extended targets detection and resolution is developed in a multistatic radar context. A cognitive waveform selection mechanism based on target probability of detection maximization in conjunction with adaptive receiver allocation/selection is proposed. Apart from the cognitive waveform selection objective, this process aims at evaluating the optimal positions for the radar receivers in an attempt to iteratively minimize the Geometric Dilution of Precision (GDOP), subsequently resulting in a high precision target geolocation estimate. The cognitive waveform selection mechanism is based on target dynamics involving time varying target scattering characteristics and clutter distribution parameters. Thus, with the proposed dual objective approach, the concept of cognition can be extended to both the radar transmitter and receiver sites. Numerical results demonstrate better target detection performance and positioning accuracy using the proposed approach as compared with conventional methods based on static transmission or stationary multistatic receivers topology.

This chapter shares the same review of literature as a publication by the same author. Some passages are taken directly from (Ben-Kilani et al., 2016), with additional information which applies to this thesis.

2.1   Introduction

Cognitive Radar (CR) is an innovative paradigm for optimizing traditional radar performances within dynamic environments (Haykin, 2006). The concept is essentially based on a continuous learning through radar interactions with its surrounding world, and an

iterative feedback from the receiver to the transmitter facilitates the adaptation of radar transmission parameters in real time (Haykin, 2006). The continuous target tracking is ensured by preservation of the information content of the radar returns (Haykin, 2006).

The reaction of the transmitter to the updated information coming from the feedback loop has a crucial impact on the ability of the CR to intelligently adapt to the environment. As a result, a lot of the research efforts have been focused on the waveform design and optimization. Waveform optimization was emphasized by the need to properly detect extended targets. In contrast to point targets, which have a flat response across the operating frequency band of the radar, extended targets exhibit random scattering characteristics due to their range extent. Thus, optimal waveform could be designed in order to maximize the energy reflected from the target.

The topic of CR waveform optimization has been treated following several optimization criteria. A principal waveform design approach is to directly optimize the receiver detection statistics of extended targets in the presence of clutter and additive noise. In (Pillai et al., 2000); (Garren, 2001); (Estephan, 2010), the dynamic choice of both the waveform and the receiver impulse response is dictated by a maximization process of the output Signal-to-Clutter plus Noise Ratio (SCNR). in (Kay et al., 2009), the Neyman-Pearson (NP) detector is derived in case of extended target and clutter. The detailed waveform design process is based on a maximization process of the symmetrized Kullback-Liebler measure directly linked to the target detection performance. A Generalized Canonical Correlation (GCC) detector for multistatic passive detection is proposed in (Liu & Himed, 2014). It is shown that the proposed detector performs better than the Generalized Likelihood Ratio Test (GLRT) detector only in case of known noise statistics (Liu & Himed, 2014). A comparative study between the Adaptive Matched Filter (AMF) detector and the GLRT detector is carried out in (Bruyere & Goodman, 2008), It is shown that the GLRT outperforms AMF in case of unknown noise and target scattering statistics. Both detectors exhibit better performances with an increasing number of receiver platforms (Bruyere & Goodman, 2008).

Multistatic radars offer many advantages compared to monostatic radars especially increased coverage and improved target resolution and classification (Stinco et al., 2014), in addition to higher tolerance to sources of interference due to their spatial diversity and the potential for improved physical survivability owing to the multiplicity of stations (Derham et al., 2010). However, a minimum level of synchronization between different units is required to achieve multistatic signal processing (Derham et al., 2010).

Geometric Dilution of Precision (GDOP) is a metric initially used in satellite navigation to characterize the impact of system geometry on the positioning accuracy (Yarlagadda et al., 2000). Recently applied to general sensor network systems design (Sharp et al., 2009); (Torrieri, 1984); (Sharp et al., 2012), GDOP is defined as the ratio of the root-mean-square position error to the root-mean-square ranging error (Torrieri, 1984). Consequently, higher GDOP value for a particular topological distribution of the sensor networks represents poor positioning performance. From the above GDOP definition, a good positioning accuracy could be achieved with an optimal choice of the sensor network geometry.

Following from the above discussions, it is interesting to study the performances of cognitive multistatic radar where the selection of the transmitted waveform and the placement of the receivers are dynamically changed to adapt to the time-varying environment. Some works (Anastasio et al., 2010); (Gumiero et al., 2011); (Nguyen et al., 2014) relate to the optimization of the multistatic radar geometry for enhanced target positioning accuracy. In (Anastasio et al., 2010), the selection of two transmitters of opportunity and a single receiver location in a passive multistatic radar is performed using a Cramer-Rao Lower Bound (CRLB) based algorithm, which considers a set of constraints for the relative positions of the transmitter and receiver units. The proposed solution is considered accurate but computationally expensive (Anastasio et al., 2010). A joint approach based on transmitter waveform and receiver path optimization for target tracking by multistatic radar is proposed in (Nguyen et al., 2014). The developed algorithm minimizes the tracking mean square error, however it doesn't account for extended target processing. In addition, the environment is assumed to be clutter free. In our work context, we propose a joint approach to optimize both

detection and positioning accuracy of extended targets in clutter plus noise corrupted environment.

The contributions of the current work can be summarized as:

1) Design of a cognitive waveform selection mechanism, based on the principle of maximization of target detection probability;

2) Development of a receiver positioning strategy, with an objective of GDOP minimization, which supplements the previous contribution concerning cognitive waveform selection;

3) Fusion of both parts to form a hybrid system that shows better detection performances in comparison with only the cognitive waveform selection mechanism.

2.2   System architecture

Figure 2.1 shows the general architecture of the proposed CR system. The cognitive loop could be summarized in the following steps:

Step 1: The backscattered signals gathered from different receivers are matched filtered in the multistatic radar returns processing block where the received signals are correlated with the transmitted waveform. Consequently, the outputs of the matched filtering process are used to estimate the target impulse responses in addition to the clutter and noise covariance matrices through successive measurements. Then, the central processor uses the estimated dynamic radar scene information to select the waveform that maximizes the probability of target detection. The waveform selector block in the central processor chooses the waveform to transmit within an ensemble of Hadamard phase coded waveforms according to the detection maximization criterion.

Step 2: The range-Doppler responses relative to different bistatic transmitter-receiver pairs are computed after matched filtering. Subsequently, multiple information relative to bistatic target ranges and bistatic Doppler shifts are extracted from different range-Doppler responses and injected into a LS geolocation process in order to compute the absolute position and velocity estimates of the target. The target position estimate is then used to compute the GDOP of the target positioning algorithm. Finally, a GDOP-based minimization approach is carried out in order to obtain the optimal positions of the receivers according to the actual target position estimate.

Step 3: The central processor sends a waveform selection command to the transmitter in order to transmit the waveform chosen according to Step 1. Meanwhile, the central processor will evaluate the optimal positions obtained from Step 2 and will instruct the receivers to update their locations accordingly in real-time as shown in Figure 2.1.

Different steps are then repeated iteratively allowing the cognitive system to continuously adapt its operational mode to the dynamic scene.
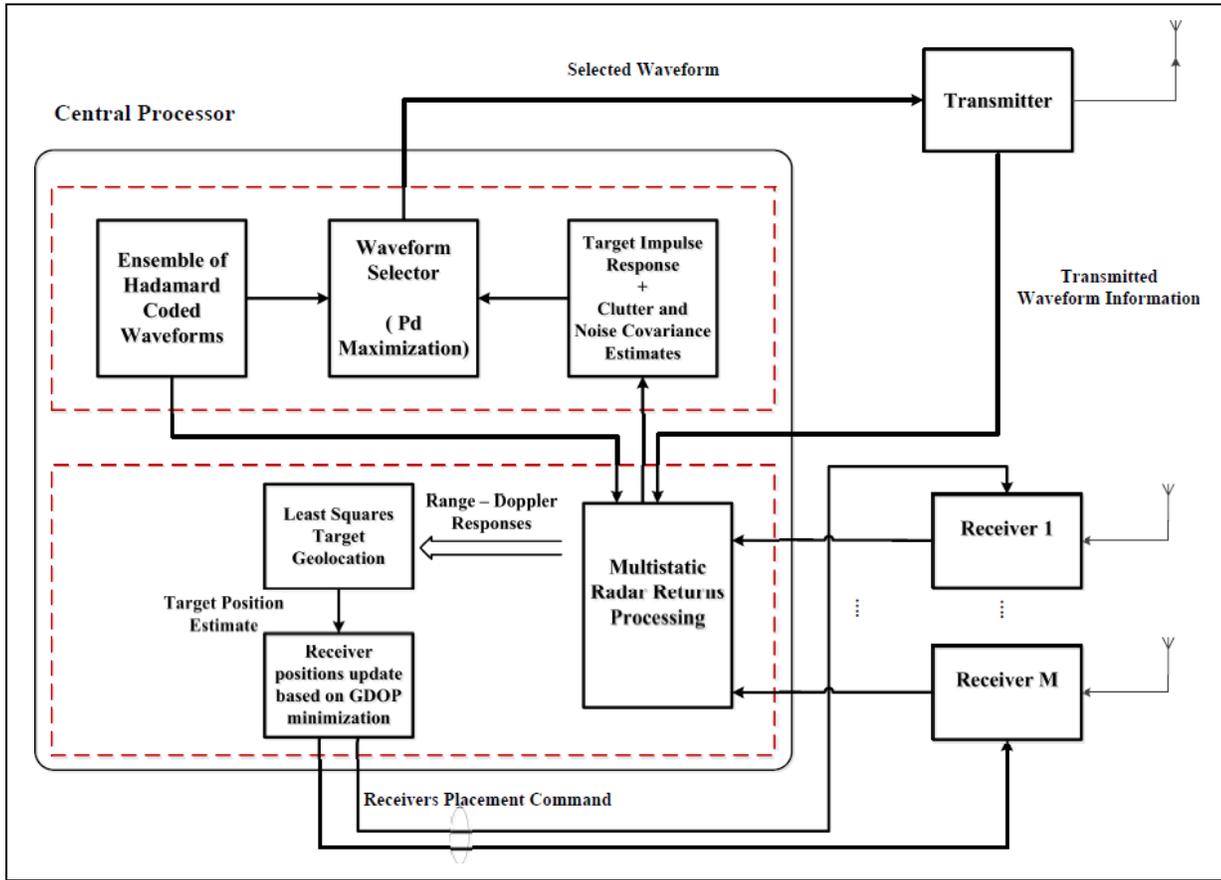
Figure 2.1 Proposed CR architecture

2.3   Signal model

2.3.1   Phase-coded waveforms

In this work, we use phase-coded waveforms as they can fully exploit the transmit power with sufficient variability unlike traditional Linear Frequency Modulated (LFM) waveforms (Skolnik, 2001). Each phase-coded waveform comprises a train of phase-coded Gaussian pulses. Each pulse is divided into $N = 512$ subpulses each of duration $\delta = 6.6\,ns$. A unimodular Hadamard code is used to modulate the phases of the subpulses, which corresponds to a specific row of the $N \times N$ Walsh-Hadamard matrix. Hadamard sequences,

with sufficient length, are chosen in order to improve the Doppler resolution of the radar system. Each normalized Gaussian pulse takes the following form:

$$f(t) = \frac{1}{\sqrt{2\pi T}} \, exp(\frac{-t^2}{T^2})$$

(2.1)

Where T is the pulse width.

We denote by $f_n(t)$ the nth subpulse of the pulse $f(t)$. The complex envelope of one transmitted phase-coded pulse is expressed as:

$$I(t) = \sum_{n=1}^{N} c_n f_n(t)$$

(2.2)

Where c_n is the Hadamard sequence code of the subpulse $f_n(t)$. The transmitted burst is a train of U phase-coded pulses (i.e., delayed versions of $I(t)$) given by:

$$s(t) = \sum_{u=1}^{U} I(t - uT_{PR})$$

(2.3)

Where $s(t)$ is the complex envelope of the narrowband transmitted signal and T_{PR} is the pulse repetition time.

2.3.2 Target RCS model

RCS is a measure of target size and ability to reflect radar energy. The RCS unit is m^2, which corresponds to an area. Effectively, if all the incident radar energy on the target were reflected equally in all directions, then the radar cross section would be equal to the target's cross-sectional area as seen by the transmitter. In practice, some energy is absorbed and the reflected energy is not distributed equally in all directions. Therefore, the RCS characterization task is not straightforward and is normally determined by measurement. The target RCS depends on several factors:

- Material of which target is made;
- Absolute size of the target;
- Relative size of the target (relative to radar transmitted signal wavelength);
- The incident and reflected angles;
- The polarization of transmitted and received radiation in respect to the orientation of the target.

Swerling target models are special cases of the Chi-Squared target models with specific degrees of freedom. There are five different Swerling models, numbered I through V (Skolnik, 2001); (Rihaczek, 1996):

Swerling I

A model where the RCS varies according to a Chi-squared probability density function with two degrees of freedom. This applies to a target that is made up of many independent scatterers of roughly equal areas. As little as half a dozen scattering surfaces can produce this distribution. Swerling I model describes a target whose radar cross-section is constant throughout a single scan, but varies independently from scan to scan. This case is known as slow fluctuation. In this case, the pdf reduces to:

$$p(\xi) = \frac{1}{\xi_{av}} exp\left\{-\frac{\xi}{\xi_{av}}\right\}$$

(2.4)

Where $\xi > 0$ represents the variance of RCS fluctuations and ξ_{av} is the average RCS. Swerling I model has been shown to be a good approximation when determining the RCS of objects in aviation.

Swerling II

Similar to Swerling I, except the RCS values returned are independent from pulse to pulse, instead of scan to scan. This case is known as fast fluctuation.

Swerling III

A model where the RCS varies according to a Chi-squared probability density function with four degrees of freedom. This pdf approximates an object with one large scattering surface with several other small scattering surfaces. The RCS is constant through a single scan just as in Swerling I. This is again a case of slow fluctuation. The pdf becomes:

$$p(\xi) = \frac{4\xi}{\xi_{av}^2} exp\left\{-\frac{2\xi}{\xi_{av}}\right\}$$

$$(2.5)$$

Swerling IV

Similar to Swerling III, but the RCS varies from pulse to pulse rather than from scan to scan. This is a case of fast fluctuation.

Swerling V (Also known as Swerling 0)

Constant RCS as degrees of freedom approaches infinity.

In contrast to point targets, which have a flat response across the operating frequency band of the radar, extended targets exhibit random scattering characteristics due to their physical extent (which is comparable to the radar range resolution). In fact, the received radar signal from extended target is the sum of multiple delayed versions of transmitted waveform (Bell., 1993).

2.3.3   NP detection in multistatic radar context

We consider M physically separated receive sensors so that all the received clutter and noises are statistically independent from one sensor to sensor.

We denote by $x_i(t)$ the complex input of the ith receiver, $c_i(t)$ denotes clutter and $n_i(t)$ the sum of ambient noise and interference, i.e., jamming. $n_i(t)$ and $c_i(t)$ are modeled as zero mean complex wide sense stationary (WSS) Gaussian random processes.

The detection problem of an extended target in the presence of clutter and noise can be summarized as:

$$H_0: x_i(t) = c_i(t) + n_i(t)$$
$$H_1: x_i(t) = [h_i(t) * s(t)] + c_i(t) + n_i(t) \qquad (2.6)$$

where H_0 is the hypothesis of target absence (i.e., only clutter and noise are present), H_1 is the hypothesis of target presence in addition to clutter and noise, $h_i(t)$ is the extended target impulse response relative to the ith receiver and $*$ denotes convolution. For ease of illustration, we suppose that the clutter is stationary.

We consider the Swerling I target model, which implies that the target is made up of many independent scatterers of roughly equal areas. Under such assumption, the backscattered signal coming from the target can be expressed as:

$$h_i(t) * s(t) = A_i[g_i(t) * s(t)]$$
$$= A_i \sum_{k=1}^{N_s} b_{ik} s(t - \tau_{ik}) \, exp(2\pi j f_{ik} t) \qquad (2.7)$$

Where A_i is a complex reflection factor proportional to the extended target Radar Cross Section (RCS) with the Probability Density Function (PDF) $A_i \sim CN(0, \sigma_{A_i}^2)$. $g_i(t)$ is the deterministic part of the extended target impulse response, N_s represents the number of scatterers composing the target, b_{ik} is a deterministic coefficient relative to the kth scatterer and the ith path, τ_{ik} is the total delay experienced by the transmitted signal from the transmitter to the ith receiver and after reflection by the kth scatterer in between and f_{ik} represents the bistatic Doppler shift experienced by the transmitted signal along the ith path and caused by the movement of the kth scatterer.

Consequently, the expression of the received signal at the ith receiver under Hypothesis H_1 is now derived as:

$$x_i(t) = A_i \sum_{k=1}^{N_s} b_{ik} s(t - \tau_{ik}) \, exp(2\pi j f_{ik} t) \, + \, c_i(t) + n_i(t) \tag{2.8}$$

We take Q samples of each received signal $x_i(t)$ and we define the vector $X_i, i = 1, \dots, M$ of dimension $1 \times Q$, which is composed of the received samples.

Also, we define the column vector of all sensor outputs $X = [X_1, \dots, X_M]^T$. Hence the detection problem of (2.6) can be represented as (Kay et al., 2009):

$$H_0: X_i = C_i + N_i$$
$$H_1: X_i = T_i + C_i + N_i$$
$$= A_i G_i + C_i + N_i \tag{2.9}$$

Where $c_i(t)$ and $n_i(t)$ are replaced by their corresponding column vectors of samples C_i and N_i, T_i denotes the vector of backscattered signal samples coming from the target and G_i is the vector of samples related to the deterministic part of the target response $g_i(t) * s(t)$. It follows that T_i, C_i and N_i are all complex multivariate Gaussian random vectors with a zero-mean vector. The PDF of the received vector X_i under H_0 is given by (Kay et al., 2009):

$$p(X_i; H_0) = \frac{1}{\pi^Q det(K_i)} \, exp[-X_i{}^H K_i^{-1} X_i] \tag{2.10}$$

where K_i is the covariance matrix of $C_i + N_i$.

Since A_i, C_i and N_i are assumed independent of each other, the PDF under H_1 can be represented as (Kay et al., 2009):

$$p(X_i; H_1) = \frac{1}{\pi^Q det(\sigma_{A_i}^2 G_i G_i{}^H + K_i)} exp[-X_i{}^H(\sigma_{A_i}^2 G_i G_i{}^H + K_i)^{-1} X_i] \tag{2.11}$$

Furthermore, all sensor outputs X_i are considered independent. Thus,

$$p(X; H_w) = \prod_{i=1}^{M} p(X_i; H_w), \qquad w = 0,1 \tag{2.12}$$

After deriving the distribution of the NP detection statistic, the probability of false alarm P_{FA} and detection P_D expressions can be obtained following the derivations in (Kay et al., 2009):

$$P_{FA} = \sum_{i=1}^{M} P_i \, exp[-\gamma/(2\alpha_i^{(0)})] \tag{2.13}$$

$$P_D = \sum_{i=1}^{M} Q_i \, exp[-\gamma/(2\alpha_i^{(1)})] \tag{2.14}$$

Where

$$P_i = \prod_{\substack{i=1 \\ n \neq i}}^{M} \frac{1}{1 - \alpha_n^{(0)}/\alpha_i^{(0)}} \tag{2.15}$$

$$Q_i = \prod_{\substack{i=1 \\ n \neq i}}^{M} \frac{1}{1 - \alpha_n^{(1)}/\alpha_i^{(1)}} \tag{2.16}$$

$$\alpha_i^{(0)} = \frac{\sigma_{A_i}^2 G_i{}^H K_i{}^{-1} G_i}{1 + \sigma_{A_i}^2 G_i{}^H K_i{}^{-1} G_i} \tag{2.17}$$

$$\alpha_i^{(1)} = \sigma_{A_i}^2 {G_i}^H {K_i}^{-1} G_i$$

<div align="right">(2.18)</div>

γ is the detection threshold. The weighting term $\alpha_i^{(0)}$ characterizes the contribution of the ith receiver in the detection process. If a small target return is measured at the ith receiver (i.e., $\sigma_{A_i}^2 {G_i}^H {K_i}^{-1} G_i \ll 1$), then its contribution will not be included in the detection decision. As a result, the proposed approach allows to efficiently leverage the signal diversity offered by the multistatic topology in order to optimize the target detection capabilities.

2.4   Cognitive waveform selection mechanism

Following from the above discussions, a multistatic cognitive waveform selection process could be devised in order to maximize the probability of detection expressed in (2.14) for a given probability of false alarm. Indeed, the threshold value γ could be dynamically derived by solving (2.13) for a fixed value of the probability of false alarm and the real-time scene parameters (i.e., the extended target impulse responses in addition to clutter plus noise covariance estimates). The resulting threshold γ is then used to compute the probability of detection.

The waveform selection process could be formulated as:

$$s_{opt} = max_{s_k \in S} P_D$$

<div align="right">(2.19)</div>

where s_{opt} is the selected waveform that maximizes P_D, S is the ensemble of Hadamard phase-coded sequences and s_k is a particular probing waveform from S.

The probability of target detection is maximized at each iteration. Subsequently, new waveform is selected for transmission. Each waveform is composed of a train of Hadamard phase-coded pulses where the subpulses coding sequence corresponds to a specific

Hadamard sequence as described in section III. The procedure of cognitive waveform selection could be summarized as follows:

1) Select a waveform from the ensemble S for transmission.

2) The received signals are used to estimate the real-time covariance matrices of clutter and noise K_i in addition to the extended target impulse responses and scattering coefficient variances $\sigma_{A_i}^2$ corresponding to the ith receiver.

3) For each waveform s_k in the ensemble S, use the information regarding actual Doppler shifts and total delays contained in the estimated target impulse responses to compute the deterministic vectors G_i relative to s_k as detailed in (2.8) and (2.9). Then compute the actual values of $\alpha_i^{(0)}$ and $\alpha_i^{(1)}$ in (2.17) and (2.18) based on the current estimates of G_i, K_i and $\sigma_{A_i}^2$ and update the threshold γ by solving (2.13) for the fixed value of probability of false alarm P_{FA}. Finally calculate the value of P_D, which corresponds to the waveform s_k based on actual values of $\alpha_i^{(0)}$, $\alpha_i^{(1)}$ and γ as described in (2.14).

4) Choose the waveform s_{opt} corresponding to the maximum P_D.

5) Transmit s_{opt}, collect the return signals and process it in each receiver. Repeat steps 2-5.

2.5   Multistatic GDOP-based receiver locations update strategy

2.5.1   LS geolocation process

The backscatter signals coming from the target are matched filtered at each receiver and the bistatic range-Doppler responses relative to different receivers are processed. Consequently, bistatic ranges and Doppler shifts relative to different transmitter-receiver pairs could be easily extracted from the range-Doppler responses. Theoretical expressions of bistatic range and bistatic Doppler shift are given by (Skolnik, 2001):

$$r_i = \sqrt{R_T \times R_{ri}} \qquad (2.20)$$

$$f_i = 2\frac{V}{\lambda}\cos\phi_i \, \cos(\beta_i/2)$$

$$= 2\frac{V}{\lambda}\cos\phi_i \sqrt{\frac{1}{2} + \frac{R_T - L_i \sin\theta_T}{2\sqrt{R_T^2 + L_i^2 - 2R_T L_i \sin\theta_T}}} \qquad (2.21)$$

Where r_i is the bistatic range relative to the transmitter and the ith receiver, R_T is the transmitter to target range, R_{ri} is the ith receiver to target range. f_i is the bistatic Doppler shift, L_i is the baseline separating the transmitter from the ith receiver, $V = \sqrt{v_x^2 + v_y^2 + v_z^2}$ is the target velocity, i^{th} is the carrier wavelength, β_i is the the bistatic angle, ϕ_i is the angle between the target velocity vector and the bistatic bisector and θ_T is the angle between the transmitter and the target.

The aim of the geolocation step is to estimate the absolute target position and velocity from the measured bistatic ranges and Doppler shifts relative to different receivers. The LS geolocation system can be modeled as:

$$\boldsymbol{Z} = \boldsymbol{\psi}(\boldsymbol{\rho}) + \eta \qquad (2.22)$$

where $\boldsymbol{Z} = [r_1, \ldots, r_M, f_1, \ldots, f_M]^T$ is the measurement vector, $\boldsymbol{\rho} = [x, y, z, v_x, v_y, v_z]^T$ is the vector of unknown target parameters (i.e., target position and velocity vectors) and η is the measurement noise vector.

From (2.20), (2.21) and (2.22), we can represent the hybrid system as,

$$
\psi(\boldsymbol{\rho}) =
\begin{bmatrix}
\sqrt{R_T \times R_{r1}} \\
\sqrt{R_T \times R_{r2}} \\
\vdots \\
\sqrt{R_T \times R_{rM}} \\
2\dfrac{\sqrt{v_x^2 + v_y^2 + v_z^2}}{\lambda}\cos\phi_1 \sqrt{\dfrac{1}{2} + \dfrac{R_T - L_1 \sin\theta_T}{2\sqrt{R_T^2 + L_1^2 - 2R_T L_1 \sin\theta_T}}} \\
2\dfrac{\sqrt{v_x^2 + v_y^2 + v_z^2}}{\lambda}\cos\phi_2 \sqrt{\dfrac{1}{2} + \dfrac{R_T - L_2 \sin\theta_T}{2\sqrt{R_T^2 + L_2^2 - 2R_T L_2 \sin\theta_T}}} \\
\vdots \\
2\dfrac{\sqrt{v_x^2 + v_y^2 + v_z^2}}{\lambda}\cos\phi_M \sqrt{\dfrac{1}{2} + \dfrac{R_T - L_M \sin\theta_T}{2\sqrt{R_T^2 + L_M^2 - 2R_T L_M \sin\theta_T}}}
\end{bmatrix}
$$

$$(2.23)$$

The range-velocity estimation problem can be expressed as,

$$\widehat{\boldsymbol{\rho}} = \min_\rho \|\boldsymbol{Z} - \boldsymbol{\psi}(\boldsymbol{\rho})\| \qquad (2.24)$$

We solve the optimization problem of (2.24) by using the Trust-Region-Reflective algorithm (Sorensen, 1982). The real-time estimate of target position is forwarded to the GDOP based multilateration process in order to optimize the receiver locations for better target positioning accuracy.

2.5.2 GDOP-based receivers placement strategy

GDOP is a vital metric, which indicates the efficacy of the sensor network topological distribution in aiding the geolocation process as detailed in works like (Sharp et al., 2009); (Chen et al., 2009). Large GDOP values correspond to a poor geometry topology, which will result in poor geolocation performance. Hence, an optimization algorithm is necessary to determine the best set of the sensor locations to be utilized in order to aid the target

geolocation process. This optimization would be dynamic and dependent on the current target estimate generated by the LS geolocation process, which has been detailed in the previous section.

The position of the target according to different sensor receivers in the multistatic topology has a crucial impact on the accuracy of target estimation capabilities of the system. Such effects are prominent when the target is very close to or on the bistatic baseline.

In our work context, we assume that the receivers are able to move so that real-time optimal locations could be chosen for better target estimation accuracy. To do so, we devise a multistatic GDOP based optimization approach, which is detailed as follows:

We can express the relationships between the measurement vector and the target parameters as:

$$Z = F(\zeta) + \eta \tag{2.25}$$

Where $Z = [r_1, ..., r_M, f_1, ..., f_M]^T$ is the measurement vector composed of radar range measurements r_i and Doppler shift measurements f_i, $\zeta = [x, y, z]^T$ is the vector of unknown target position coordinates and η is the measurement noise vector.

In case of a single extended target and the general case of M receivers, we have:

$$F(\zeta) = \begin{bmatrix} F_1 \\ F_2 \\ \vdots \\ \vdots \\ F_M \\ F_{M+1} \\ F_{M+2} \\ \vdots \\ F_{2M} \end{bmatrix}$$

$$= \begin{bmatrix} \sqrt{R_T \times R_{r1}} \\ \sqrt{R_T \times R_{r2}} \\ \vdots \\ \sqrt{R_T \times R_{rM}} \\ 2\dfrac{v}{\lambda}\cos\phi_1 \sqrt{\dfrac{1}{2} + \dfrac{R_T - L_1 \sin\theta_T}{2\sqrt{R_T^2 + L_1^2 - 2R_T L_1 \sin\theta_T}}} \\ 2\dfrac{v}{\lambda}\cos\phi_2 \sqrt{\dfrac{1}{2} + \dfrac{R_T - L_2 \sin\theta_T}{2\sqrt{R_T^2 + L_2^2 - 2R_T L_2 \sin\theta_T}}} \\ \vdots \\ 2\dfrac{v}{\lambda}\cos\phi_M \sqrt{\dfrac{1}{2} + \dfrac{R_T - L_M \sin\theta_T}{2\sqrt{R_T^2 + L_M^2 - 2R_T L_M \sin\theta_T}}} \end{bmatrix}$$

$$(2.26)$$

And the noise column vector is expressed as:

$$\eta = \begin{bmatrix} \eta_{r1} \\ \eta_{r2} \\ \cdot \\ \cdot \\ \eta_{rM} \\ \eta_{f1} \\ \eta_{f2} \\ \vdots \\ \eta_{fM} \end{bmatrix}$$

$$(2.27)$$

We define the noise covariance matrix $\chi = E[(\eta - E[\eta])(\eta - E[\eta])^T]$. In order to derive the GDOP for the LS geolocation process F, it is essential to linearize F by expanding it in a Taylor series about a reference vector $\zeta_0 = [x_0, y_0, z_0]^T$. ζ_0 should be sufficiently close to the actual ζ (could be an estimate of ζ determined from previous iteration).

$$\boldsymbol{F}(\boldsymbol{\zeta}) = \boldsymbol{F}(\boldsymbol{\zeta_0}) + \boldsymbol{\Gamma}(\boldsymbol{\zeta} - \boldsymbol{\zeta_0}) \qquad (2.28)$$

Where $\boldsymbol{\Gamma}$ is the $2M \times 3$ matrix of derivatives evaluated at $\boldsymbol{\zeta_0}$.

$$\boldsymbol{\Gamma} = \begin{bmatrix} \left.\dfrac{\partial F_1}{\partial x}\right|_{\zeta_0} & \left.\dfrac{\partial F_1}{\partial y}\right|_{\zeta_0} & \left.\dfrac{\partial F_1}{\partial z}\right|_{\zeta_0} \\[2ex] \left.\dfrac{\partial F_2}{\partial x}\right|_{\zeta_0} & \left.\dfrac{\partial F_2}{\partial y}\right|_{\zeta_0} & \left.\dfrac{\partial F_2}{\partial z}\right|_{\zeta_0} \\[2ex] \vdots & \vdots & \vdots \\[2ex] \left.\dfrac{\partial F_M}{\partial x}\right|_{\zeta_0} & \left.\dfrac{\partial F_M}{\partial y}\right|_{\zeta_0} & \left.\dfrac{\partial F_M}{\partial z}\right|_{\zeta_0} \\[2ex] \left.\dfrac{\partial F_{M+1}}{\partial x}\right|_{\zeta_0} & \left.\dfrac{\partial F_{M+1}}{\partial y}\right|_{\zeta_0} & \left.\dfrac{\partial F_{M+1}}{\partial z}\right|_{\zeta_0} \\[2ex] \left.\dfrac{\partial F_{M+2}}{\partial x}\right|_{\zeta_0} & \left.\dfrac{\partial F_{M+2}}{\partial y}\right|_{\zeta_0} & \left.\dfrac{\partial F_{M+2}}{\partial z}\right|_{\zeta_0} \\[2ex] \vdots & \vdots & \vdots \\[2ex] \left.\dfrac{\partial F_{2M}}{\partial x}\right|_{\zeta_0} & \left.\dfrac{\partial F_{2M}}{\partial y}\right|_{\zeta_0} & \left.\dfrac{\partial F_{2M}}{\partial z}\right|_{\zeta_0} \end{bmatrix}$$

$$(2.29)$$

The noise elements composing η are assumed independent and identically distributed zero mean Gaussian random variables. Thus, the matrix $\boldsymbol{\chi}$ is diagonal with non-zero diagonal elements.

The maximum likelihood or LS estimator for the linearized model is given by (Torrieri, 1984):

$$\hat{\zeta} = \zeta_0 + (\boldsymbol{\Gamma}^T \boldsymbol{\chi}^{-1} \boldsymbol{\Gamma})^{-1} \boldsymbol{\Gamma}^T \boldsymbol{\chi}^{-1} (\boldsymbol{Z} - \boldsymbol{F}(\zeta_0)) \tag{2.30}$$

The covariance matrix of the target parameters estimate vector $\hat{\zeta}$ is computed in (Torrieri, 1984) as:

$$\boldsymbol{P} = E[(\hat{\zeta} - E[\hat{\zeta}])(\hat{\zeta} - E[\hat{\zeta}])^T] = (\boldsymbol{\Gamma}^T \boldsymbol{\chi}^{-1} \boldsymbol{\Gamma})^{-1} \tag{2.31}$$

Finally, the GDOP is defined as $\sqrt{trace[\boldsymbol{P}]}$.

The choice of the appropriate locations of the radar receivers is carried out by minimizing the GDOP at the actual target estimate obtained from the LS geolocation algorithm. Let us denote by Y_i the 3D space where the ith receiver could be located in. Moreover, let the optimum set of receiver locations be represented as $\Lambda = [x_1, y_1, z_1 \ldots, x_M, y_M, z_M]$. Consequently, the minimization problem, which estimates the optimum set of receiver locations Λ for better target positioning accuracy, can be formulated as:

$$\widehat{\Lambda} = \min_{(x_i, y_i, z_i) \in Y_i} GDOP_{(\hat{x}_a, \hat{y}_a, \hat{z}_a)} \tag{2.32}$$

Where (x_i, y_i, z_i) are the ith receiver coordinates and $[.]_{(\hat{x}_a, \hat{y}_a, \hat{z}_a)}$ represents the GDOP evaluation at the actual target position estimate, which is obtained from the LS geolocation process. Several non-linear minimization algorithms could be used to solve the optimization problem in (2.32). One of them is the interior-point method (Waltz et al., 2006).

From practical perspective, the update of the radar receivers placement based on the proposed approach in (2.32) is only carried out when the target positioning error starts to be high and a time interval is elapsed from the last update.

2.6   Simulation results

In order to validate the proposed approach, a multistatic radar topology of one stationary transmitter and three widely spaced receivers is adopted for all the numerical examples. The transmitter is considered as the reference point and the origin of the system coordinates. We also consider a Swerling I extended target, which consists of seven closely-spaced scatterers moving at the same velocity. The range extent of the target is proportional to the system range resolution, which is the basic condition for extended target consideration as mentioned in (Bell., 1993).

2.6.1 Range-Doppler responses

Figures 2.2, 2.3 and 2.4 show different range-Doppler plots when an arbitrary waveform from the Hadamard phase-coded waveforms set is selected and transmitted. The bistatic range extents of the slow-moving extended target relative to different receivers are: [75.8 m , 76.7 m] relative to the transmitter-receiver 1 pair, [56.5 m , 56.75 m] relative to the transmitter-receiver 2 pair and [53.13 m , 54.28 m] relative to the transmitter-receiver 3 pair.

A stationary extended clutter is also present as shown in Figures 2.2, 2.3 and 2.4, its bistatic range extents are given by: [23.84 m , 24.66 m] relative to the transmitter-receiver 1 pair, [28.46 m , 29.31 m] relative to the transmitter-receiver 2 pair and [17.71 m , 18.09 m] relative to the transmitter-receiver 3 pair. The Signal-To-Clutter ratio (SCR) is assumed the same at each receiver and equal to 13.97 dB. An Additive White Gaussian Noise (AWGN) is added to the received signals prior to match filtering. The SNR at each receiver is chosen to be 26.98 dB. This value is justified by the high transmitted power from the radar.

As seen from Figures 2.2, 2.3 and 2.4, using Hadamard sequences of sufficient length (N = 512) allows us to have higher integration time, which results in better Doppler resolution. This value is chosen as a trade-off to yield the required Doppler resolution while avoiding long integration time. Nevertheless, due to the nature of the transmitted waveform (i.e., a train of phase-coded pulses), additional peaks nearby the target responses are generated from range sidelobes. We have noticed that these peaks are at least 20 dB lower than the target responses and they have a low impact on the target detection performance (the detection threshold γ is adjusted accordingly) as validated by the detection results in the following section.
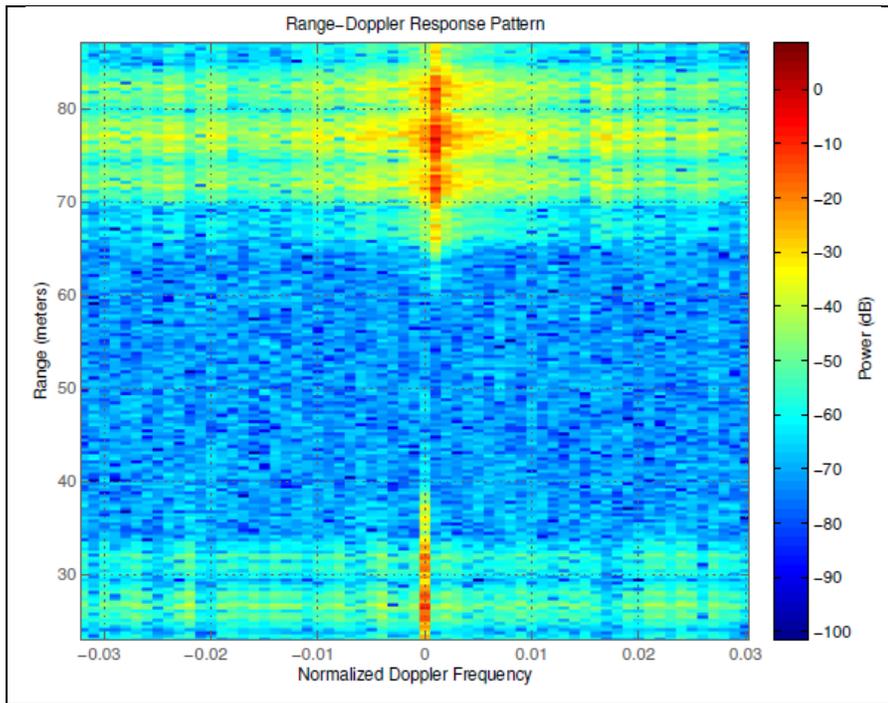
Figure 2.2 Bistatic range-Doppler map at receiver 1
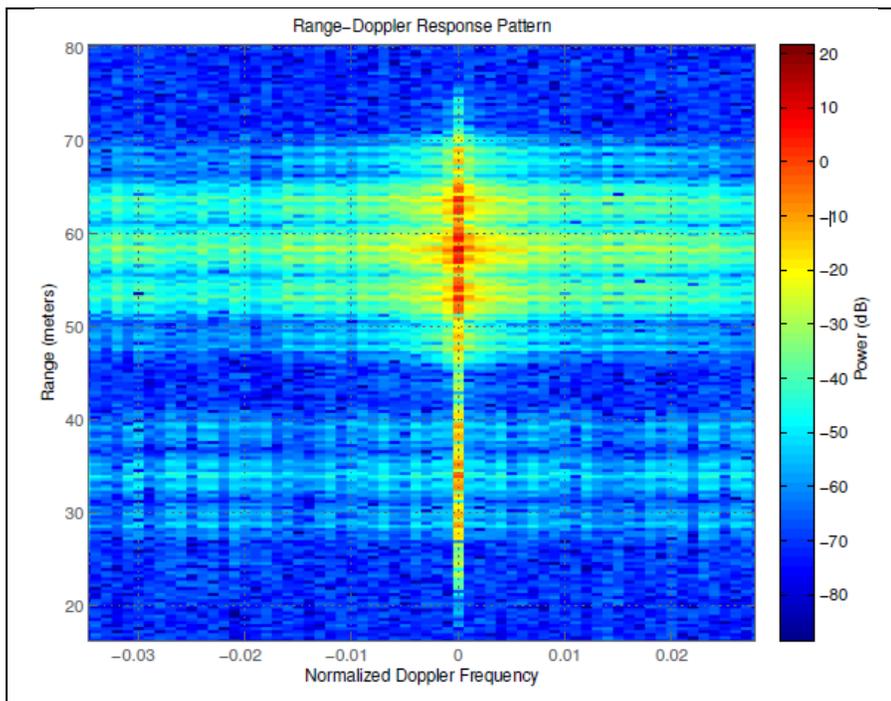
Figure 2.3 Bistatic range-Doppler map at receiver 2
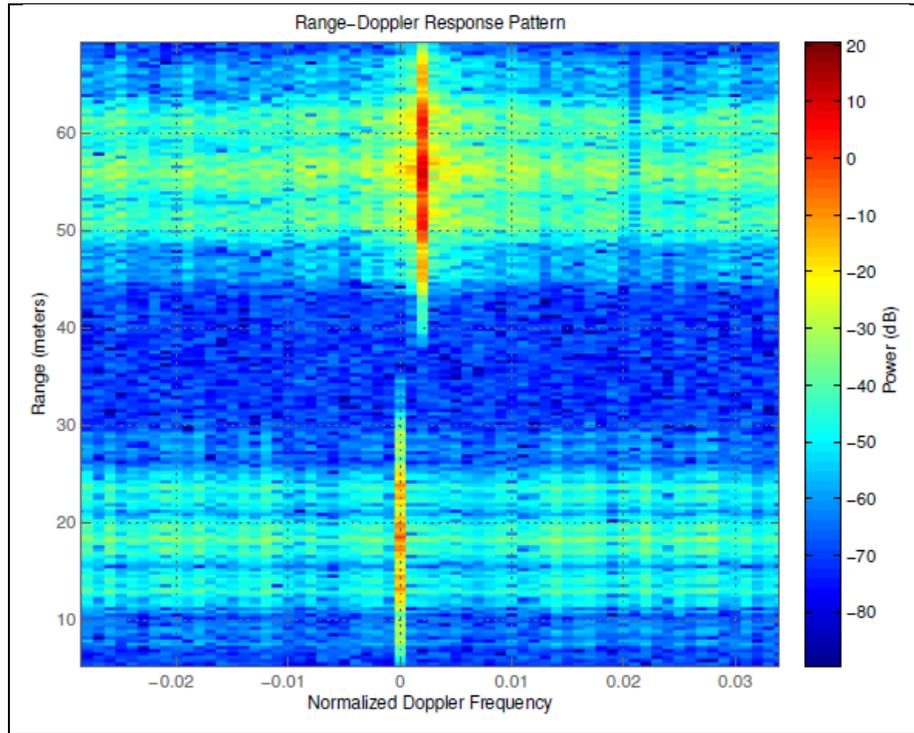
Figure 2.4 Bistatic range-Doppler map at receiver 3

2.6.2 Probability of target detection

Figure 2.5 depicts the probability of target detection in the presence of AWGN and clutter interference. The SCNR expressed in (2.18) is used to evaluate the probability of target detection, since this expression takes into account the extended target impulse responses and scattering characteristics, in addition to clutter and noise covariance.

For each value of SCNR, the threshold γ is computed in order to ensure a fixed probability of false alarm equal to 10^{-5} then the probability of detection is computed based on (2.14). In the simulations context, we assume that all the three receivers have the same SCNR.

In Figure 2.5(a), we compare the values of the probability of detection for the cognitive selection of waveforms that maximize the probability of detection to the values for an

arbitrary static waveform. As the proposed approach adapts the choice of waveform to the dynamic scene (i.e., the target RCS fluctuations and the clutter distribution), better detection performances are illustrated compared to the static assignment case where the waveform is unable to match the time-varying target response. For instance, the proposed approach achieves a probability of detection of 0.82 compared to 0.75 when a static waveform is used, for a given SCNR of 10 dB.

Figure 2.5(b) depicts the gain in target detection when multiple spatially separated receivers are used compared to a single receiver case. An improvement in the probability of target detection is illustrated for increased number of receivers as predicted from (2.14) where we clearly see the spatial diversity contribution of the multistatic topology in detection performances. As shown in Figure 2.5(b), the use of $M=6$ receivers allows to reach a probability of detection equal to 1 compared to 0.94 in the case of $M=3$ receivers, and 0.45 in the case of $M=1$ receivers, for a given SCNR of 10 dB.
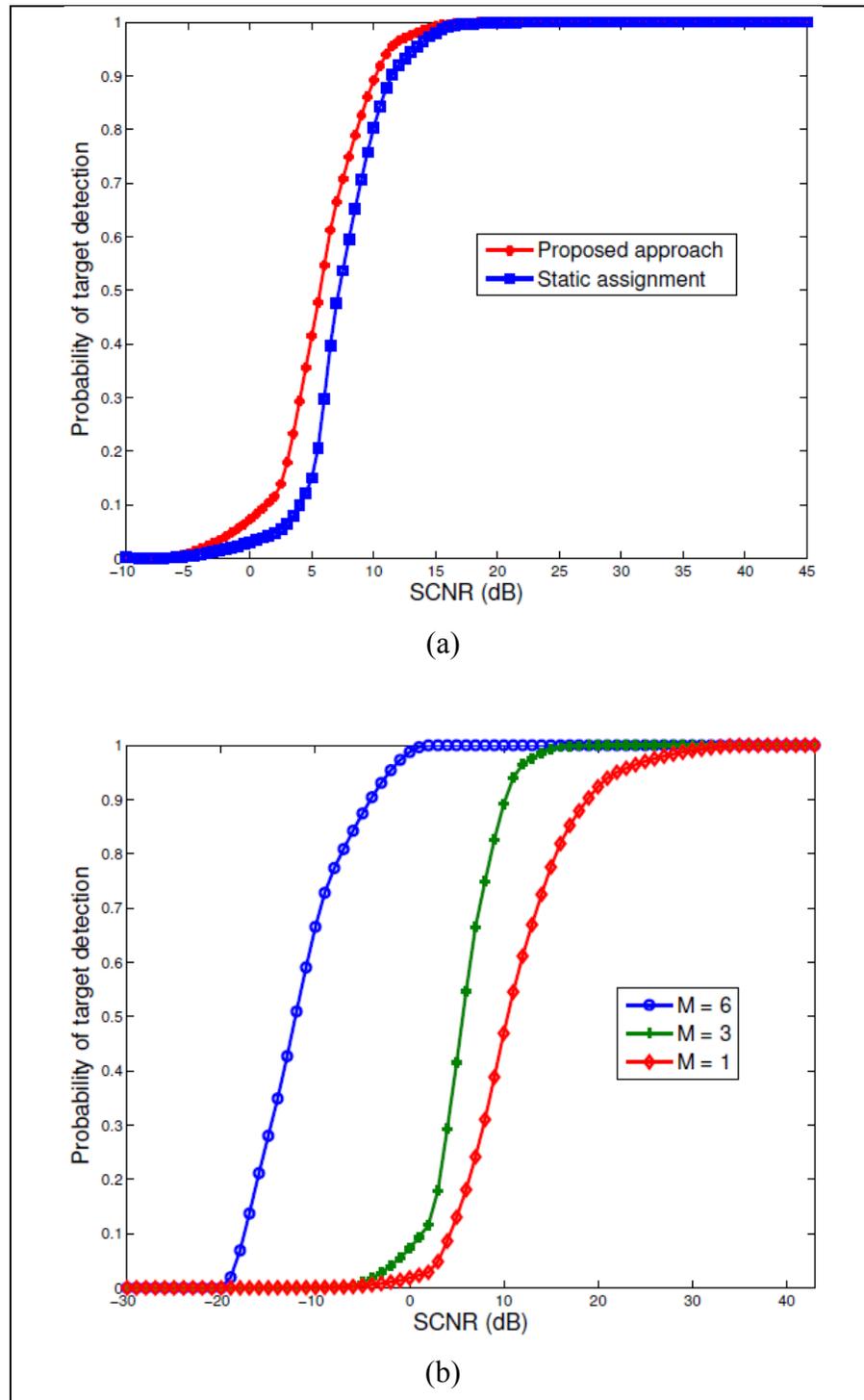
Figure 2.5 (a) Probability of target detection for waveform selection approach and static waveform assignment, (b) Probability of target detection for waveform selection approach with different number of receivers (M = 1, 3 and 6)

2.6.3 LS geolocation process

Figure 2.6 shows the Cumulative Distribution Function (CDF) of the target absolute position error in both cases where static receiver locations are used and GDOP based receiver locations update is applied (*M=3* radar receivers). The CDF curves are obtained by simulating different values of the target position over an entire area of 150 m × 150 m and storing the estimated values by the LS geolocation process. The error is computed as the Euclidean distance between the true and the estimated values. We can notice that better target positioning accuracy is achieved by the receivers placement update mechanism compared to the case of static receivers. In fact, the target positioning error is 90% less than or equal to 0.1 m when the proposed GDOP based receiver locations update process is used compared to a target positioning error which is 90% less than or equal to 0.6 m when static receivers locations are used.
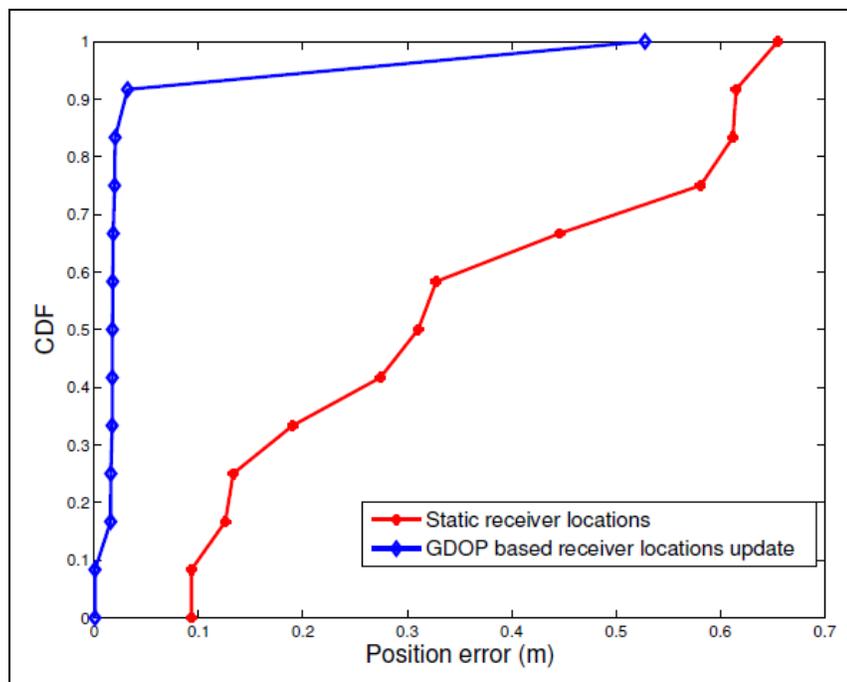
Figure 2.6 CDF of the target position estimate error for M=3 radar receivers

2.6.4 GDOP-based receiver locations update

Figure 2.7 shows the improvement in GDOP values as a function of the number of algorithm iterations considering the GDOP minimization problem of (2.32). The locations of different receivers are first chosen randomly, then we run the GDOP minimization algorithm according to the current target position estimate. All along the processing duration, the algorithm search iteratively for the optimal receiver locations that minimize the GDOP value within specific error tolerance constraints. As we can see from Figure 2.7, the achieved GDOP value is less than 1 m starting from the 17th iteration.

Figure 2.8 shows the receiver positions computed by the GDOP optimization process at iterations 1, 5, 10, 15 and 20 (the index "i" refers to iteration count) as depicted in Figure 2.7. The transmitter is placed at the origin and the target position is kept the same during the iterative GDOP optimization process (the optimization process lasts only few milliseconds. During this time interval, the target is kept in the same range bin and thus could be considered as not moving). Figure 2.8(b) shows the 2-D projection for receiver location updates over iterations onto the x-y plane.
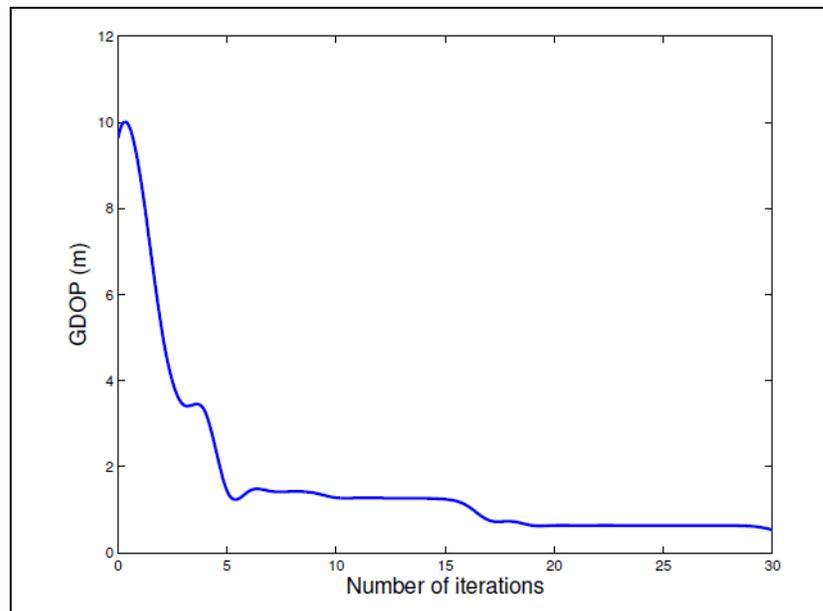
Figure 2.7 GDOP iterative minimization process
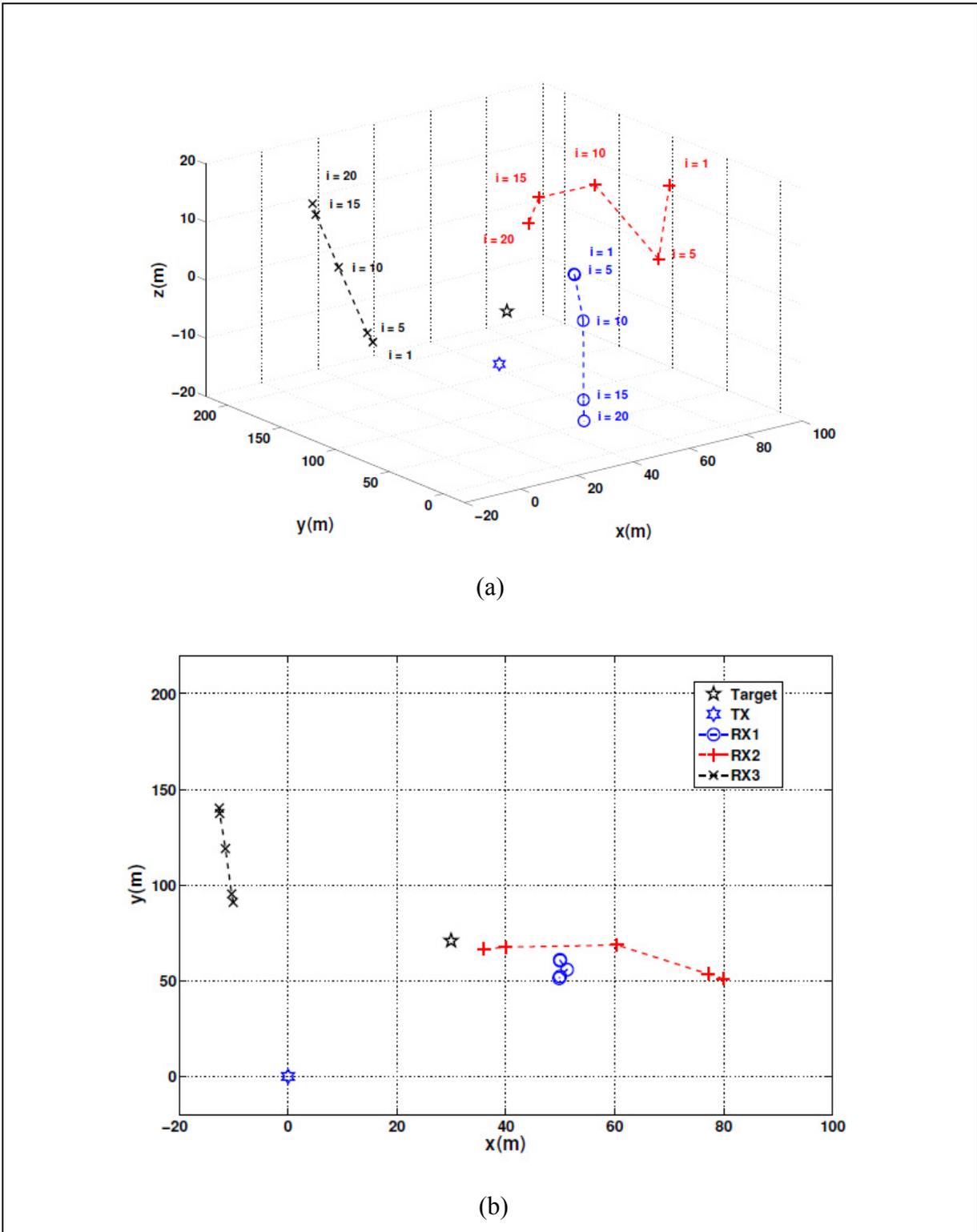
Figure 2.8 (a) 3-D receiver location updates over iterations, (b) 2-D projection for receiver location updates over iterations

2.6.5 Joint approach detection performance

Figure 2.9 depicts the Receiver Operating Characteristics (ROC) curves in both cases where only waveform selection based on detection maximization process is carried out, and the proposed approach of waveform selection based on detection maximization in conjunction with adaptive receiver locations selection mechanism is used. We deliberately choose low SCNR values at different receivers in order to study the impact of the adaptive receiver allocation on the overall system detection performances (the chosen SCNR is equal to -5 dB at each receiver). Low SCNR values cause a drop on the detection performances, but as we can see from Figure 2.9, the GDOP based receiver locations update process allows a better target positioning accuracy, which results in detection performance enhancement.
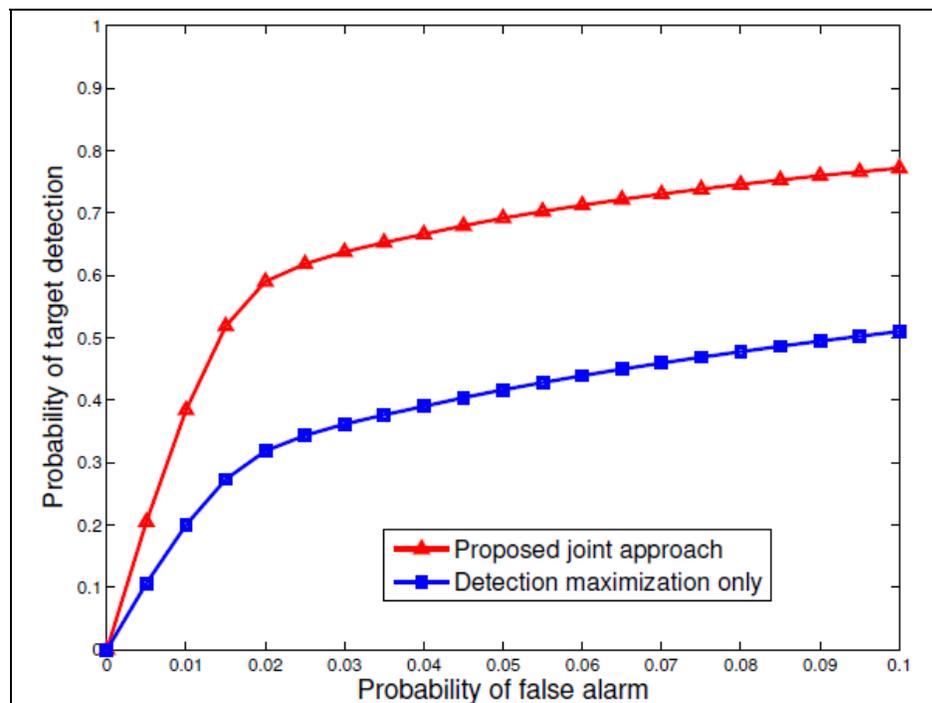
Figure 2.9 Low SCNR ROC curves for the proposed approach and the detection maximization process

2.6.6   Multistatic ambiguity function

The Ambiguity Function (AF) is a practical tool to verify the suitability of the transmitted waveforms to the system requirements. In fact, the capability of the radar system to resolve two present targets is determined by the half-power width of the ambiguity function main lobe, while the accuracy of a specific target estimation is dictated by the sharpness of the main lobe (Skolnik, 2001).

In bistatic configuration, the relationships between delay-Doppler and range velocity pairs are non-linear (Yang et al., 2006). If the transmitter is chosen as the reference point, the bistatic AF can be expressed as (Tsao et al., 1997):

$$
\begin{aligned}
\theta(R_{T_h}, & R_{T_a}, V_h \cos\phi, V_a \cos\phi, \theta_T, L) \\
&= \left| \int_{-\infty}^{+\infty} s(t - \tau_a(R_{T_a}, \theta_T, L)) s^*(t - \tau_h(R_{T_h}, \theta_T, L)) \right. \\
&\quad \left. \times \exp[-j\left(f_h(R_{T_h}, V_h \cos\phi, \theta_T, L) - f_a(R_{T_a}, V_a \cos\phi, \theta_T, L)\right) t] dt \right|^2
\end{aligned}
$$

$$(2.33)$$

where the subscripts a and h are used to denote respectively the actual and the hypothesized values of the parameter associated with the target, f is the bistatic Doppler shift already expressed in (2.21) and τ is the bistatic delay expressed as (Tsao et al., 1997):

$$
\tau(R_T, \theta_T, L) = \left[R_T + \sqrt{R_T^2 + L^2 - 2R_T L \sin\theta_T} \right] / c
$$

$$(2.34)$$

where c is the wave propagation speed.

We can notice from (2.21), (2.33) and (2.34) that the bistatic AF depends on the bistatic geometry in addition to the transmitted waveform. In case of multiple widely-spaced

receivers and fluctuating extended target, the signal fluctuations are independent at different receivers and the notion of multistatic AF is defined according to (Bradaric et al., 2006); (Derham et al., 2010) as a weighting combination of bistatic ambiguity functions related to different transmitter-receiver pairs. The weights used to form the multistatic AF are directly related to the SCNR at each receiver (Bradaric et al., 2006); (Derham et al., 2010) and depend on the target scattering characteristics.

We consider a Swerling I extended target composed of seven powerful scattering points. The absolute range extent of the target is about $1\,m$, which is proportional to the radar range resolution (basic condition for extended target consideration). The target scattering center is located at $(30\,\text{m}, 71\,\text{m}, 0\,\text{m})$. We assume three receivers with equal SCNR.

We plot in Figure 2.10(a) the multistatic ambiguity function after applying the proposed approach: we jointly select the waveform that maximizes the multistatic probability of detection expression in (2.14) according to the estimated target impulse responses by matched filtering process, in addition to the clutter plus noise estimates. Meanwhile the receivers are moved to the optimal locations, which are dictated by the GDOP minimization process. The optimal receiver locations are computed according to the target scattering center estimate. On the other hand, we plot in Figure 2.10(b) the multistatic ambiguity function related to a random choice of waveform and receivers placement. It is clearly seen that the proposed cognitive approach offers more target accuracy (i.e., sharpness of the main lobe) than any random assignment of waveform and receiver locations.
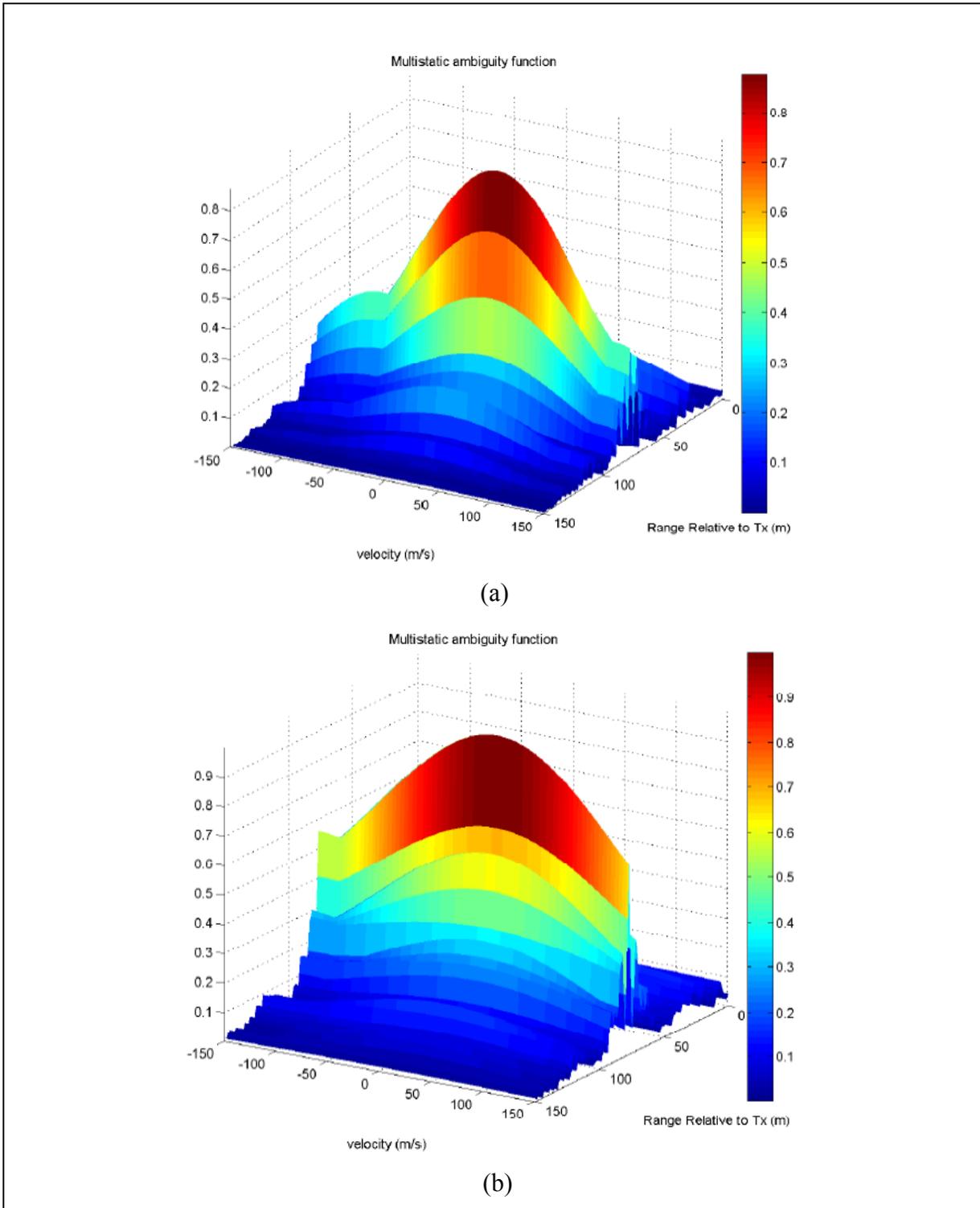
Figure 2.10 (a) Multistatic AF using the proposed approach, (b) Multistatic AF with a
random choice of waveform and receivers placement

2.7   Chapter summary

We have presented in this chapter a practical framework for joint cognitive waveform selection and adaptive GDOP based receiver locations update strategy in the context of changing environment (moving target and clutter). Relevant information about the real-time extended target impulse responses in addition to the clutter plus noise covariance estimates are processed by the central processor via matched filtering, each time backscattered signals are sent from different receivers. Maximization of the target probability of detection is carried out in the central processor to select the optimal waveform, meanwhile the target position estimate obtained from the LS geolocation algorithm is forwarded to a GDOP minimization process, which compute the optimal locations of the receivers that maximize the target positioning accuracy. The destined commands for the transmitter and the receivers are then sent simultaneously and the multistatic radar is able to quickly adapt to the dynamically changing environment.

From practical perspective, the update of the radar receivers placement based on the proposed approach is only carried out when the target positioning error starts to be high and a time interval is elapsed from the last update.

Optimal system performance is conditioned by synchronization between waveform selection and receivers placement strategy, which should be controlled at the processor level. The proposed approach leverages the benefits of multistatic topology, especially the spatial diversity and the wider coverage, to enhance the extended target probability of detection in the presence of clutter and noise. On the other hand, the receivers are able to move within specific areas to maximize the target positioning accuracy. From a practical point of view, the proposed approach is suitable for a moving multistatic platforms as is the case of Unmanned Aerial Vehicle (UAV) based multistatic topology, or moving radar platforms during tactical military missions.

In the next chapter, we leverage the spatial diversity offered by multistatic radar in the context of joint radar and communication operation, wherein several communication nodes in a network operate separately in frequency. The aim is to propose a novel joint radar and communication architecture based on cooperative scheme to optimize the radar operation.

CHAPTER 3

JOINT OFDM RADAR AND COMMUNICATION SYSTEM DESIGN AND APPLICATIONS

In this chapter, the channel statistics are of crucial importance for both radar and communication operation. In a scenario, where multiple nodes are able to communicate with each other, the presence of multiple objects in the environment can introduce relevant information in terms of channel characteristics. This information could jointly be leveraged from a communication point of view for better demodulation performance, and also for improvement of radar sensing capabilities. In this chapter, we consider the presence of multiple communicating nodes and multiple objects (especially, targets and clutters) in the environment. We examine the relationship between channel average Peak to Average Power Ratio (PAPR) and the resolvability of received components and we demonstrate that the bistatic radar performance could be improved at each node level by enabling radar processing on the bistatic stream exhibiting the highest PAPR value.

3.1   Introduction

Joint radar and communication operation has been increasingly encouraged in last years. The motivation behind such dual functionality is essentially related to the spectrum sharing supported by incremental similarities between carrier frequencies of radar and communication functions (Sturm & Wiesbeck, 2010). Radar and communication bandwidth sharing dictates the design of new mechanisms for simultaneous dual processing tasks. Incorporating communication as secondary to the primary radar function is reported in a number of papers (Euziere et al., 2014); (Hassanien et al., 2015); (Blunt & Yantham, 2007). Recent contributions such as (Chiriyath et al., 2015); (Paul et al., 2016); (Chiriyath & Bliss, 2015); (Chiriyath et al., 2016); (Masarik & Subotic, 2016) consider the coexistence of both radar and communication systems as source of interference and investigate cooperative signalling schemes by proposing novel waveform spectrum design approaches.

In a multi-node scenario, each node is able to sense the environment while decoding the information gathered from other communicating nodes. Communication information received from other nodes could be leveraged for bistatic radar processing since each transmitted remote signal will experience reflections by targets and clutters in the environment. As a result, each received communication stream will be composed of the direct communication link, if Line of Sight (LOS) condition is present, in addition to multiple backscattered versions of the signal by the objects in the environment.

In this chapter, we are interested in joint radar and communication operation, where the communication part can help the radar block to select the best bistatic stream in terms of channel statistics among a multiplicity of orthogonal streams. We study the analytical relationship between the channel PAPR and the resolvability of the received components from a radar point of view. The proposed architecture offers significant benefits in target detection by taking advantage of the multi-look diversity of the distributed system.

3.2 System architecture

Consider a joint radar and communication architecture in a multi-node environment, where several nodes can transmit data simultaneously to other nodes. To ensure multi-user communication system operability, we use a spectrally-interleaved multi-carrier scheme initially proposed in (Sturm, 2013). In this scheme, the total amount of available sub-carriers is distributed among different users in an interleaved way, where successive sub-carriers are assigned to different users in a cyclic manner (Sturm, 2013). Among the reserved sub-carriers per user, few of them are used as private pilots for channel estimation purpose and the remaining sub-subcarriers are used for user data transmission. Following the described transmission scheme, the frequency diversity per user is optimized by maximizing the separation between the sub-carriers allocated to the same user. In addition, the highest range resolution of the full system bandwidth is achieved, while enabling the simultaneous operation of multiple transmitters (Sturm, 2013). Each node is also a monostatic radar composed of collocated transmitter and receiver. As a result, the multi-node communication

network operates at the same time as a distributed radar sensor network. In fact, each node is able to communicate with some other remote nodes while doing its radar processing tasks. The nodes are synchronized in frequency by a common 10 MHz signal and in time by a common Pulse Per Second (PPS) signal. In addition, the transmitter and receiver parts inside each node are synchronized with the same internal clock.
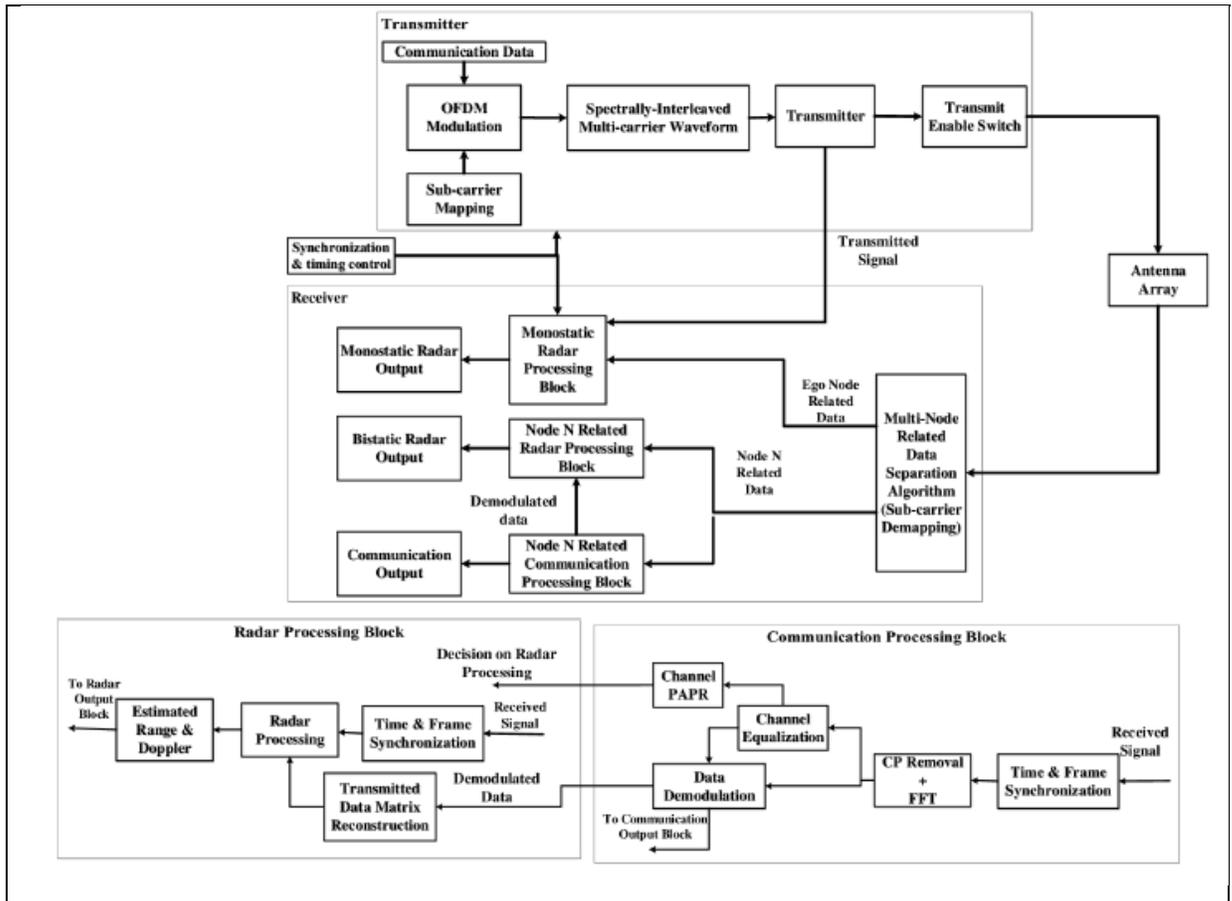

Figure 3.1 Node architecture

3.3   Channel PAPR selection mechanism

We consider the spectrally-interleaved multi-carrier scheme initially proposed in (Sturm, 2013). The total amount of available sub-carriers is distributed among different users in an interleaved way. We illustrate each node transceiver architecture in Figure 3.1. Each node is

able to send its own multi-carrier waveforms to other communicating nodes in the network following the sub-carrier mapping scheme. Among the sub-carriers reserved to a specific node, some sub-carriers are used to send reference signals as pilots specific to each user. The pilot sub-carriers are distributed over the reserved frequencies at each transmitter level following the comb-type pattern design (Shen & Martinez, 2013). This pattern is well suited to fast varying environments, when proper equalization is carried out at each symbol period level. In addition, the repartition of the pilot signals over the sub-carriers takes into consideration the system coherence bandwidth in order to allow for the flat fading assumption to be valid between successive pilot repartitions for proper channel estimation and correct recovery of data at the receiver. In the context of this work, the channel is assumed slow-fading during the OFDM frame. It should be noted that each node should send his own reference signals to the receiving node for proper channel estimation. Therefore, specific reference signals used by each node are well known by the other communicating nodes. The remaining sub-carriers per node are used for data transmission. We assume the presence of P nodes. A transmitted frame from the Pth node is composed of M_s OFDM symbols and expressed as (Sturm, 2013):

$$s_p(t) = \sum_{k=0}^{M_s-1} \sum_{i=0}^{N_p-1} d_{ikp} \, exp\big(2\pi j f_{i,p} t\big) \, g(t - kT_s) \qquad (3.1)$$

Where $s_p(t)$ is the transmitted OFDM frame of the pth node. N_p frequencies out of the total N_c sub-carriers are reserved to the pth node in order to transmit its data plus its own reference signals (i.e., $N_P = \frac{N_c}{P}$). T_s is the elementary OFDM symbol duration, $f_{i,p} = (p - 1 + iP)\Delta f$ is the ith reserved frequency to the pth node for data or reference signal transmission. Δf is the sub-carrier spacing, which is chosen a lot larger than the Doppler spread to ensure that the Doppler shift does not destroy orthogonality between sub-carriers, d_{ikp} is the modulated data symbol or reference symbol related to the ith sub-carrier, k^{th} OFDM symbol and the pth node. Finally, $g(t)$ is the rectangular filter of duration T_s.

The complete set of the system transmission parameters is shown in Table 3.1. The choice of parameter values is motivated by the characteristics of the propagation environment and dictated by the following conditions:

1) T_G is chosen larger than the maximum excess delay in the environment.

2) The sub-carrier spacing Δf is smaller than the coherence bandwidth for flat fading consideration at each sub-carrier level. In addition, Δf should be a lot larger than the Doppler spread to ensure that the Doppler shift does not destroy orthogonality between sub-carriers.

3) The coherence time i.e., the time over which a channel can be assumed approximately constant, easily exceeds the elementary OFDM symbol duration T_s.

Table 3.1 Transmission parameters

Symbol	Parameter	Value
f_c	Carrier Frequency	24 GHz
N_c	Total Number of Sub-carriers	1024
M_s	Frame Length	512
T_s	Elementary OFDM Symbol duration	11 us
T_G	Cyclic Prefix Duration	1.375 us
$T = T_s + T_G$	Total OFDM Symbol Duration	12.375 us
BW	Overall System Bandwidth	93.1 MHz
ΔR	Radar Resolution	1.61 m
Δf_D	Doppler Resolution	157 Hz

It should be noted that the unambiguous range of the spectrally-interleaved multi-carrier scheme is reduced by a factor of P (Sturm, 2013). This reduction is a limitation in our work. However, its value is still superior to the minimum desirable value when the system parameters of Table 3.1 are used and a maximum of $P = 8$ transmitters are simultaneously active.

We consider the receiver platform of a remote ego node as depicted in Figure 3.1. The pth bistatic pair refers to the pair composed of the pth remote transmitting node and the ego node receiver. We assume the presence of $P - 1$ transmitting nodes in addition to the ego node. Orthogonal streams composing the received signal and relative to different nodes are separated at the ego receiver. Backscattered signals, relative to the ego transmitter, are directly fed to a monostatic radar processing block. On the other hand, each received bistatic stream is fed to distinct communication and radar blocks for processing as depicted in Figure 3.1.

At each communication block, after cyclic prefix removal and FFT operation, the LS estimates of the channel conditions at the pilot sub-carriers are computed, then used to estimate the channel conditions at the data sub-carriers by the mean of Low-Pass Interpolation (LPI) technique at every OFDM symbol duration. This type of interpolation is known for good computational complexity and performance trade-off (Shen & Martinez, 2013). Then, we use the channel estimates at the data sub-carriers to compensate for the channel effects at data symbols level. The final step is to demodulate the data.

The LS frequency-domain channel transfer function samples at pilots are estimated during channel equalization by proceeding to an element-wise division between the received and the transmitted reference data matrices (Sturm, 2013). In case a LOS component is present, its contribution at the channel transfer function at pilots could be easily compensated for as the position and velocities of different nodes are assumed known at each instant (each node will transmit information regarding his current position while sending the other communication

information to the receiving node). At the final step, we obtain the frequency-domain channel transfer function samples $H_p(n, k)$ at pilot sub-carriers and relative to the pth bistatic pair:

$$H_p(n, k) = \sum_{l=0}^{L_p} b_{p,l} \, exp\left(-2\pi j f_{n,p} \frac{R_{tot_{l,p}}}{c_0}\right) exp\left(2\pi j f_{D_{p,l}} kT\right) \tag{3.2}$$

Where L_p is the number of received components relative to the pth bistatic pair, $b_{p,l}$, $R_{tot_{l,p}}$ and $f_{D_{p,l}}$ are respectively the path attenuation, the total path distance and the Doppler shift related to the lth received component and p^{th} bistatic pair, $f_{n,p}$ is the nth reserved pilot frequency to the pth node, c_0 is the wave propagation speed and T is the total OFDM symbol duration. We consider the point-scatterer model, where we assume the presence of point targets and clutters in the environment. The multipath components originated from multiple reflections in the environment arrive very attenuated at the receiver, and therefore are ignored for clarity.

The channel estimate at pilot sub-carriers could be used to give insight into how much multiple received components are resolvable.
To do so, we define the channel PAPR as:

$$PAPR_H = \frac{|H|^2_{Peak}}{(|H|_{rms})^2} \tag{3.3}$$

where the nominator is the peak value of the frequency-domain channel power samples at pilot sub-carriers $|H|^2$ and the denominator is the average frequency-domain channel power at pilot sub-carriers. PAPR values are superior or equal to 1. In fact, the worst case (PAPR =1) would apply when all the received components in (3.2) are superimposed in delays, Doppler shift and magnitudes.

The real part of the expression of the channel transfer function samples in (3.2) is a summation over the number of received components L_p of independent and identically distributed random variables (for a specific p^{th} bistatic pair, we assume that $b_{p,l}$ are identically distributed). From the central limit theorem, the real part of $H_p(n,k)$ follows a normal distribution with zero mean and a variance $\sigma_p^2 = \frac{\sum_{l=1}^{L_p} E[b_{p,l}^2]}{2} = \frac{L_p E[b_{p,l}^2]}{2}$. The same case is concluded for the imaginary part of $H_p(n,k)$. Since the real and imaginary parts of $H_p(n,k)$ are also uncorrelated, the square magnitude $|H_p(n,k)|^2$ follows an exponential distribution:

$$f\left(|H_p(n,k)|^2\right)(h) = \frac{1}{\alpha} exp\left\{-\frac{h}{\alpha}\right\}, h > 0$$

(3.4)

Where the variance $\sigma_{p_{|H|^2}}^2$ of $|H_p(n,k)|^2$ is:

$$\sigma_{p_{|H|^2}}^2 = (2\sigma_p^2)^2 = (L_p E[b_{p,l}^2])^2 = (L_p(\sigma_{b_{p,l}}^2 + (E[b_{p,l}])^2))^2$$

(3.5)

From the expression in (3.5), we prove that the variance $\sigma_{p_{|H|^2}}^2$ depends on two factors when the pth remote transmitting node and the ego node receiver are in communication: L_p, which is the number of reflecting objects in the environment and the statistics of the path attenuation $b_{p,l}$ (i.e., its variance $\sigma_{b_{p,l}}^2$ and its mean).

More distinguishable received components specific to the pth bistatic communicating pair will arrive with higher difference in phases and magnitudes, which result in higher statistics

of $b_{p,l}$. From expression (3.5), it will result in higher variance of the channel transfer function samples, which leads to higher channel PAPR value.

Consequently, the communication processing block could decide whether to authorize the bistatic radar processing block to proceed based on the channel PAPR values as shown in Figure 3.1. In fact, by taking into consideration the presence of distinct orthogonal streams coming form different remote nodes, the bistatic radar processing could be carried out only on the stream showing the highest channel PAPR values, which results in better radar target resolution.

Once the bistatic stream with highest channel PAPR selected, we compute the element-wise division of the received modulation symbols matrix by the equivalent transmitted matrix at the radar processing block. Then we apply an FFT operation on each row of the obtained matrix followed by and IFFT operation on each column of the matrix resulting from the previous step (Sturm, 2013). The range and Doppler values are computed after peaks search approach on the magnitude squared final matrix. We apply an interference cancellation algorithm as in (Sit, 2012) if a LOS component is present in the chosen bistatic stream. We define the radar SNR ρ_{rad} as:

$$\rho_{rad} = \frac{M_s N_p L_p E[b_{p,l}^2]}{\sigma_{noise}^2} \tag{3.6}$$

where σ_{noise}^2 is the radar noise power, $M_s N_p$ is the radar processing gain and $\rho = \frac{E[b_{p,l}^2]}{\sigma_{noise}^2}$ is the average SNR per receive component after element-wise matrices division operation.

3.4 Simulation results

3.4.1 Radar range-Doppler responses

We consider the ego node in receive mode and two remote transmitting nodes ($P = 3$ in this case) in addition to the presence of three targets in the environment. Nodes and targets are moving with random relative velocities. For all the simulations, we use the transmission parameters of Table 4.1 and we consider a BPSK data modulation at each transmitter level. The targets are simulated with the same average Radar Cross Section (RCS) of $1\ m^2$.

We plot in Figure 3.2(a) and Figure 3.2(b) two bistatic range-Doppler maps related to each transmitter-ego receiver pair and generated from bistatic radar processing blocks. From Figure 3.2(a) and Figure 3.2(b), we notice better target resolution for the high PAPR channel case compared to the lowest case. Indeed, radar signatures of the three targets are discernible at the range-Doppler plot relative to the high PAPR channel. The three targets have been simulated with close velocity values. Nevertheless, in case of low PAPR channel, the signatures of the three targets arrive superimposed, which results in only one resolvable target signature at the correspondent range-Doppler plot.

The radar processing offers an additional processing gain related to information redundancy, which is inherent to the nature of OFDM signals.
We plot in Figure 3.3(a) the frequency-domain time average power samples at pilot sub-carriers of the channel exhibiting low PAPR and to which the range-Doppler map of Figure 3.2(a) is associated. Similarly Figure 3.3(b) represents the channel time average power samples relative to the range-Doppler map with high channel PAPR in Figure 3.2(b). Higher PAPR values mean high fluctuations of the channel power peak values compared to the average values, which are essentially due to better resolvability of received components originated from target reflections.
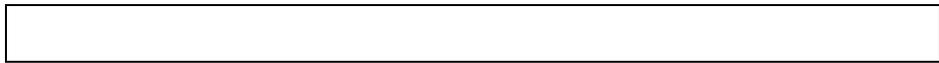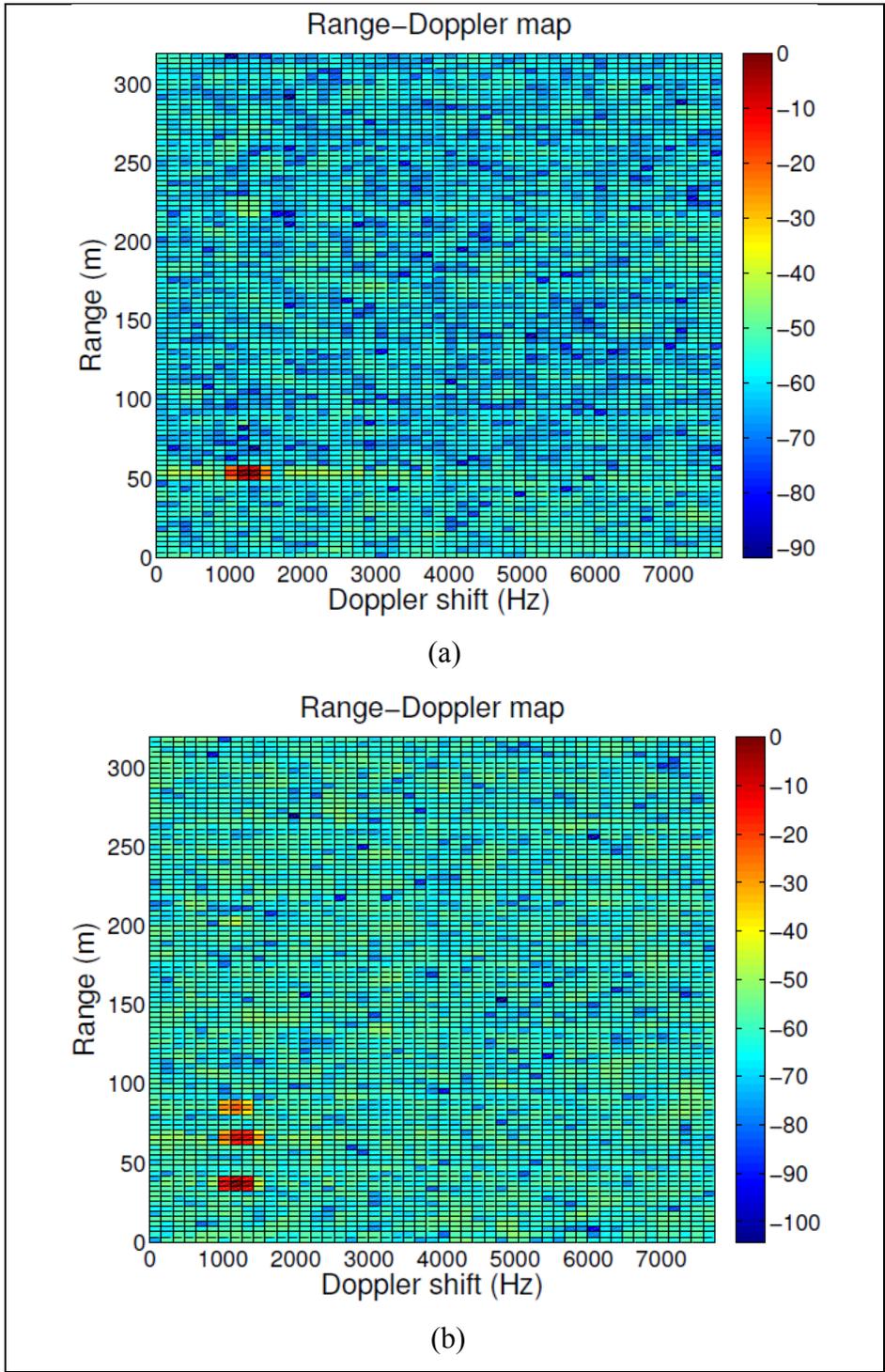
Figure 3.2 (a) Bistatic range-Doppler map (Low channel PAPR), (b) Bistatic range-Doppler map (High channel PAPR)
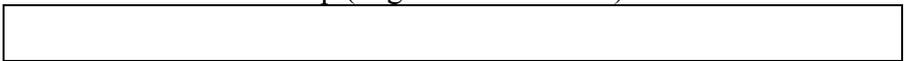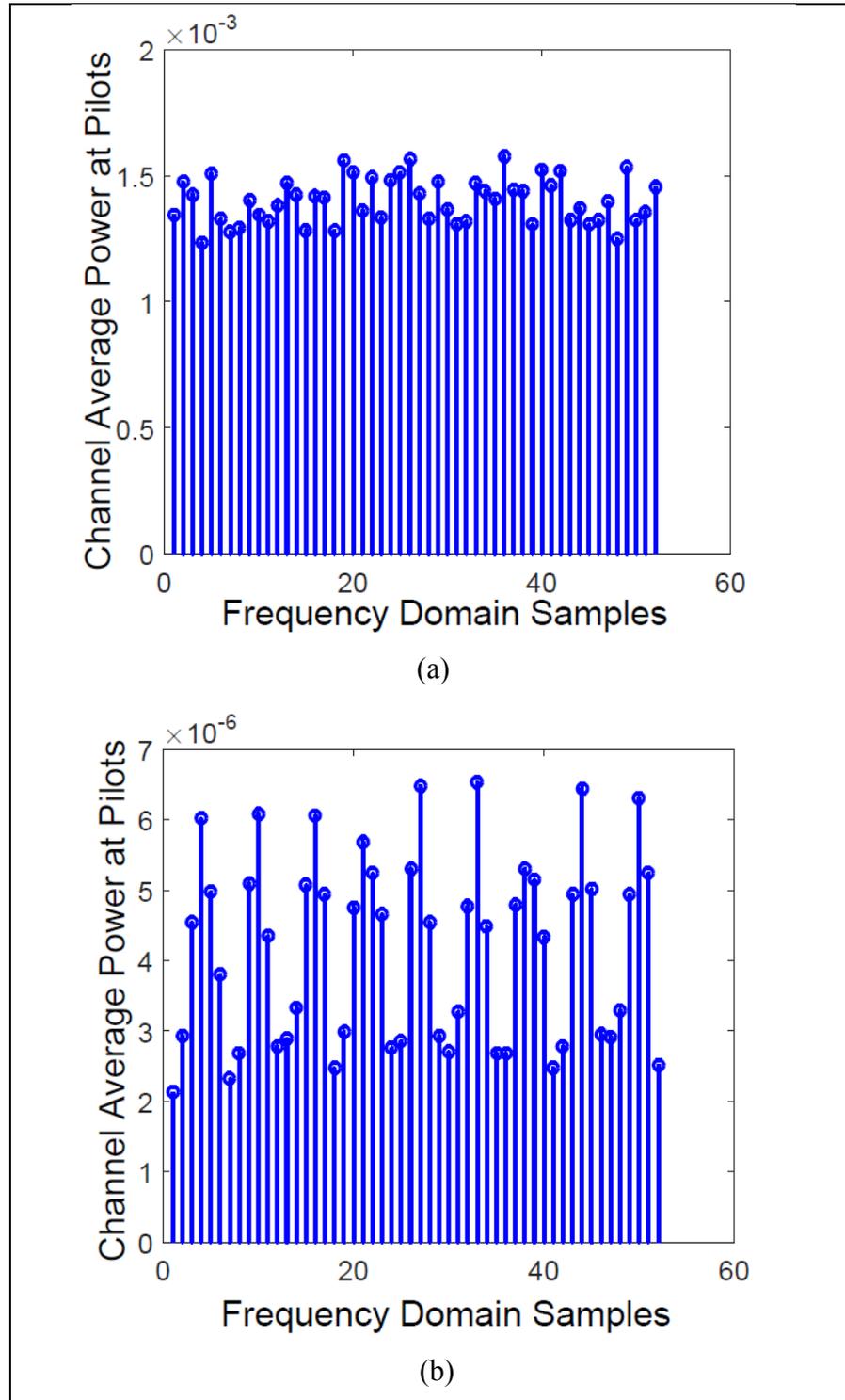
Figure 3.3 (a) Time average channel power samples (Low channel PAPR), (b) Time average channel power samples (High channel PAPR)

112

3.4.2   Percentage of detected targets and SNR

We plot in Figure 3.4(a) the percentage of detected targets as a function of the number of present targets for two different values of N_p. Uniformly distributed targets in the surveillance area are simulated for a high number of iterations. During each iteration, the PAPR values corresponding to the two transmitter streams are computed at the ego receiver level and then identified (high and low). For each stream, the number of detected targets out of the total number of targets is computed. Finally, the percentage of detection is computed after a high number of iterations. The results shown in Figure 3.4(a) are in agreement with the expression in (3.6). Indeed, higher N_p value would result in higher ρ_{rad}, which enhances the radar detection capabilities in the presence of multiple targets. In both N_p cases, high PAPR channels offer better detection performances compared to the lower PAPR cases. In fact, the selection of the high PAPR channel allows to detect 84 % of the six present targets compared to only 77% for the low PAPR channel, when 512 subcarriers per node are used. Moreover, we remark that average SNR ρ is higher for the high PAPR cases compared to the its value for low PAPR cases. We show in Figure 3.4(b) the variation of the radar SNR ρ_{rad} as a function of system parameters and ρ as in (3.6). We can see that for the same values of M_s and N_p, higher number of received components results in slightly higher values of ρ_{rad} as expressed in (3.6).
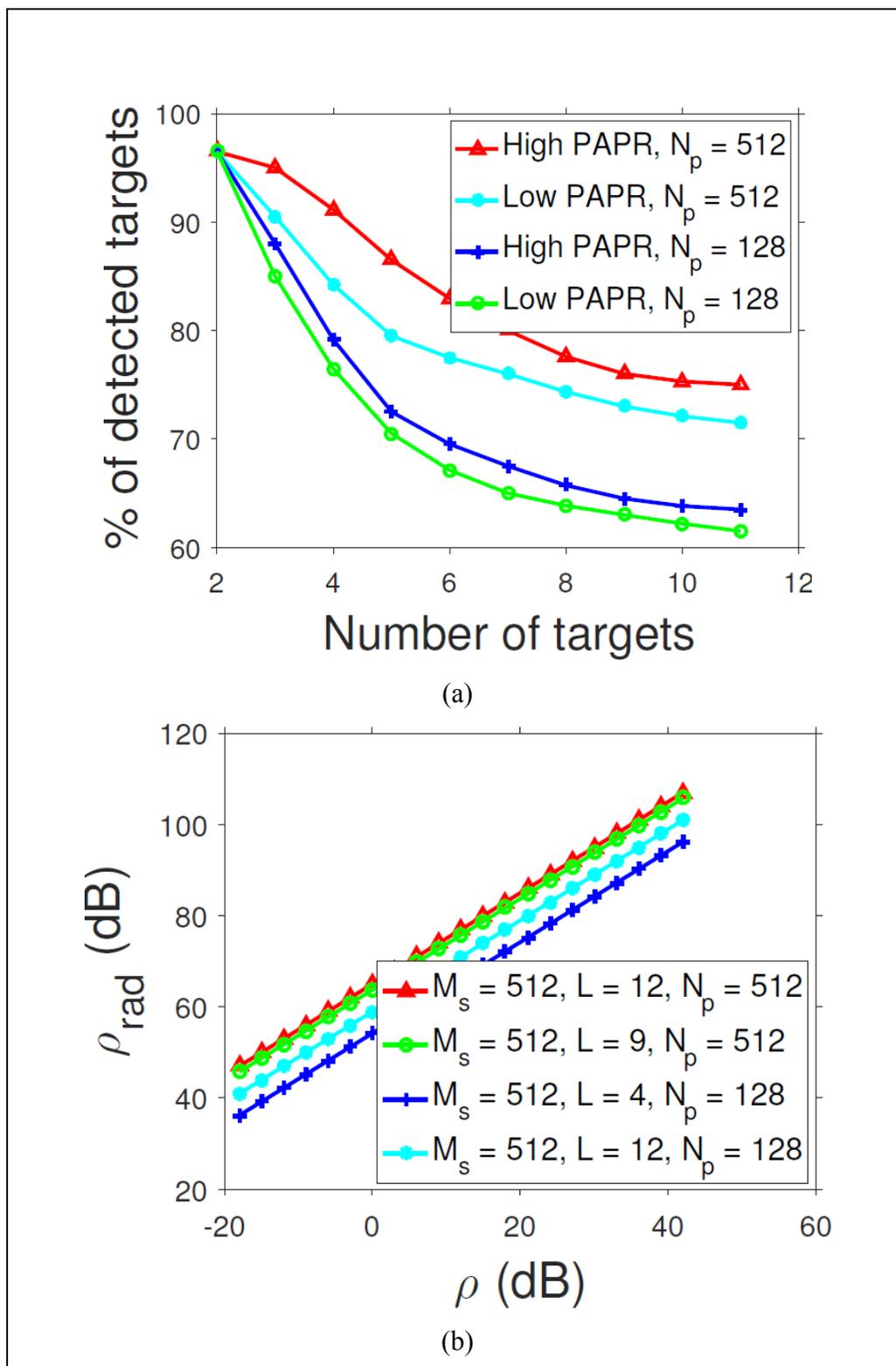
Figure 3.4 Percentage of detected targets and SNR

3.5   Chapter summary

This chapter analyzes the relationship between the channel PAPR and the channel statistics i.e., the number of received components and the path attenuation amplitude statistics. We have also shown that the radar SNR depends on the parameters of the spectrally-interleaved multi-carrier scheme when implemented (M_s and N_p) in addition to the channel statistics. Moreover, we have shown that the radar functionality can benefit from the presence of the communication part to improve its own sensing performance. Indeed, higher percentage of detected targets is achieved for the selected bistatic streams that is characterized by high PAPR channels. Future work will investigate the ability of each node to directly construct its own geolocation map of the environment by processing the monostatic and the selected high PAPR channel-based bistatic radar information.

The next chapter further extends our proposed joint radar and communication work via a different architecture, where separate point-to-point communication and multistatic radar systems are present with partial or total spectrum overlap. The next chapter investigates the optimum placement of radar receivers in order to minimize the radar ranging errors caused by the communication interference, while enhancing the target positioning accuracy.

CHAPTER 4

COEXISTENCE OF RADAR AND COMMUNICATION SYSTEMS WITH SPECTRUM SHARING CHALLENGE

In this work, we investigate a scenario where both multistatic radar and point-to-point communication systems are present with partial or total spectrum sharing constraint. We propose a new adaptive radar receivers placement mechanism that jointly maximizes the signal to interference plus noise ratio (SINR) of each communication transmitter-radar receiver channel while minimizing the geometric dilution of precision (GDOP). The proposed joint approach takes advantage of the cooperation between radar and communication systems and performs well in presence of communication interference on the radar side. Moreover, the proposed approach helps to increase the capability to properly demodulate communication data at each radar receiver resulting in less radar measurement errors due to communication interference, while enhancing the target positioning accuracy.

This chapter shares the same review of literature as a publication by the same author. Some passages are taken directly from (Ben-Kilani et al., 2017), with additional information which applies to this thesis.

4.1   Introduction

Radar and communication systems are recently facing more and more the challenging constraint of spectrum sharing. The dual functionality is driven by incremental similarities between carrier frequencies of both systems., which results in higher spectrum congestion especially below 6 GHz (Blunt & Yantham, 2007); (Jacyna et al., 2016); (Richmond et al., 2016); (Bliss, 2014); (Chiriyath et al., 2015).

Both radar and communication systems are facing some similar challenges as a growth of user numbers and robust performance requirements. On the other hand, each system is

targeting specific objectives: the objective of any radar system is target detection, tracking and discrimination in case of multi-target environment. The communication system is used for data transfer with an minimum bit error objective. Both systems actively inject RF energy into the environment to accomplish the aforementioned objectives (Jacyna et al., 2016). Thus, a simultaneous operation of both systems in the same frequency band and without any cooperation scheme would result in suboptimal overall system operation essentially caused by mutual interference effect.

In this chapter, we will investigate how cooperative spectrum sharing between the radar and communication systems could allow each system to operate at acceptable performance. In fact, we will demonstrate that information sharing between the systems at near real-time and then specific optimization metrics execution could really help to minimize the mutual inference and enable systems to operate at acceptable levels of performance. We will try to develop a novel joint optimization metric based on radar receiver placement strategy. Before we describe the actual proposed work, we provide a general background on the recently proposed joint metrics in literature.

4.2 Recent advances on cooperative radar and communication operation

An overview of the fundamental limits studies for the Shared Spectrum Access for Radar and Communications (SSPARC) program has been made in (Blunt & Yantham, 2007). This program is developing sharing technologies that result in joint spectrum access for both radar and communications systems which maintains or increases individual system performance while ensuring each system achieves its mission objectives (Blunt & Yantham, 2007). The fundamental limits part is a theoretical research effort, based on information theory, to determine joint radar and communications performance bounds for spectrum sharing (Blunt & Yantham, 2007). The fundamental limits study is supported by a combination of universities, research institutions and commercial companies, which resulted in the release of several recent research papers related to the topic so far. As detailed in (Blunt & Yantham, 2007), one of the main objectives of the fundamental limits study is to develop measures and

metrics that can be used to judge the merits of a given sharing system design (those that incorporate both communications and radar functionalities). It should be noted that several challenges are related to the aforementioned objective (Blunt & Yantham, 2007): multiple modes of radar (monostatic, bistatic, etc..) and communications (multiple access..), understanding the interactions between radar and communication waveforms when evaluating signal separation approaches such as: spatial, spectral, temporal, polarization and coding diversities, understanding adaptation to the environment using common waveform designs based on both robust channel estimation techniques and nonlinear optimization approaches (Blunt & Yantham, 2007). The general goal is to expand the boundaries of information theory for better understanding and mastery of joint radar and communication operation in any specific scenario.

A joint performance bound in terms of communication rate and a novel radar estimation rate has been developed in (Richmond et al., 2016); (Bliss, 2014). This performance bound has been leveraged in (Chiriyath et al., 2015) to design radar waveform that jointly maximize radar estimation rate and communication rate for a shared spectrum. The performance of radar and communication cooperative bound in presence of two different types of clutter is analyzed in (Paul et al., 2016). The impact of clutter cancellation residual (due to phase noise) on the cooperative bounds also studied in (Chiriyath & Bliss, 2015). It has been shown that the clutter residual could be treated as an additional noise source, which negatively impact both radar estimation rate and communication performance. In work (Chiriyath et al., 2016), the radar CRLB expressions have been derived in both cases of presence and absence of communication interfering signal. It has been shown that the use of additional target-reflected communications path of sufficient strength could help improve the radar detection capability. In addition, the derived CRLB expressions have been used to define an objective function to be used for waveform co-design. The work in (Masarik & Subotic, 2016) focus on the radar as an encoder of information in an interference-limited environment. Such assumption allows to define achievable information-theoretic limits of both radar and communication and consider the problem of a radar operating in the presence of

communication interference as a Gaussian multiple access channel problem to which fundamental performance bounds have derived.

An interesting joint radar communication risk metric has been proposed in (Jacyna et al., 2016), where the NP criterion has been extended to include the communication data rate. The model for the cooperative risk metric definition assumes that data received by both the radar and communication can be observed simultaneously and instantly with a near real-time feedback between both systems. The ideal linked cooperation has been shown to yield a structured covariance-based water-filling solution. A second case of unlinked cooperation has been also analyzed, where radar and communication settings are known by both systems (codebooks, waveforms, timing...) but received data is not relayed between them. It has been shown based on this second case that depending on the rate of communication channel in comparison to the capacity of the radar communication data link, the defined risk metric could be whether decoupled or not.

Recent contribution in (Reed et al., 2016) focuses in particular upon the development of new expression for radar capacity, which has been combined to the traditional communication capacity for a unified radar-communication capacity measure optimization. The proposed research makes use of advance radar-communication channel estimation techniques along with adaptive space-time transmit and receive scheme to maximize the overall signal to noise ratio while minimizing the co-channel interference.

The proposed technique in this paper extends the work of (Richmond et al., 2016), (Bliss, 2014); (Chiriyath et al., 2016) by considering the spatial diversity of the multistatic radar and controlling the multistatic radar receivers placement in an attempt to reduce the impact of a separate communication system interference on radar performance. In (Zheng et al., 2018), an adaptive approach is proposed to minimize the interference originated from several radars at the communication receiver in a non-moving environment and under simplistic direct path-only interference condition.

Radar systems are traditionally composed of static elements. However, application scenarios where the radar receivers can be viewed as moveable devices are increasingly encountered in military, tactical or emergency deployments. In these cases, the receivers can be mounted on vehicles, motorized platforms, or even UAVs.

In this chapter, we thus consider the presence of radar and communication systems with partial spectrum overlap in a moving environment. We control the placement of the multistatic radar receivers in order to improve target ranging and positioning performances in presence of the communication system interference. In fact, we propose a novel joint metric optimization process that uses the real-time scene parameters to dynamically update the radar receivers placement. This practical process attempts to increase the communication data demodulation capability at each radar receiver while improving the target positioning accuracy of the multistatic radar system in presence of extended clutter and noise.

4.3   System architecture
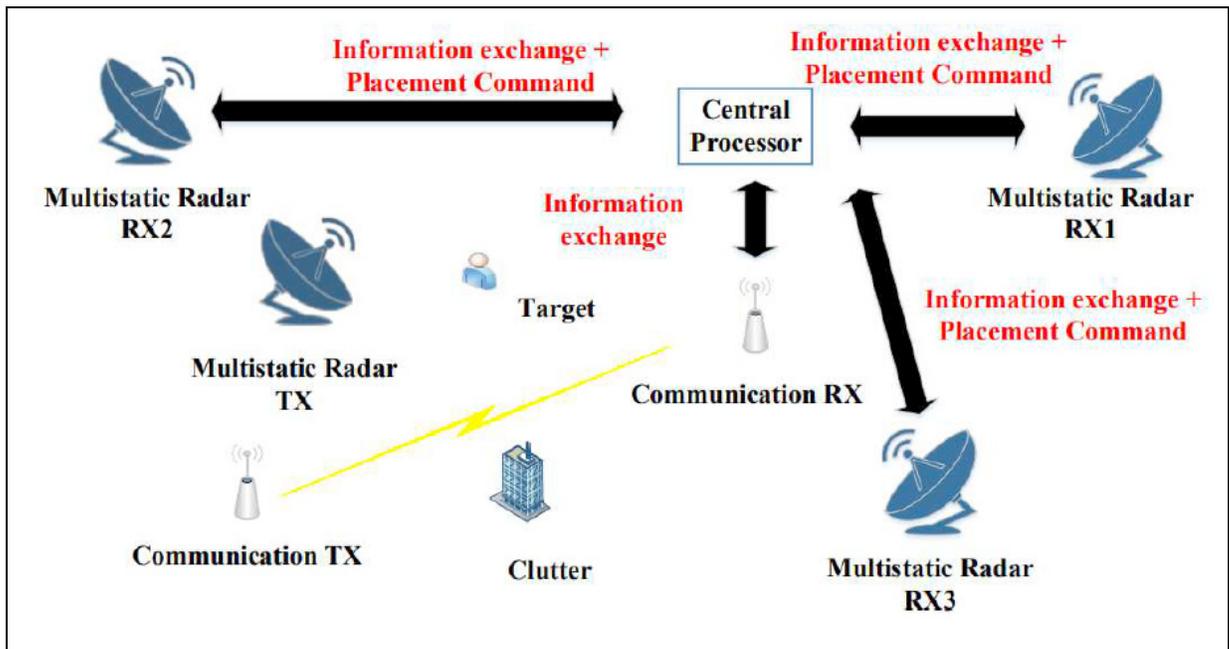
Figure 4.1 Joint radar and communication scenario

We consider the presence of separate point-to-point communication system and a <u>multistatic</u> radar, composed of one transmitter and M receivers as shown in Figure 4.1. Extended target and clutter are also present in the environment. The communication nodes, the radar receivers and the objects in the environment are able to move. Therefore, the Doppler effect is considered at the received signals level. We assume the presence of a central processor as depicted in Figure 4.1, where all received radar signals are fed to in real-time. In addition, the central processor has the knowledge of radar and communication parameters (radar waveform, communication modulation and coding schemes, bandwidth of each system and the updated positions of different nodes).

4.4 Signal model

Let $s_R(t)$ and $s_C(t)$ be respectively the transmitted radar and communication waveforms. The received signal at the communication receiver $r_{Com}(t)$ is expressed as:

$$
\begin{aligned}
r_{Com}(t) &= r_C(t) + r_D(t) + r_T(t) + r_L(t) + n(t) \\
&= r_C(t) + r_D(t) + g_T s_R(t) * d(t) + r_L(t) + n(t)
\end{aligned}
$$

$$(4.1)$$

Where $r_C(t)$ denotes the communication signal, which is composed of line of sight (LOS) communication signal in addition to multipath components, $r_D(t)$ is the direct signal from the radar, which is known and compensated for at the communication receiver. $r_T(t)$ is the target return, $r_L(t)$ is the clutter return and $n(t)$ is the noise signal. It should be noted that radar multipath returns received as a result of signal scattered by target and clutter and reflected in the surrounding environment are very weak compared to first-order reflections generated by target and clutter, and therefore are ignored for clarity purpose. g_T is a complex reflection factor proportional to the extended target <u>bistatic</u> radar cross section (<u>RCS</u>) relative to the radar transmitter and the communication receiver. $d(t)$ is the deterministic part of the extended target impulse response.

On the other hand, the received radar signal $r_{Rad_i}(t)$ at the ith radar receiver is:

$$r_{Rad_i}(t) = \tilde{r}_{C_i}(t) + \tilde{r}_{T_i}(t) + \tilde{r}_{L_i}(t) + \tilde{n}_i(t)$$
$$= \tilde{r}_{C_i}(t) + \tilde{g}_{T_i}s_R(t) * \tilde{d}_i(t) + \tilde{r}_{L_i}(t) + \tilde{n}_i(t)$$

$$(4.2)$$

Where $\tilde{\ }$ is used to distinguish the received signal components at the different multistatic radar receivers from those received at the communication receiver. The received communication signal at the ith radar receiver $\tilde{r}_{C_i}(t)$ is composed of LOS communication signal in addition to multipath components. It is assumed that direct radar signal is automatically suppressed at each radar receiver. $\tilde{g}_{T_i}$ is a complex reflection factor proportional to the extended target bistatic radar cross section (RCS) relative to the radar transmitter and ith radar receiver pair. We consider a Swerling I extended target (i.e., $\tilde{g}_{T_i} \sim CN\left(0, \sigma^2_{\tilde{g}_{T_i}}\right)$, $\tilde{d}_i(t)$ is the deterministic part of the extended target impulse response relative to the radar transmitter and the ith radar receiver.

$r_T(t), r_L(t), \tilde{r}_{T_i}(t), \tilde{r}_{L_i}(t), n(t)$ and $\tilde{n}_i(t)$ are all modeled as independent zero mean complex Gaussian random processes. In addition, all radar receivers are widely spaced so that the received radar signals $r_{Rad_i}(t)$ are considered independent.

4.5   Receivers placement update strategy

We are interested in the case where radar and communication systems are operating simultaneously and sharing a part or the whole of the spectrum resources. This case study is the most encountered in real scenarios as opposed to the straightforward case, where radar and communication operations are separated in time, space or frequency band.

As detailed in the beginning of the present chapter, the increasing demands of spectrum from both radar and communication application dictates cooperative spectrum sharing between both systems for proper operation of each system with acceptable performance in presence of the other one.

In order to leverage the received radar signals $r_{Rad_i}(t)$ for target detection at the central processor, the communication component $\tilde{r}_{C_i}(t)$ in (4.2) should be estimated and compensated for. The communication data demodulation is carried out at the central processor on each received radar signal. After time and frequency synchronization via respectively preamble detection and carrier recovery, the communication data is demodulated after channel equalization based on the modulation constellation.

Let $\delta_{\tilde{r}_{C_i}(t)}$ be the residual communication signal after data demodulation at communication transmitter- i^{th} radar receiver channel. For a specific deployment scenario of communication and radar nodes, the rate supportable by the communication channel could either be inferior or superior to what is supportable by the communication- i^{th} radar channel. If the rate of information transmitted by the communication system is lower than the communication- i^{th} radar data link capacity, the ith radar receiver will be able to perfectly demodulate and reconstruct the communication signal yielding negligible $\delta_{\tilde{r}_{C_i}(t)}$. In the opposite case, $\delta_{\tilde{r}_{C_i}(t)}$ would be a non-zero vector.

From the above discussion, by adjusting the radar nodes placement, the rate of the communication-radar channel could be enhanced for better communication data demodulation at the radar. This would minimize the impact of communication interference on received radar signals and as a result maximize radar measurement accuracy. A straightforward approach to do that, is to maximize the SINR of each communication-radar channel.

The multiplicity of widely-spaced radar receivers enables the geolocation operation in order to extract the target absolute parameters (i.e., absolute position and velocity). In fact, the

backscattered signals coming from the target are matched filtered and the bistatic range-Doppler responses relative to different receivers are processed. Consequently, bistatic range and Doppler information relative to different radar receivers are extracted from the range-Doppler responses. In addition, real-time target impulse response and clutter plus noise covariance matrices are estimated through successive measurements. Finally, the estimated bistatic range and Doppler information are supplied to a LS geolocation process with the purpose of absolute target parameters extraction.

4.5.1   LS geolocation process

The backscatter signals coming from the target are matched filtered at each receiver and the bistatic range-Doppler responses relative to different receivers are processed. Consequently, bistatic ranges and Doppler shifts relative to different transmitter-receiver pairs could be easily extracted from the range-Doppler responses. Theoretical expressions of bistatic range and bistatic Doppler shift are given by (Skolnik, 2001):

$$r_i = \sqrt{R_T \times R_{ri}} \tag{4.3}$$

$$f_i = 2\frac{V}{\lambda}\cos\phi_i \, \cos(\beta_i/2)$$

$$= 2\frac{V}{\lambda}\cos\phi_i \sqrt{\frac{1}{2} + \frac{R_T - L_i \sin\theta_T}{2\sqrt{R_T^2 + L_i^2 - 2R_T L_i \sin\theta_T}}} \tag{4.4}$$

Where r_i is the bistatic range relative to the transmitter and the ith receiver, R_T is the transmitter to target range, R_{ri} is the ith receiver to target range. f_i is the bistatic Doppler shift, L_i is the baseline separating the transmitter from the ith receiver, $V = \sqrt{v_x^2 + v_y^2 + v_z^2}$ is the target velocity, i^{th} is the carrier wavelength, β_i is the the bistatic angle, ϕ_i is the angle between the target velocity vector and the bistatic bisector and θ_T is the angle between the transmitter and the target.

The aim of the geolocation step is to estimate the absolute target position and velocity from the measured bistatic ranges and Doppler shifts relative to different receivers. The LS geolocation system can be modeled as:

$$Z = \psi(\rho) + \eta \qquad (4.5)$$

where $Z = [r_1, \ldots, r_M, f_1, \ldots, f_M]^T$ is the measurement vector, $\rho = [x, y, z, v_x, v_y, v_z]^T$ is the vector of unknown target parameters (i.e., target position and velocity vectors) and η is the measurement noise vector.

From (4.3), (4.4) and (4.5), we can represent the hybrid system as,

$$\psi(\boldsymbol{\rho}) = \begin{bmatrix} \sqrt{R_T \times R_{r1}} \\ \sqrt{R_T \times R_{r2}} \\ \vdots \\ \sqrt{R_T \times R_{rM}} \\ 2\dfrac{\sqrt{v_x^2 + v_y^2 + v_z^2}}{\lambda} \cos\phi_1 \sqrt{\dfrac{1}{2} + \dfrac{R_T - L_1 \sin\theta_T}{2\sqrt{R_T^2 + L_1^2 - 2R_T L_1 \sin\theta_T}}} \\ 2\dfrac{\sqrt{v_x^2 + v_y^2 + v_z^2}}{\lambda} \cos\phi_2 \sqrt{\dfrac{1}{2} + \dfrac{R_T - L_2 \sin\theta_T}{2\sqrt{R_T^2 + L_2^2 - 2R_T L_2 \sin\theta_T}}} \\ \vdots \\ 2\dfrac{\sqrt{v_x^2 + v_y^2 + v_z^2}}{\lambda} \cos\phi_M \sqrt{\dfrac{1}{2} + \dfrac{R_T - L_M \sin\theta_T}{2\sqrt{R_T^2 + L_M^2 - 2R_T L_M \sin\theta_T}}} \end{bmatrix}$$

$$(4.6)$$

The range-velocity estimation problem can be expressed as,

$$\hat{\boldsymbol{\rho}} = \min_{\rho} \|\boldsymbol{Z} - \boldsymbol{\psi}(\boldsymbol{\rho})\| \qquad (4.7)$$

We solve the optimization problem of (4.7) by using the Trust-Region-Reflective algorithm (Sorensen, 1982).

4.5.2 Conventional GDOP Approach

GDOP is a vital metric that indicates the efficiency of the sensor network topological distribution in aiding the geolocation process. Large GDOP values correspond to a poor geometry topology, which result in poor geolocation performance. We assume that the multistatic radar receivers are able to move so that real-time optimal locations could be chosen for target parameters estimation accuracy.

We can express the relationships between the measurement vector and the target parameters as:

$$\boldsymbol{Z} = \boldsymbol{F}(\boldsymbol{\zeta}) + \eta \qquad (4.8)$$

Where $Z = [r_1, \dots, r_M, f_1, \dots, f_M]^T$ is the measurement vector composed of radar range measurements r_i and Doppler shift measurements f_i, $\zeta = [x, y, z]^T$ is the vector of unknown target position coordinates and η is the measurement noise vector.

In case of a single extended target and the general case of M receivers, we have:

$$F(\zeta) = \begin{bmatrix} F_1 \\ F_2 \\ \vdots \\ F_M \\ F_{M+1} \\ F_{M+2} \\ \vdots \\ F_{2M} \end{bmatrix}$$

$$F(\zeta) = \begin{bmatrix} \sqrt{R_T \times R_{r1}} \\ \sqrt{R_T \times R_{r2}} \\ \vdots \\ \sqrt{R_T \times R_{rM}} \\ 2\dfrac{v}{\lambda} \cos\phi_1 \sqrt{\dfrac{1}{2} + \dfrac{R_T - L_1 \sin\theta_T}{2\sqrt{R_T^2 + L_1^2 - 2R_T L_1 \sin\theta_T}}} \\ 2\dfrac{v}{\lambda} \cos\phi_2 \sqrt{\dfrac{1}{2} + \dfrac{R_T - L_2 \sin\theta_T}{2\sqrt{R_T^2 + L_2^2 - 2R_T L_2 \sin\theta_T}}} \\ \vdots \\ 2\dfrac{v}{\lambda} \cos\phi_M \sqrt{\dfrac{1}{2} + \dfrac{R_T - L_M \sin\theta_T}{2\sqrt{R_T^2 + L_M^2 - 2R_T L_M \sin\theta_T}}} \end{bmatrix}$$

(4.9)

And the noise column vector is expressed as:

$$\eta = \begin{bmatrix} \eta_{r1} \\ \eta_{r2} \\ . \\ . \\ . \\ \eta_{rM} \\ \eta_{f1} \\ \eta_{f2} \\ \vdots \\ \eta_{fM} \end{bmatrix}$$

(4.10)

We define the noise covariance matrix $\chi = E[(\eta - E[\eta])(\eta - E[\eta])^T]$. In order to derive the GDOP for the LS geolocation process F, it is essential to linearize F by expanding it in a Taylor series about a reference vector $\boldsymbol{\zeta_0} = [x_0, y_0, z_0]^T$. $\boldsymbol{\zeta_0}$ should be sufficiently close to the actual $\boldsymbol{\zeta}$ (could be an estimate of $\boldsymbol{\zeta}$ determined from previous iteration).

$$F(\zeta) = F(\boldsymbol{\zeta_0}) + \boldsymbol{\Gamma}(\zeta - \boldsymbol{\zeta_0})$$

(4.11)

Where $\boldsymbol{\Gamma}$ is the $2M \times 3$ matrix of derivatives evaluated at $\boldsymbol{\zeta_0}$.

$$\boldsymbol{\Gamma} = \begin{bmatrix} \frac{\partial F_1}{\partial x}\Big|_{\zeta_0} & \frac{\partial F_1}{\partial y}\Big|_{\zeta_0} & \frac{\partial F_1}{\partial z}\Big|_{\zeta_0} \\ \frac{\partial F_2}{\partial x}\Big|_{\zeta_0} & \frac{\partial F_2}{\partial y}\Big|_{\zeta_0} & \frac{\partial F_2}{\partial z}\Big|_{\zeta_0} \\ \vdots & \vdots & \vdots \\ \frac{\partial F_M}{\partial x}\Big|_{\zeta_0} & \frac{\partial F_M}{\partial y}\Big|_{\zeta_0} & \frac{\partial F_M}{\partial z}\Big|_{\zeta_0} \\ \frac{\partial F_{M+1}}{\partial x}\Big|_{\zeta_0} & \frac{\partial F_{M+1}}{\partial y}\Big|_{\zeta_0} & \frac{\partial F_{M+1}}{\partial z}\Big|_{\zeta_0} \\ \frac{\partial F_{M+2}}{\partial x}\Big|_{\zeta_0} & \frac{\partial F_{M+2}}{\partial y}\Big|_{\zeta_0} & \frac{\partial F_{M+2}}{\partial z}\Big|_{\zeta_0} \\ \vdots & \vdots & \vdots \\ \frac{\partial F_{2M}}{\partial x}\Big|_{\zeta_0} & \frac{\partial F_{2M}}{\partial y}\Big|_{\zeta_0} & \frac{\partial F_{2M}}{\partial z}\Big|_{\zeta_0} \end{bmatrix}$$

(4.12)

The noise elements composing η are assumed independent and identically distributed zero mean Gaussian random variables. Thus, the matrix χ is diagonal with non-zero diagonal elements.

The maximum likelihood or LS estimator for the linearized model is given by:

$$\hat{\zeta} = \zeta_0 + (\boldsymbol{\Gamma}^T \chi^{-1} \boldsymbol{\Gamma})^{-1} \boldsymbol{\Gamma}^T \chi^{-1} (\boldsymbol{Z} - \boldsymbol{F}(\zeta_0)) \tag{4.13}$$

The covariance matrix of the target parameters estimate vector $\hat{\zeta}$ is computed as:

$$\boldsymbol{P} = E[(\hat{\zeta} - E[\hat{\zeta}])(\hat{\zeta} - E[\hat{\zeta}])^T] = (\boldsymbol{\Gamma}^T \chi^{-1} \boldsymbol{\Gamma})^{-1} \tag{4.14}$$

Finally, the GDOP is defined as $\sqrt{trace[\boldsymbol{P}]}$.

The choice of the appropriate locations of the radar receivers is carried out by minimizing the GDOP at the actual target estimate obtained from the LS geolocation algorithm. Let us denote by Y_i the 3D space where the ith receiver could be located in. Moreover, let the optimum set of receiver locations be represented as $\boldsymbol{\Lambda} = [x_1, y_1, z_1 \ldots, x_M, y_M, z_M]$.

Consequently, the minimization problem, which estimates the optimum set of receiver locations $\boldsymbol{\Lambda}$ for better target positioning accuracy, can be formulated as:

$$\widehat{\boldsymbol{\Lambda}} = \min_{(x_i, y_i, z_i) \in Y_i} GDOP_{(\hat{x}_a, \hat{y}_a, \hat{z}_a)} \tag{4.15}$$

Where (x_i, y_i, z_i) are the ith receiver coordinates and $[.]_{(\hat{x}_a, \hat{y}_a, \hat{z}_a)}$ represents the GDOP evaluation at the actual target position estimate, which is obtained from the LS geolocation process. Several non-linear minimization algorithms could be used to solve the optimization problem in (4.15). One of them is the interior-point method (Waltz et al., 2006).

4.5.3 Proposed joint metric

As previously mentioned in this chapter, for a specific deployment scenario of communication and radar nodes, the rate supportable by the communication channel could either be superior or inferior to what is supportable by each radar-communication channel. In case the rate supportable by each communication-radar channel is superior or equal to the communication channel rate, the radar would be able to perfectly decode and compensate for the received communication signal $\tilde{r}_{C_i}(t)$ resulting in a minimized interference level for radar operation. From this perspective, it become reasonable to take into consideration communication interference minimization at each radar receiver while searching for the best receiver placement that optimizes the target positioning. To do so, we extend the GDOP minimization problem in (4.15) to account for communication-radar channel SINR maximization at each radar receiver. Thereby, a joint metric optimization is defined as follows:

$$\hat{\Lambda} = \min_{(x_i, y_i, z_i) \in Y_i} [\, GDOP_{(\hat{x}_a, \hat{y}_a, \hat{z}_a)} - \mu \sum_i SINR_{CR_i}] \qquad (4.16)$$

where (x_i, y_i, z_i) are the ith receiver coordinates, $SINR_{CR_i}$ is the signal to interference plus noise ratio relative to the communication transmitter - i^{th} radar receiver channel, μ weighs the relative importance of the $SINR_{CR}$ part in the joint objective function (chosen equal to or higher than 1 if the radar ranging error is high due to the communication interference) and $[\,.\,]_{(\hat{x}_a, \hat{y}_a, \hat{z}_a)}$ represents the joint metric evaluation at the actual target position estimate, which is obtained from the LS geolocation process.

We can solve the non-linear optimization problem of (4.16) using the interior-point method (Waltz et al., 2006).

From practical perspective, the update of the radar receivers placement based on the proposed joint approach in (4.16) is only carried out when the ranging error starts to be high and a time interval is elapsed from the last update.

For each (x_i, y_i, z_i) coordinates, the value of $SINR_{CR_i}$ in (4.16) is defined based on the transmitter node coordinates, communication transmission parameters, target scattering coefficient variance, estimated target absolute position and velocity based on the LS geolocation process in addition to estimated clutter and noise powers:

$$SINR_{CR_i} = \frac{P_{\tilde{r}_{c_i}}}{P_{\tilde{r}_{T_i}} + P_{\tilde{r}_{L_i}} + P_{\tilde{n}_i}} \tag{4.17}$$

where $P_{(.)}$ is defined as signal power. The received power of the communication signal at the ith radar receiver $P_{\tilde{r}_{c_i}}$ is expressed as:

$$P_{\tilde{r}_{c_i}} = \vartheta G_{t_{com}} G_{r_{R_i}} P_{t_{com}} \left(\frac{\lambda}{4\pi d_{CR_i}}\right)^{\eta} \tag{4.18}$$

where ϑ is a random variable used to model the communication multipath propagation. $G_{t_{com}}$ and $G_{r_{R_i}}$ are respectively the communication transmitter and the ith radar receiver gains. $P_{t_{com}}$ is the communication transmitted power, λ is the wavelength, d_{CR_i} is the distance between the communication transmitter and i^{th} radar receiver and η is the path loss exponent.

The received scattered target signal power at the ith radar receiver is given by:

$$P_{\tilde{r}_{T_i}} = \sigma_{\tilde{g}_{T_i}}^2 \left| \sum_{k=1}^{N_s} b_{ik} s(t - \tau_{ik}) \exp(2\pi j f_{ik} t) \right|^2 \tag{4.19}$$

where N_s is the number of scatterers composing the extended target, b_{ik} is a deterministic coefficient relative to the kth scatter and the radar transmitter- i^{th} radar receiver path. τ_{ik} is the total delay experienced by the transmitted signal from the radar transmitter to i^{th} radar receiver and after reflection by the kth scatter and f_{ik} is the bistatic Doppler shift experienced by the transmitted signal along the ith path and caused by the movement of the kth scatterer. Finally, $P_{\tilde{r}_{L_i}}$ and $P_{\tilde{n}_i}$ are respectively the clutter and noise powers, which are estimated through successive measurements.

From (4.16), the SINR maximization part will allow to enhance the capacity of different communication-radar channels, which would result in better communication data demodulation and compensation at different radar receivers and therefore less radar measurement errors due to communication interference. At the same time, the minimization of the GDOP will help increase the target positioning accuracy. The resultant positions of the radar receivers are optimal for enhanced target detection and positioning performances.

4.6 Simulation results and discussion

We consider the presence of a point-to-point BPSK-OFDM system, where the communication waveform bandwidth is 17 MHz with a transmitted power of 7 dBW. A multistatic radar composed of one stationary transmitter and three widely-spaced receivers is deployed in the same environment. The radar waveform is composed of Hadamard phase-coded pulses with a total bandwidth of 75 MHz and a transmitted power of 40 dBW. We consider the same 2.4 GHz central frequency of operation for both radar and communication

systems, which results in partial spectrum overlap. We assume the presence of an extended target and an extended clutter (with random positions) in addition to the ambient noise. The locations of radar receivers are initially chosen randomly and μ is set to 1.

4.6.1   Target probability of detection

We show in Figure 4.2 the probability of detection (P_D) as a function of SCNR for the proposed scenario and a fixed probability of false alarm equal to 10^{-5}. It can be seen that the GDOP-only optimization metric yields poor detection performances when communication interference is present. The joint metric performs well in presence of communication link because it jointly maximizes the demodulation capability of the communication-radar link, which results in less detection and radar ranging errors while optimizing the target positioning accuracy via the GDOP term. For instance, the proposed approach achieves a P_D of 0.84 compared to 0.49 when only the GDOP approach is used in the presence of communication interference and 0.76 when only the GDOP approach is used in absence of communication interference, for a given SCNR of -20 dB. For an SCNR of -5 dB and higher, the detection probability is close to 1 for all cases due to the spatial diversity contribution of the multistatic topology.
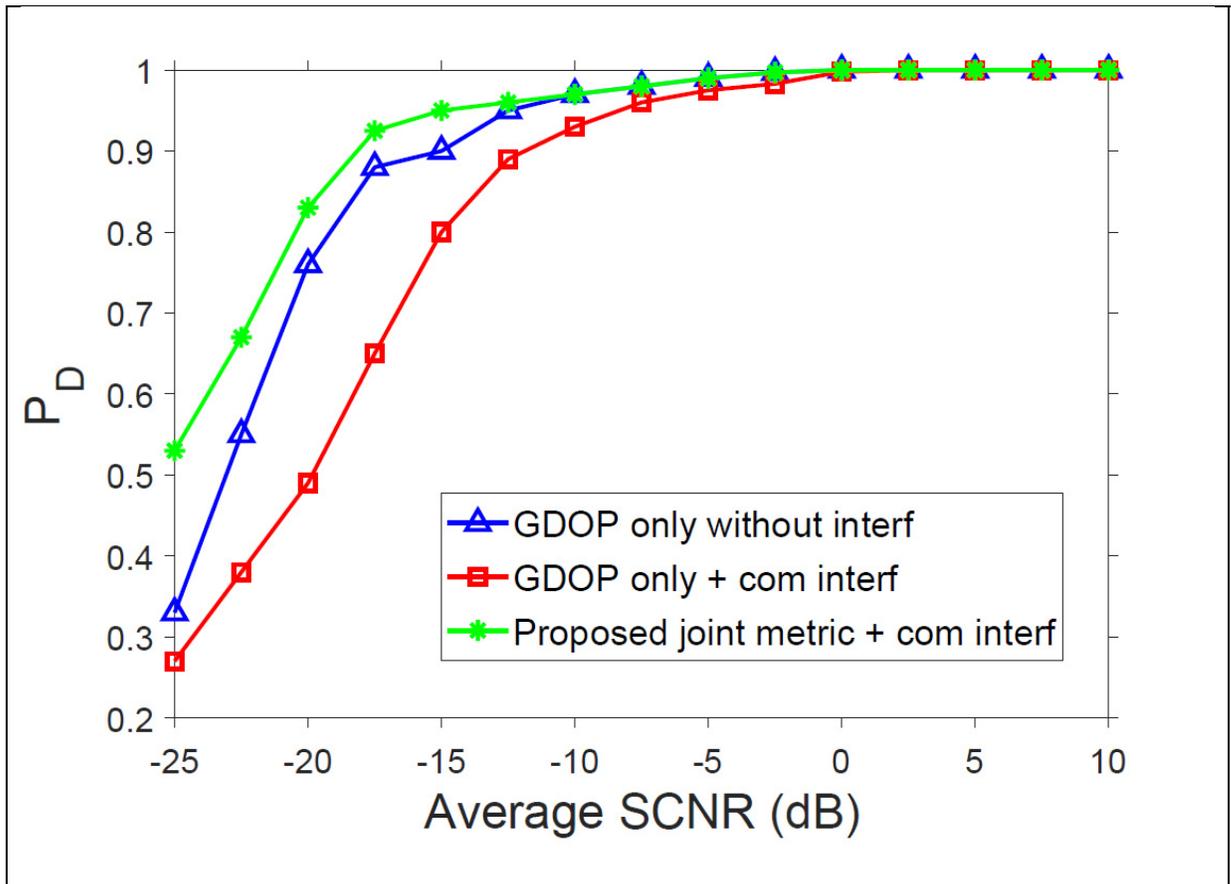
Figure 4.2 Probability of target detection using the proposed 3D location optimization technique for 3 widely spaced receivers in presence of extended clutter

4.6.2 BER curves

We show in Figure 4.3 the BER results relative to one communication-radar (ComRad) link. The joint metric allows to find the multistatic radar receivers placement that partially maximizes the SINR at each communication transmitter-radar receiver channel while optimizing the target positioning accuracy based on the multistatic radar ranging measurements. As a result, the BER values of the communication-radar channels are lower when the joint metric is applied compared to the case where the GDOP-only optimization is applied. In fact, the radar receivers placement resulting from the GDOP-only optimization helps only to improve the target positioning accuracy but could easily degrade the

communication-radar link as shown in Figure 4.3. The degradation in communication-radar link causes more radar ranging errors due to communication interference and therefore less target detection and positioning performance. It should be noted that the obtained values of BER in Figure 4.3 are suboptimal because of the BPSK-OFDM scheme chosen for the case study.
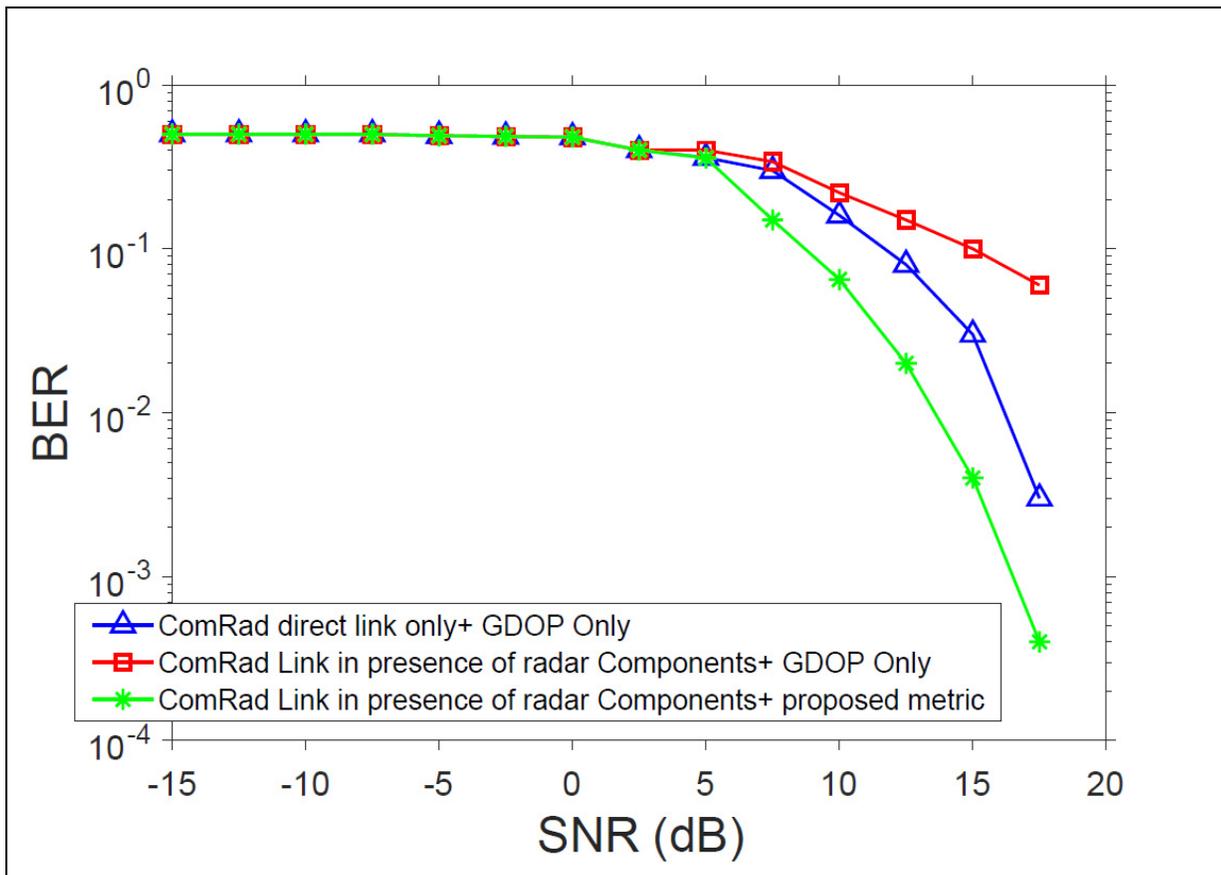
Figure 4.3 Bit error rate curves

4.6.3   Joint metric-based radar receiver locations update

Figure 4.4 shows the joint metric minimization process described in (4.16) as a function of algorithm iterations.

Figures 4.5 and 4.6 shows respectively the 2D and the 3D radar receiver positions update from initial to final iterations. The radar transmitter is placed at the origin and the extended target and clutter positions are kept the same during the iterative joint metric optimization process with their relative scattering center shown in Figures 4.5 and 4.6. A point-to-point communication system is also present in the same environment. The new radar positions are the result of the trade-off between SINR maximization of each communication transmitter-radar receiver channel and target positioning accuracy enhancement based on radar ranging measurements. Figure 4.5 shows the 2D projection for all the system components onto the x-y plane.
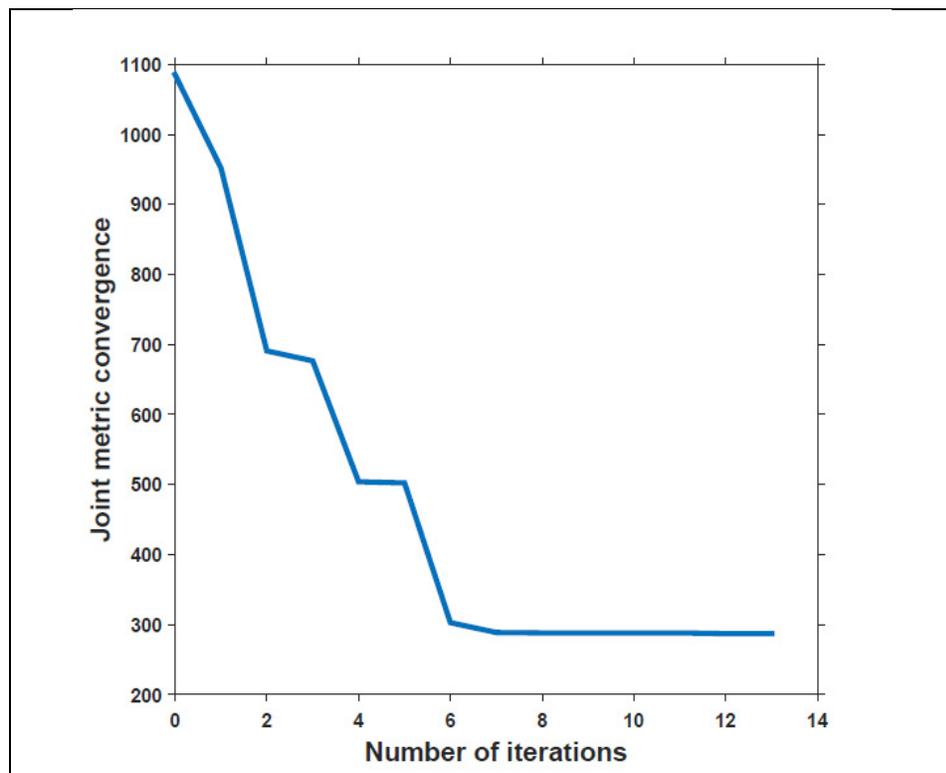
Figure 4.4 Joint metric iterative minimization process
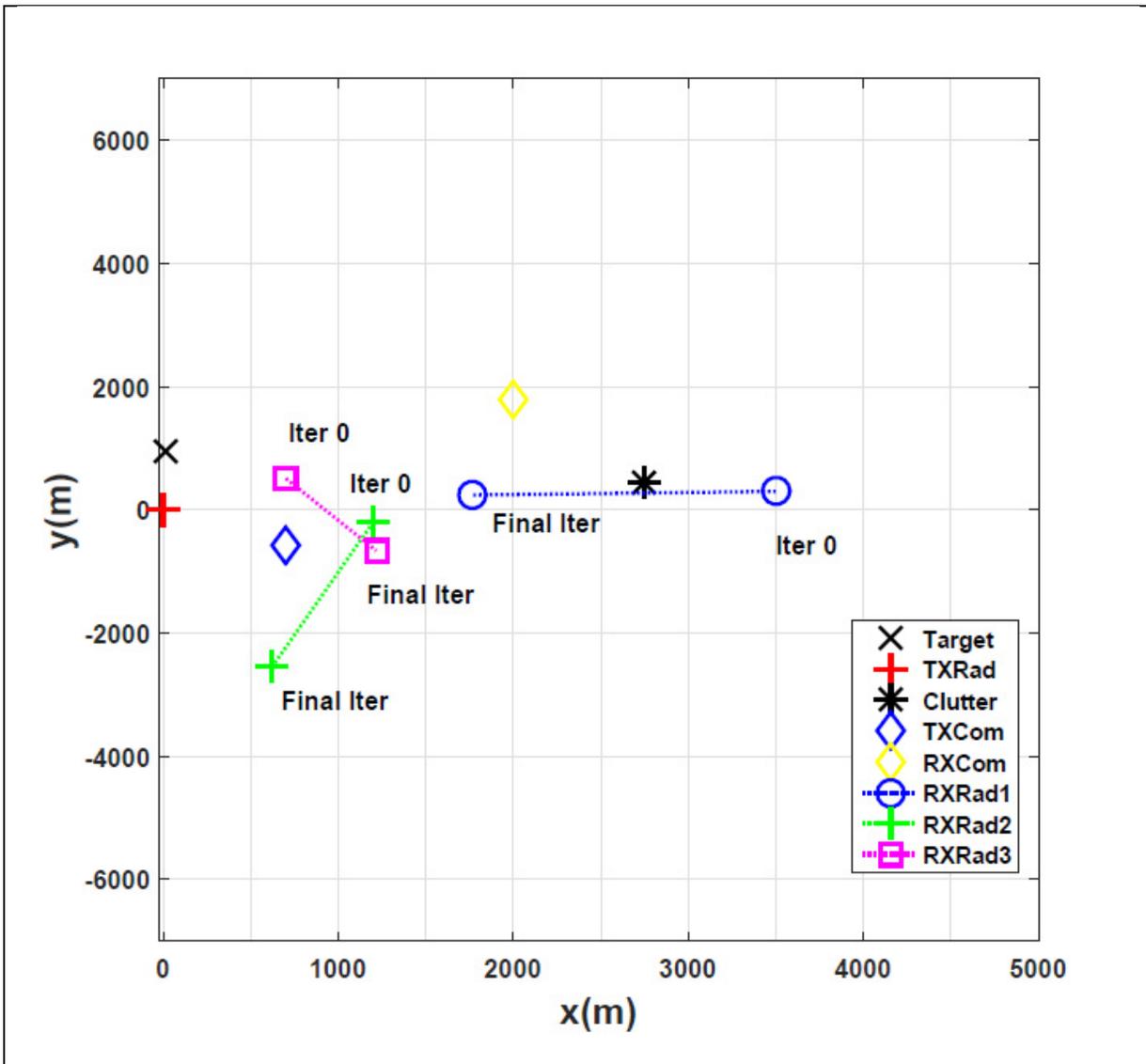
Figure 4.5 2D projection for radar receiver location updates throughout
the optimization process
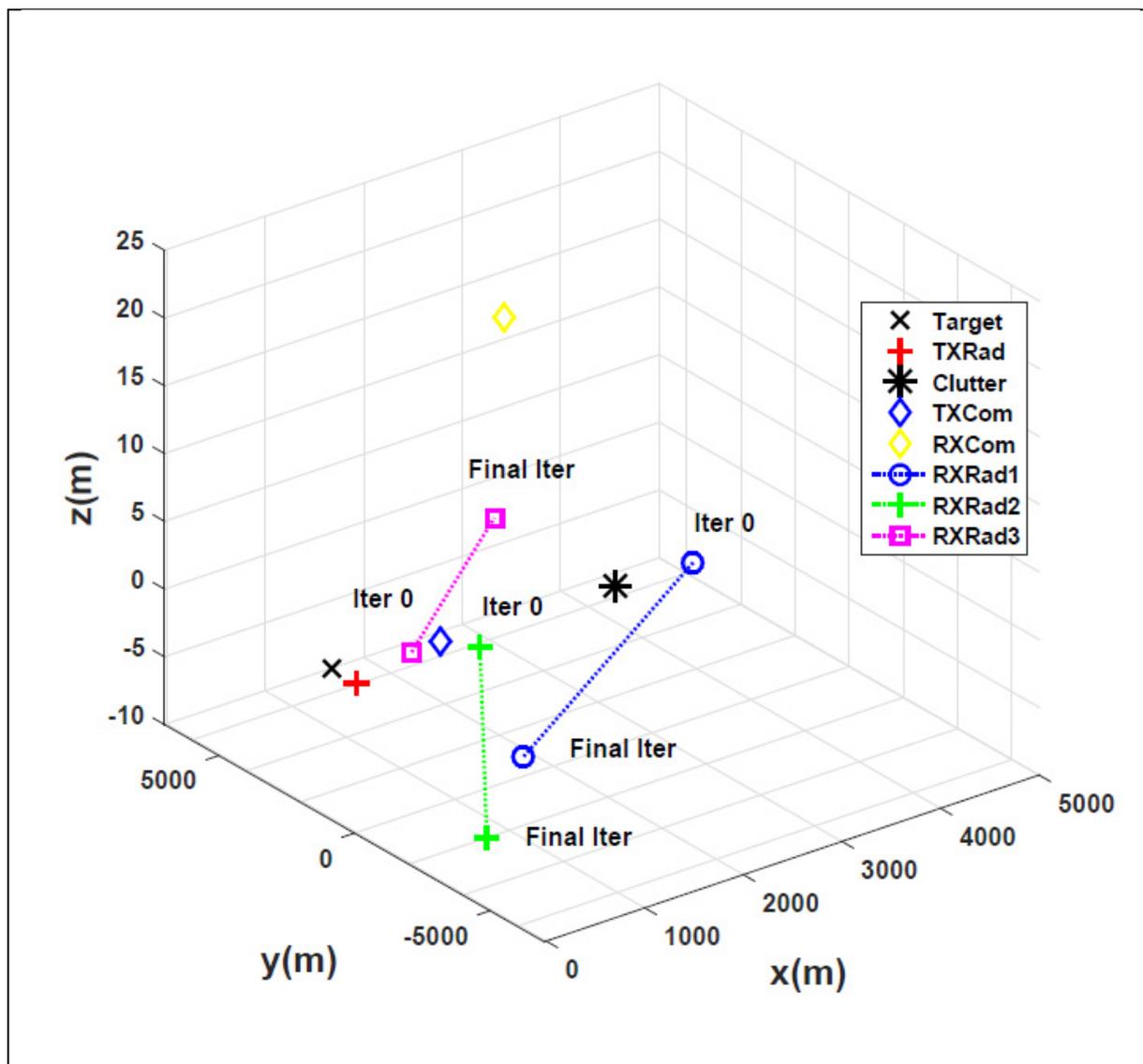
Figure 4.6 3D radar receiver location updates throughout
the optimization process

4.6 Chapter Summary

This chapter proposed an adaptive multistatic radar receivers placement mechanism based on optimization of a joint metric in presence of a point-to-point communication system with spectrum sharing constraint. In fact, the proposed joint metric optimization takes into consideration the presence of communication interference in an attempt to jointly maximize

the SINR of each communication transmitter-radar receiver channel for better interference decoupling at the radar level, while minimizing the GDOP for enhanced target positioning accuracy. Better performance in terms of communication interference handling and suppression at the radar level, have been obtained with the proposed joint approach compared to the GDOP-only minimization metric.

CONCLUSION

In this thesis, we have investigated cognitive Radar Sensor Network (RSN) architectures aiming to optimize the target detection and its parameters estimation accuracy. The context is a realistic time-varying radar scene, where mobile extended targets and clutters are permanently present in the environment. We show in this thesis that the RSN can adjust its operational transmission parameters (waveform shape and coding) and reception parameters (dynamic receivers selection and placement) to efficiently adapt to the radar scene.

The main motivation behind the research presented in this thesis was to develop and analyze RSN architectures capable of adapting its operational modes in accordance with target scintillation characteristics and its surrounding environment dynamics. A special focus is upon distributed (statistical) MIMO RSN systems, where spatial diversity could be utilized in conjunction with cognitive waveform selection and design techniques for target detection optimization.

In chapter 2, we investigate a cognitive selection mechanism of the radar waveform based on target probability of detection maximization in conjunction with adaptive receivers placement mechanism. Apart from the cognitive waveform selection objective, the proposed process aims at evaluating the optimal positions for the radar receivers in an attempt to iteratively minimize the geometric dilution of precision (GDOP). Subsequently, the proposed dual objective approach aims to optimize the target detection and positioning accuracy by extending the concept of cognition to both the radar transmitter and receivers sites. A gain in target detection is achieved when multiple specially separated receivers are used compared to a single receiver. In fact, the use of $M=6$ receivers allow to reach a probability of detection equal to 1 compared to 0.94 in the case of $M=3$ receivers, and 0.45 in the case of $M=1$ receivers, for a given SCNR of 10 dB. On the other hand, the proposed joint approach achieves an increase of 30% in detection probability compared to only detection maximization process for a given SCNR of -5 dB and a probability of false alarm equal to 0.05. In addition, the target positioning error is 90% less than or equal to 0.1 m when the

proposed GDOP based receiver locations update process is used compared to a target positioning error which is 90% less than or equal to 0.6 m when static receivers locations are used.

In chapter 3, we investigate a special category of joint radar and communication operation, where several communication nodes in a network operate separately in frequency. A novel architecture at each node level has been proposed to leverage the multi-look diversity of the distributed system by activating radar processing on the bistatic stream exhibiting the highest PAPR value in addition to the already existent monostatic processing. The OFDM waveform has been used at the same time for communication and radar operation. The main advantage of this architecture is a dual radar and communication capabilities at each node hardware level, while leveraging the spatial diversity offered by the network geometry to enable multistatic radar processing. In fact, the selection of the high PAPR channel allows to detect 84 % of the six present targets compared to only 77% for the low PAPR channel, when 512 subcarriers per node are used.

In chapter 4, we focus upon a different category of joint radar and communication operation, where separate point-to-point communication and multistatic radar systems are present with partial or total spectrum sharing constraint. This chapter investigates the optimum placement of radar receivers with the goal of optimizing target positioning accuracy while minimizing the interference caused by the simultaneous operation of the communication system. In fact, the proposed joint objective approach attempts to maximize the signal to interference plus noise ratio (SINR) of each communication transmitter-radar receiver channel while minimizing the geometric dilution of precision. In this way, the proposed approach helps to increase the capability to demodulate the communication data at each radar receiver (resulting in less radar measurement errors due to communication interference) and simultaneously enhance the target positioning accuracy. In fact, the proposed approach achieves a P_D of 0.84 compared to 0.49 when only the GDOP approach is used in the presence of communication interference and 0.76 when only the GDOP approach is used in

absence of communication interference, for a given SCNR of -20 dB and a fixed probability of false alarm equal to 10^{-5}.

Future work in this research field could involve extending the idea of cognitive radar sensor network in the context of multiple extended targets. In fact, the spatial diversity offered by RSN could be leveraged in conjunction with machine learning / deep learning techniques with the goal of enabling the multiple targets identification and classification in the context of dynamic radar scene. More specifically, the radar receivers placement optimization techniques and the waveform selection mechanisms investigated in the context of this thesis, could be applied with the classification techniques based on machine learning algorithms to enhance multiple extended targets recognition, detection and feature extraction in harsh indoor and outdoor environments.

Another interesting avenue of research is related to the joint radar and communication systems operation. Future research could extend the work presented in chapter 4 to take into consideration the radar transmitter mobility (not only the radar receivers mobility) in an attempt to minimize the interference at the communication receiver caused by the simultaneous operation of the multistatic radar. In this way, the cooperation between the radar and the communication systems could be widened to improve the simultaneous operation with minimum allowable level of mutual interference. In addition, the point-to-point communication system could be replaced by multipoint architecture. In this case, the joint cooperative radar and communication objective process should be adjusted accordingly. The results presented in this thesis open up new possibilities for implementation of distributed (statistical) MIMO RSN systems, efficient sensing and development of cooperative radar systems and intelligent signal processing techniques for future wireless communication and radar coexistence.

LIST OF REFERENCES

Mahafza, B.R., & Esherbeni, A. Z. (2005). *Matlab Simulations for Radar systems Design*. 1st Ed. CRC Press, Chapman and Hall.

Chernyak, V. S. (1998). *Fundamentals of Multisite Radar Systems*. London, U.K: Gordon and Breach Science Publisher.

Liang, J., & Liang, Q. (2011). Design and Analysis of Distributed Radar Sensor Networks. *IEEE Transactions on Parallel and Distributed Systems, 22*(11), pp. 1926-1933.

Fishler, E., Haimovich, A., Blum, R., Chizhik, D., Cimini, L., & Valenzuela, R. (2004, April). MIMO radar: an idea whose time has come. Paper presented at the IEEE Radar Conference, Philadelphia, PA, USA.

Stoica, P., Li, J., & Xie, Y. (2007). On probing signal design for MIMO radar. *IEEE Transactions on Signal Processing, 55*(8), pp. 4151-4161.

Li, J., & Stoica, P. (2007). MIMO radar with colocated antennas. *IEEE SIGNAL PROCESSING MAGAZINE, 24*(5), pp. 106-114.

Xu, L., Li, J., & Stoica, P. (2008). Target detection and parameter estimation for MIMO radar systems. *IEEE Transactions on Aerospace and Electronic Systems, 44*(3), pp. 927–939.

Li, J., Stoica, P., Xu, L., & Roberts, W. (2007). On parameter identifiability of MIMO radar. *IEEE Signal Processing Letters, 14*(12), pp. 968-969.

Bliss, D., & Forsythe, K. (2003, Nov). *Multiple-input multiple-output (MIMO) radar and imaging: degrees of freedom and resolution.* Paper presented at the Thirty-Seventh Asilomar Conference on Signals, Systems and Computers, Pacific Grove, CA, USA.

Forsythe, K., Bliss, D., & Fawcett, G. (2004, Nov). *Multiple-input multiple-output (MIMO) radar: performance issues.* Paper presented at the Thirty-Eighth Asilomar Conference on Signals, Systems and Computers, Pacific Grove, CA, USA.

Fishler, E., Haimovich, A. M., Blum, R. S., Cimini, L. J., Chizhik, D., & Valenzuela, R. A. (2006). Spatial diversity in radars—models and detection performance. *IEEE Transactions on Signal Processing, 54*(3), pp. 823-838.

Baker, C. J., & Hume, A. L. (2003). Netted radar sensing. *IEEE Aerospace and Electronic Systems Magazine, 18*(2), pp. 3-6.

Hume, A. L., & Baker, C. J. (2001, May). *Netted Radar Sensing.* Paper presented at the IEEE Radar Conference, Atlanta, GA, USA.

Haykin, S. (2006). Cognitive radar: a way of the future. *IEEE Signal Processing Magazine, 23*(1), pp. 30-40.

Pillai, S. U., Oh, H. S., Youla, D. C., & Guerci, J. R. (2000). Optimal transmit-receiver design in the presence of signal-dependent interference and channel noise. *IEEE Transactions on Information Theory, 46*(2), pp. 577-584.

Garren, D., Osborn, M., Odom, A., Goldstein, J., Pillai, S., & Guerci, J. (2001). Enhanced target detection and identification via optimised radar transmission pulse shape. *IEE Proceedings - Radar, Sonar and Navigation, 148*(3), pp. 130-138.

Estephan, H., M. G. Amin, M. G., & Yemelyanov, K. M. (2010). Optimal waveform design for improved indoor target detection in sensing through-the-wall applications. *IEEE Transactions on Geoscience and Remote Sensing, 48*(7), pp. 2930-2941.

Bell, M. (1993). Information theory and radar waveform design. *IEEE Transactions on Information Theory, 39*(12), pp. 1578-1597.

Goodman, N. A., Venkata, P. R., & Neifeld, M. A. (2007). Adaptive Waveform Design and Sequential Hypothesis Testing for Target Recognition with Active Sensors. *IEEE Journal of Selected Topics in Signal Processing, 1*(1), pp. 105-113.

Romero, R., & Goodman, N. A. (2008, May). *Information-theoretic matched waveform in signal dependent interference.* Paper presented at the IEEE Radar Conference, Rome, Italy.

Kay, S. (2009). Waveform Design for Multistatic Radar Detection. *IEEE Transactions on Aerospace and Electronic Systems, 45*(3), pp. 1153-1166.

Zhang, J., Wang, H., & Zhu, X. (2010). Adaptive waveform design for separated transmit/receive ULA-MIMO radar. *IEEE Transactions on Signal Processing, 58*(9), pp. 4936-4942.

Yang, Y., & Blum, R. S. (2006, August). *Radar Waveform Design using Minimum Mean-Square Error and Mutual Information.* Paper presented at the IEEE Workshop on Sensor Array and Multichannel Process, Waltham, Massachusetts, USA.

Tang, B., Tang, J., & Peng, Y. (2011). Waveform Optimization for MIMO Radar in Colored Noise: Further Results for Estimation-Oriented Criteria. *IEEE Transactions on Signal Processing, 60*(3), pp. 1517-1522.

Jajamovich, G. H., Lops, M., & Wang, X. (2010). Space-Time Coding for MIMO Radar Detection and Ranging. *IEEE Transactions on Signal Processing, 58*(12), pp. 6195-6206.

Yang, Y., Blum, R. S., Zishu, H., & Fuhrmann, D. R. (2009). MIMO Radar Waveform Design via Alternating Projection. *IEEE Transactions on Signal Processing, 58*(3), pp. 1440-1445.

Song, X., Zhou, S., & Willett, P. (2010). Reducing the Waveform Cross Correlation of MIMO Radar with Space–Time Coding. *IEEE Transactions on Signal Processing, 58*(8), pp. 4213-4224.

Nijsure, Y., Kaddoum, G., & Leung, H. (2015). Cognitive chaotic UWB-MIMO radar based on nonparametric Bayesian technique. *IEEE Transactions on Aerospace and Electronic Systems, 51*(3), pp. 2360-2378.

Chen, Y., Nijsure, Y., Yuen, C., Chew, Y. H., Ding, Z., & Boussakta, S. (2013). Adaptive Distributed MIMO Radar Waveform Optimization Based on Mutual Information. *IEEE Transactions on Aerospace and Electronic Systems, 49*(2), pp. 1374-1385.

Yarlagadda, R., Ali, I., Al-Dhahir, N., & Hershey, J. (2000). GPS GDOP metric. *IEE Proceedings - Radar, Sonar and Navigation, 147*(5), pp. 259-264.

Sharp, I., Kegen, Y., & Guo, Y. J. (2009). GDOP Analysis for Positioning System Design. *IEEE Transactions on Vehicular Technology, 58*(7), pp. 3371-3382.

Torrieri, D. J. (1984). Statistical Theory of Passive Location Systems. *IEEE Transactions on Aerospace and Electronic Systems, AES-20*(2), pp. 183-198.

Sharp, I., Yu, K., & Hedley, M. (2012). On the GDOP and Accuracy for Indoor Positioning. *IEEE Transactions on Aerospace and Electronic Systems, 48*(3), pp. 2032-2051.

Anastasio, V., Colone, F., Lallo, A. D., Farina, A., Gumiero, F., & Lombardo, P. (2010, September/October). *Optimization of multistatic passive radar geometry based on CRLB with uncertain observations.* Paper presented at the European Radar Conference, Paris, France.

Gumiero, F., Santarelli, S., Bongioanni, C., Colone, F., & Lombardo, P. (2011, October). *Using real data for the implementation of multistatic passive radar geometry optimization procedure.* Paper presented at the European Radar Conference, Manchester, UK.

Nguyen, N. H., Dogancay, K., & Davis, L. M. (2014, June/July). *Joint transmitter waveform and receiver path optimization for target tracking by multistatic radar system.* Paper presented at the IEEE Workshop on Statistical Signal Processing, Gold Coast, VIC, Australia.

Nguyen, N. H., & Doğançay, K. (2016). Optimal Geometry Analysis for Multistatic TOA Localization. *IEEE Transactions on Signal Processing, 64*(16), pp. 4180-4193.

Nguyen, N. H., & Doğançay, K. (2015, May). *Optimal sensor placement for Doppler shift target localization.* Paper presented at the IEEE Radar Conference, Arlington, VA, USA.

Yang, Y., Yi, W., Zhang, T., Cui, G., Kong, L., & Yang, X. (2016, July). *Antenna placement of multistatic radar system with detection and localization performance.* Paper presented at the International Conference on Information Fusion, Heidelberg, Germany.

Lei, P., Huang, X., Wang, J., & Ma, X. (2012, July). *Sensor placement of multistatic radar system by using genetic algorithm.* Paper presented at the IEEE International Geoscience and Remote Sensing Symposium, Munich, Germany.

Lackpour, A., & Proska, K. (2016, May). *GOMERS: Genetic optimization of a multistatic extended radar system*, Philadelphia, PA, USA.

Bradaric, I., Capraro, G. T., Weiner, D. D., & Wicks, M. C. (2006, April). *Multistatic radar systems signal processing.* Paper presented at the IEEE Radar Conference, Verona, NY, USA.

Bradaric, I., Capraro, G. T., & Wicks, M. C. (2009, February). *Multistatic ambiguity function - A tool for waveform selection in distributed radar systems.* Paper presented at the International Waveform Diversity and Design Conference, Kissimmee, FL, USA.

Derham, T., Doughty, S., Baker, C., & Woodbridge, K. (2010). Ambiguity Functions for Spatially Coherent and Incoherent Multistatic Radar. *IEEE Transactions on Aerospace and Electronic Systems, 46*(1), pp. 230-245.

Sturm, C., & Wiesbeck, W. (2011). Waveform design and signal processing aspects for fusion of wireless communications and radar sensing. *Proceedings of the IEEE, 99*(7), pp. 1236-1259.

Garmatyuk, D., Schuerger, J., Morton, Y. T., Binns, K., Durbin, M., & Kimani, J. (2007). *Feasibility study of a multi-carrier dual-use imaging radar and communication system.* Paper presented at the European Radar Conference, Munich, Germany.

Garmatyuk, D., Schuerger, J., & Kauffman, K. (2011). Multifunctional software defined radar sensor and data communication system. *IEEE Sensors Journal, 11*(1), pp. 99-106.

Nijsure, Y., Chen, Y., Boussakta, S., Yuen, C., Chew, Y. H., & Ding, Z. (2012). Novel System Architecture and Waveform Design for Cognitive Radar Radio Networks. *IEEE Transactions on Vehicular Technology, 61*(8), pp. 3630-3642.

Surender, S. C., & Narayanan, R. M. (2011). UWB Noise-OFDM Netted Radar: Physical Layer Design and Analysis. *IEEE Transactions on Aerospace and Electronic Systems, 47*(2), pp. 1380-1400.

Euziere, J., Guinvarc'h, R., Lesturgie, M., Uguen, B., & Gillard, R. (2014, October). *Dual function radar communication time-modulated array.* Paper presented at the International Radar Conference, Lille, France.

Hassanien, A., Amin, M. G., Zhang, Y. D., & Ahmad, F. (2015). A dual function radar-communications system using sidelobe control and waveform diversity. *IEEE Transactions on Signal Processing, 64*(8), pp. 2168-2181.

Blunt, S. D., & Yantham, P. (2007, June). *Waveform design for radar-embedded communications.* Paper presented at the International Waveform Diversity and Design Conference, Pisa, Italy.

Jacyna, G. M., Fell, B., & McLemore, D. (2016, May). *A high-level overview of fundamental limits studies for the DARPA SSPARC program.* Paper presented at the IEEE Radar Conference, Philadelphia, PA, USA.

Richmond, C. D., Basu, P., Learned, R. E., Vian, J., Worthen, A., & Lockard, M. (2016, May). *Performance bounds on cooperative radar and communication systems operation.* Paper presented at the IEEE Radar Conference, Philadelphia, PA, USA.

Bliss, D. W. (2014, May). *Cooperative radar and communications signaling: The estimation and information theory odd couple.* Paper presented at the IEEE Radar Conference, Cincinnati, OH, USA.

Chiriyath, A. R., Paul, B., Jacyna, G. M., & Bliss, D. W. (2015). Inner Bounds on Performance of Radar and Communications Co-Existence. *IEEE Transactions on Signal Processing, 64*(2), pp. 464-474.

Paul, B., Chiriyath, A. R., & Bliss, D. W. (2016, May). *Joint communications and radar performance bounds under continuous waveform optimization: The waveform awakens.* Paper presented at the IEEE Radar Conference, Philadelphia, PA, USA.

Chiriyath, A. R., & Bliss, D. W. (2015, November). *Effect of clutter on joint radar-communications system performance inner bounds.* Paper presented at the Asilomar Conference on Signals, Systems and Computers, Pacific Grove, CA, USA.

Chiriyath, A. R., Paul, B., & Bliss, D. W. (2016, May). *Joint radar-communications information bounds with clutter: The phase noise menace.* Paper presented at the IEEE Radar Conference, Philadelphia, PA, USA.

Masarik, M. P., & Subotic, N. S. (2016, May). *Cramèr-Rao lower bounds for radar parameter estimation in noise plus structured interference.* Paper presented at the IEEE Radar Conference, Philadelphia, PA, USA.

Reed, J. T., Odom, J. L., Causey, R. T., & Lanterman, A. D. (2016, May). *Gaussian multiple access channels for radar and communications spectrum sharing.* Paper presented at the IEEE Radar Conference, Philadelphia, PA, USA.

Guerci, J. R., Guerci, R. M., Lackpour, A., & Moskowitz, D. (2015, May). *Joint design and operation of shared spectrum access for radar and communications.* Paper presented at the IEEE Radar Conference, Arlington, VA, USA.

Turlapaty, A., & Jin, Y. (2014, May). *A joint design of transmit waveforms for radar and communications systems in coexistence.* Paper presented at the IEEE Radar Conference, Cincinnati, OH, USA.

Skolnik, M. L. (2001). *Introduction to Radar systems*. New York: 3rd Ed. McGraw-Hill Publications.

Trees, H. L. V. (1968). *Detection, Estimation, and Modulation Theory*. New York: Wiley.

Liang, Q. (2006, October). *Radar Sensor Networks for Automatic Target Recognition with Delay-Doppler Uncertainty.* Paper presented at the IEEE Military Communications conference, Washington, DC, USA.

Liang, Q. (2006, September). *Waveform Design and Diversity in Radar Sensor Networks: Theoretical Analysis and Application to Automatic Target Recognition.* Paper presented at the IEEE Communications Society on Sensor and Ad Hoc Communications and Networks, Reston, VA, USA.

Xu, L., & Liang, Q. (2010, December). *Waveform Design and Optimization in Radar Sensor Network.* Paper presented at the IEEE Global Telecommunications Conference GLOBECOM 2010, Miami, FL, USA.

Wang, W. Q., & Shao, H. (2014). Radar-to-Radar Interference Suppression for Distributed Radar Sensor Networks. *Remote Sensing Journal, 6*(1), pp. 740-755.

Ly, H. D., & Liang, Q. (2009). Diversity in Radar Sensor Networks: Theoretical Analysis and Application to Target Detection. *International Journal of Wireless Information Networks*, pp. 209-216.

Liu, Y., & Liang, J. (2014). Optimization for distributed Radar Sensor Network (RSN) and MIMO-RSN in flat fading channels. *Elsevier Journal, 13*(C), pp. 253-259.

Daher, R., & Adve, R. (2010). A Notion of Diversity Order in Distributed Radar Networks. *IEEE Transactions on Aerospace and Electronic Systems, 46*(2), pp. 818-831.

Shu, H., & Liang, Q. (2007, January). *Data Fusion in a Multi-Target Radar Sensor Network.* Paper presented at the IEEE Radio and Wireless Symposium, Long Beach, CA, USA.

Sun, B., Wang, X., & Moran, B. (2012, October). *On sensing ability of distributed MIMO radar networks.* Paper presented at the IET International Conference on Radar Systems, Glasgow, UK, UK.

Robey, F. C., Coutts, S., Weikle, D., McHarg, J. C., & Cuomo, K. (2004, November). *MIMO radar theory and experimental results.* Paper presented at the Conference Record of the Thirty-Eighth Asilomar Conference on Signals, Systems and Computers, Pacific Grove, CA, USA.

Xu, L., Li, J., Stoica, P., Forsythe, K. W., & Bliss, D. W. (2007, April). *Waveform Optimization for MIMO Radar: A Cramér-Rao Bound Based Study.* Paper presented at the IEEE International Conference on Acoustics, Speech and Signal Processing Honolulu, HI, USA.

Li, J., Xu, L., Stoica, P., Forsythe, K. W., & Bliss, D. W. (2008). Range Compression and Waveform Optimization for MIMO Radar: A CramÉr–Rao Bound Based Study. *IEEE Transactions on Signal Processing, 56*(1), pp. 218-232.

Fuhrmann, D. R., & Antonio, G. S. (2008). Transmit beamforming for MIMO radar systems using signal cross-correlation. *IEEE Transactions on Aerospace and Electronic Systems, 44*(1), pp. 171-186.

Cui, G., Li, H., & Rangaswamy, M. (2014). MIMO Radar Waveform Design with Constant Modulus and Similarity Constraints. *IEEE Transactions on Signal Processing, 62*(2), pp. 343-353.

Wang, Y. C., Wang, X., Liu, H., & Luo, Z. Q. (2012). On the Design of Constant Modulus Probing Signals for MIMO Radar. *IEEE Transactions on Signal Processing, 60*(8), pp. 4432-4438.

Maio, A. D., Nicola, S. D., Huang, Y., Zhang, S., & Farina, A. (2008). Code Design to Optimize Radar Detection Performance Under Accuracy and Similarity Constraints. *IEEE Transactions on Signal Processing, 56*(11), pp. 5618-5629.

Chen, C. Y., & Vaidyanathan, P. P. (2008). MIMO Radar Ambiguity Properties and Optimization Using Frequency-Hopping Waveforms. *IEEE Transactions on Signal Processing, 56*(12), pp. 5926-5936.

Wang, H., Liao, G., Li, J., & Lv, H. (2011) Waveform optimization for MIMO-STAP to improve the detection performance. *Elsevier Journal, 91*(11), pp. 2690-2696.

Wang, H., Liao, G., Li, J., & Guo, W. (2013). Robust waveform design for MIMO-STAP to improve the worst-case detection performance. *EURASIP Journal on Advances in Signal Processing, 52*, pp. 1-8.

Liu, Y., Wang, H., & Wang, J. (2016). Robust multiple-input multiple-output radar waveform design in the presence of clutter. *IET Radar, Sonar & Navigation, 10*(7), pp. 1249-1259.

Chen, C. Y., & Vaidyanathan, P. P. (2009). MIMO Radar Waveform Optimization with Prior Information of the Extended Target and Clutter. *IEEE Transactions on Signal Processing, 57*(9), pp. 3533-3544.

Wang, H., Pei, B., & Bai, Y. (2014, August). *Robust waveform design for MIMO-STAP with imperfect clutter prior knowledge.* Paper presented at the IEEE International Conference on Signal Processing, Communications and Computing, Guilin, China.

Ahmed, S., & Alouini, M. S. (2014). MIMO Radar Transmit Beampattern Design Without Synthesising the Covariance Matrix. *IEEE Transactions on Signal Processing, 62*(9), pp. 2278-2289.

Gao, K., Wang, W. Q., & Cai, J. (2016). Frequency diverse array and MIMO hybrid radar transmitter design via Cramér–Rao lower bound minimisation. *IET Radar, Sonar & Navigation, 10*(9), pp. 1660-1670.

Scharrenbroich, M., & Zatman, M. (2014, May). *Statistical MIMO radar experimental results.* Paper presented at the IEEE Radar Conference, Cincinnati, OH, USA.

Liu, J., Li, H., & Himed, B. (2014). Two Target Detection Algorithms for Passive Multistatic Radar. *IEEE Transactions on Signal Processing, 62*(22), pp. 5930-5939.

Bruyere, D. P., & Goodman, N. A. (2008). Adaptive detection and diversity order in multistatic radar. *IEEE Transactions on Aerospace and Electronic Systems, 44*(4), pp. 1615-1623.

Goodman, N. A., & Bruyere, D. (2007). Optimum and decentralized detection for multistatic airborne radar. *IEEE Transactions on Aerospace and Electronic Systems, 43*(2), pp. 806-813.

Nelms, M. E., & Collins, P. J. (2011, May). *Development and evaluation of a multistatic ultrawideband random noise radar network.* Paper presented at the IEEE Radar Conference, Kansas City, MO, USA.

Deng, H. (2004). Polyphase code design for Orthogonal Netted Radar systems. *IEEE Transactions on Signal Processing, 52*(11), pp. 3126-3135.

Deng, H. (2012). Orthogonal netted radar systems. *IEEE Aerospace and Electronic Systems Magazine, 27*(5), pp. 28-35.

Fink, A., & Beikirch, H. (2011, September). *Analysis of rss-based location estimation techniques in fading environments.* Paper presented at the International Conference on Indoor Positioning and Indoor Navigation, Guimaraes, Portugal.

Kanaan, M., & Pahlavan, K. (2004, March). *A comparison of wireless geolocation algorithms in the indoor environment.* Paper presented at the IEEE Wireless Communications and Networking Conference Atlanta, GA, USA.

Liu, H., Darabi, H., Banerjee, P., & Liu, J. (2007). Survey of Wireless Indoor Positioning Techniques and Systems. *IEEE Transactions on Systems, Man, and Cybernetics, Part C (Applications and Reviews), 37*(6), pp. 1067-1080.

Laitinen, H., Juurakko, S., Lahti, T., Korhonen, R., & Lahteenmaki, J. (2007). Experimental evaluation of location methods based on signal-strength measurements. *IEEE Transactions on Vehicular Technology, 56*(1), pp. 287-296.

Ben-Kilani, M., Raymond, A. J., Gagnon, F., Gagnon, G., & Lavoie, P. (2014, March). *RSSI-based indoor tracking using the extended Kalman filter and circularly polarized antennas.* Paper presented at the Workshop on Positioning, Navigation and Communication, Dresden, Germany.

Li, X. (2006). Rss-based location estimation with unknown pathloss model," Wireless Communications. *IEEE Transactions on Wireless Communications, 5*(12), pp. 3626-3633.

Mazuelas, S., Bahillo, A., Lorenzo, R. M., Fernandez, P., Lago, F. A., Garcia, E., . . . Abril, E. J. (2009). Robust indoor positioning provided by real-time rssi values in unmodified wlan networks. *IEEE Journal of Selected Topics in Signal Processing, 3*(5), pp. 821-831.

Fink, A., Beikirch, H., Voß, M., & Schröder, C. (2010, September). *Rssi-based indoor positioning using diversity and inertial navigation.* Paper presented at the International Conference on Indoor Positioning and Indoor Navigation, Zurich, Switzerland.

Kao, W. W., & Lin, S. H. (2010, September). *Dead-reckoning aided rssi based positioning system for dynamic indoor environments.* Paper presented at the International Technical Meeting of The Satellite Division of the Institute of Navigation, Oregon, USA.

Schmid, J., Gädeke, T., Stork, W., & Müller-Glaser, K. D. (2011, April). *On the fusion of inertial data for signal strength localization.* Paper presented at the Workshop on Positioning, Navigation and Communication, Dresden, Germany.

Kalman, R. E. (1960). A new approach to linear filtering and prediction problems. *Journal of Basic Engineering, 82*(1), pp. 35–45.

Welch, G. F., & Bishop, G. (1995). An introduction to the kalman filter. University of North Carolina, Chapel Hill, NC, USA.

Yim, J., Park, C., Joo, J., & Jeong, S. (2008). Extended Kalman Filter for wireless LAN based indoor positioning. *Elsevier Journal, 45*(4), pp. 960-971.

Caceres, M. A., Sottile, F., & Spirito, M. A. (2009, October). *Adaptive location tracking by kalman filter in wireless sensor networks.* Paper presented at the IEEE International Conference on Wireless and Mobile Computing, Networking and Communications, Marrakech, Morocco.

Nepa, P., Cavallo, F., Bonaccorsi, M., Aquilano, M., Carrozza, M. C., & Dario, P. (2010, October). *Experimental analysis of rssi-based indoor location systems with WLan circularly polarized antennas.* Paper presented at the International Conference on Wireless Mobile Communication and Healthcare, Cyprus.

Szumny, R., Kurek, K., & Modelski, J. (2007, October). *Attenuation of multipath components using directional antennas and circular polarization for indoor wireless positioning systems.* Paper presented at the European Radar Conference, Munich, Germany.

Rappaport, T. S., & Hawbaker, D. A. (1992). Wide-band microwave propagation parameters using circular and linear polarized antennas for indoor wireless channels. *IEEE Transactions on Communications, 40*(2), pp. 240-245.

Manabe, T., Sato, K., Masuzawa, H., Taira, K., Ihara, T., Kasashima, Y., & Yamaki, K. (1995). Polarization dependence of multipath propagation and highspeed transmission characteristics of indoor millimeter-wave channel at 60 GHz. *IEEE Transactions on Vehicular Technology, 44*(2), pp. 268-274.

Kohler, M. (1997). Using the kalman filter to track human interactive motion modelling and initialization of the kalman filter for translational motion. University of Dortmund.

Wireless Connectivity Proprietary 2.4 GHz CC2510F32. Texas Instruments, available online: http://www.ti.com/products/cc2510f32.

Godrich, H., Haimovich, A. M., & Blum, R. S. (2009). Target localisation techniques and tools for multiple-input multiple-output radar. *IET Radar, Sonar & Navigation, 3*(4), pp. 314-327.

Du, Y., & Wei, P. (2014). An explicit solution to target localization in noncoherent distributed MIMO radar systems. *IEEE Signal Processing Letters, 21*(9), pp. 1093-1097.

Godrich, H., Haimovich, A. M., & Blum, R. S. (2010). Target localization accuracy gain in mimo radar-based systems. *IEEE Transactions on Information Theory, 56*(6), pp. 2783-2803.

Niu, R., Blum, R. S., Varshney, P. K., & Drozd, A. L. (2012). Target localization and tracking in noncoherent multiple-input multiple-output radar systems. *IEEE Transactions on Aerospace and Electronic Systems, 48*(2), pp. 1466-1489.

He, Q., Blum, R. S., Godrich, H., & Haimovich, A. M. (2010). Target velocity estimation and antenna placement for mimo radar with widely separated antennas. *IEEE Journal of Selected Topics in Signal Processing, 4*(1), pp. 79-100.

Dianat, M., Taban, M. R., Dianat, J., & Sedighi, V. (2013). Target localization using least squares estimation for mimo radars with widely separated antennas. *IEEE Transactions on Aerospace and Electronic Systems, 49*(4), pp. 2730-2741.

Liang, J., Leung, C. S., & So, H. C. (2016). Lagrange Programming Neural Network Approach for Target Localization in Distributed MIMO Radar. *IEEE Transactions on Signal Processing, 64*(6), pp. 1574-1585.

Zou, Y., Wan, Q., & Cao, J. (2016, November). *Target localization in noncoherent distributed MIMO radar system using squared range-sum measurements.* Paper presented at the IEEE 13th International Conference on Signal Processing (ICSP), Chengdu, China.

Zou, Y., & Want, Q. (2016, December). *Moving target localization in noncoherent distributed MIMO radar systems using range and range rate measurements.* Paper presented at the Asia-Pacific Signal and Information Processing Association Annual Summit and Conference (APSIPA), Jeju, South Korea.

Yi, J., Wan, X., Leung, H., Lu, M., & Cheng, F. (2016). Noncooperative registration for multistatic passive radars. *IEEE Transactions on Aerospace and Electronic Systems, 52*(2), pp. 563-575.

Yang, H., & Chun, J. (2016). An Improved Algebraic Solution for Moving Target Localization in Noncoherent MIMO Radar Systems. *IEEE Transactions on Signal Processing, 64*(1), pp. 258-270.

Wanchun, L., Qiu, T., Chengfeng, H., & Yingxiang, L. (2017). Location algorithms for moving target in non-coherent distributed multiple-input multiple-output radar systems. *IET Signal Processing, 11*(5), pp. 503-514.

Noroozi, A., & Sebt, M. A. (2016). Weighted least squares target location estimation in multi-transmitter multi-receiver passive radar using bistatic range measurements. *IET Radar, Sonar & Navigation, 10*(6), pp. 1088-1097.

Gogineni, S., & Nehorai, A. (2011). Target estimation using sparse modeling for distributed MIMO radar. *IEEE Transactions on Signal Processing, 59*(11), pp. 5315-5325.

Stinco, P., Greco, M. S., Gini, F., & La-Manna, M. (2014). Non-cooperative target recognition in multistatic radar systems. *IET Radar, Sonar & Navigation, 8*(4), pp. 396-405.

Arik, M., & Akan, O. B. (2010). Collaborative Mobile Target Imaging in UWB Wireless Radar Sensor Networks. *IEEE Journal on Selected Areas in Communications, 28*(6), pp. 950-961.

Sobhani, B., Paolini, E., Giorgetti, A., Mazzotti, M., & Chiani, M. (2014). IEEE Journal of Selected Topics in Signal Processing. *Target tracking for UWB multistatic radar sensor networks, 8*(1), pp. 125-136.

Sobhani, B., Zwick, T., & Chiani, M. (2016). Target TOA association with the hough transform in UWB radars. *IEEE Transactions on Aerospace and Electronic Systems, 52*(2), pp. 743-754.

Bartoletti, S., Giorgetti, A., Win, M. Z., & Conti, A. (2015). Blind selection of representative observations for sensor radar networks. *IEEE Transactions on Vehicular Technology, 64*(4), pp. 1388-1400.

Bartoletti, S., Giorgetti, A., & Conti, A. (2013, June). *Sensor radars with subset diversity.* Paper presented at the IEEE International Conference on Communications Workshops (ICC), Budapest, Hungary.

Bartoletti, S., Conti, A., Giorgetti, A., & Win, M. Z. (2014). Sensor radar networks for indoor tracking. *IEEE Wireless Communications Letters, 3*(2), pp. 157-160.

Yang, L., Liang, J., & Liu, W. (2014, October). *Radar sensor (RS) deployment for multi-target detection.* Paper presented at the Sixth International Conference on Wireless Communications and Signal Processing (WCSP), Hefei, China.

Godrich, H., Petropulu, A. P., & Poor, H. V. (2012). Sensor Selection in Distributed Multiple-Radar Architectures for Localization: A Knapsack Problem Formulation. *IEEE Transactions on Signal Processing, 60*(1), pp. 247-260.

Kaplan, L. M. (2006). Global node selection for localization in a distributed network. *IEEE Transactions on Aerospace and Electronic Systems, 42*(1), pp. 113-135.

Kaplan, L. M. (2006). Local node selection for localization in a distributed network. *IEEE Transactions on Aerospace and Electronic Systems, 42*(1), pp. 136-146.

Tharmarasa, R., Kirubarajan, T., Hernandez, M. L., & Sinha, A. (2007). PCRLB-based multisensor array management for multitarget tracking. *IEEE Transactions on Aerospace and Electronic Systems, 43*(2), pp. 539-555.

Daher, R., & Adve, R. (2008, October). *Analysis of Random radar networks.* Paper presented at the 42nd Asilomar Conference on Signals, Systems and Computers, Pacific Grove, CA, USA.

Sorensen, D. C. (1982). Newton's method with a model trust region modification. *SIAM Journal on Numerical Analysis, 19*(2), pp. 409-426.

Chen, C. H., Feng, K. T., Chen, C. L., & Tseng, P. H. (2009). Wireless location estimation with the assistance of virtual base stations. *IEEE Transactions on Vehicular Technology, 58*(1), pp. 93-106.

Waltz, R. A., Morales, J. L., Nocedal, J., & Orban, D. (2006). An interior algorithm for nonlinear optimization that combines line search and trust region steps. *Mathematical Programming Journal, 107*(3), pp. 391-408.

Tsao, T., Slamani, M., Varshney, P., Weiner, D., Schwarzlander, H., & Borek, S. (1997). Ambiguity function for a bistatic radar. *IEEE Transactions on Aerospace and Electronic Systems, 33*(3), pp. 1041-1051.

Rihaczek, A. W. (1996). *Principles of High-Resolution Radar*: Artech House.

Sturm, C., Sit, Y. L., Braun, M., & Zwick, T. (2013). Spectrally interleaved multi-carrier signals for radar network applications and multi-input multi-output radar. *IET Radar, Sonar & Navigation, 7*(3), pp. 261-269.

Shen, Y., & Martinez, E. (2006). *Channel estimation in ofdm systems*. Freescale Semiconductor.

Sit, Y. L., Sturm, C., & Zwick, T. (2012, March). *One-stage selective interference cancellation for the OFDM joint radar-communication system.* Paper presented at the 7th German Microwave Conference, Ilmenau, Germany.

Ben-Kilani, M., Nijsure, Y., Gagnon, G., Kaddoum, G., & Gagnon, F. (2016). Cognitive waveform and receiver selection mechanism for multistatic radar. *IET Radar, Sonar & Navigation, 10*(2), pp. 417-425.

Zheng, L., Lops, M., Wang, X. (2018). Adaptive interference removal for uncoordinated radar/communication coexistence. *IEEE Journal of Selected Topics in Signal Processing, 12*(1), 45-60.